UNIVERSIDADE DE LISBOA
FACULDADE DE CIÊNCIAS
DEPARTAMENTO DE FÍSICA

Replacing Gamma Analyses with DVH Analyses for Individual Patient QA

Joana Maria dos Santos Boita

Mestrado Integrado em Engenharia Biomédica e Biofísica
Perfil em Radiações em Diagnóstico e Terapia

Dissertação orientada por:
Prof. Dr. Luís Peralta e Dr. Joep Stroom

2017

Learn from yesterday, live for today, hope for tomorrow.
The important thing is not to stop questioning.

— Albert Einstein

Acknowledgements

Firstly, I have to mention that I am very grateful to the Champalimaud Foundation for receiving me in the Radiotherapy Department. I have to thank Sandra and Joep for accepting, receiving and accompanying me throughout my internship.

I am very thankful to my supervisor, Joep Stroom for all the help, patience, attention and knowledge shared with me. Without you this project would have been very difficult to carry out. It was a pleasure to work with you.

I also would like to thank Milton Rodrigues and Maria João Cardoso for all the help, time and patience spent with me.

Thank you to Sun Nuclear, mainly to Miguel Sequeira, Eduardo Sabino and Lukasz Wlodarczyk for accompanying me and for all the assistance and knowledge shared about 3DVH.

Thank you to my internal supervisor, Professor Luís Peralta for the attention, help and support along this project.

Thank you to Tatiana Ladeira for sharing with me this journey, for integrating me in the Champalimaud Foundation, for the company and all the talks.

A big thank you to all my friends that I had the opportunity to meet during these five years which ended so quickly: my EBB's, for sharing with me this path and for all the great moments that we spent together. I mainly have to thank my top10 and my informatics guys, for all the moments, support and friendship, without you this journey would not have been the same. A big thank you for my two girls, Inês Veríssimo and Isabel Machado Barradas for all the patience, support, company, help and friendship. You were a great help in achieving this thesis.

I also have to thank my Bene friends, mainly my girls Maria Vicente, Rafaela Santos, Carolina Paciência, Sofia Castelhano and Adriana Ribeiro, for all the support, constant presence, talks, friendship and all the attempts to make me leave my house and have fun. A special thank you for Eunice Vicente, for your constant presence, support and moments shared during all these years.

A big, big thank you to my cousin Rita for all the hours spent reading and re-reading this thesis and for all the help, conversations and advices.

Last but definitely not the least, to my parents and my brothers a big and warm thank you for providing me all the experiences that I had the opportunity to live and mainly for the constant support, help and for always being by my side. Without you, all of this would not be possible.

Resumo

O tratamento de Radioterapia pretende atuar contra uma das principais causas de morte mundialmente sentidas, o cancro. Esse tratamento consiste em irradiar o tecido danificado com elevada dose de radiação, de modo a cessar a proliferação das células cancerígenas. O mesmo é realizado com a máxima de tentar proteger o melhor possível o tecido envolvente, de modo a minimizar os efeitos secundários do tratamento no paciente.

Ao longo dos últimos anos têm-se verificado inúmeros desenvolvimentos e mudanças na forma como a Radioterapia se procede, devido ao grande crescimento tecnológico ocorrido. Tendo sempre em mente o objetivo de minimizar a dose entregue no tecido saudável, novas técnicas de tratamento foram desenvolvidas, como por exemplo, IMRT (*Intensity-Modulated Radiation Therapy*) e VMAT (*Volumetric-Modulated Arc Therapy*), as quais permitem a irradiação mais precisa do tecido cancerígeno, através da sua conformação por parte das folhas, um constituinte integrante do acelerador. Também foram desenvolvidas novas técnicas de imagem que melhoraram tanto os processos de planeamento como o tratamento em si. Com o aparecimento de novos, precisos e eficazes softwares e sistemas, também o planeamento do tratamento mudou. Assim, em resposta às necessidades requeridas pela entrada de novos e complexos modos de tratamento e sistemas utilizados, o processo de controlo de qualidade tornou-se essencial no planeamento do tratamento. Com este processo pretende-se assegurar que o tratamento seja administrado ao paciente da forma mais segura e precisa. O controlo de qualidade em IMRT, e neste caso, específico a cada paciente, consiste numa medição do plano do paciente previamente realizado recorrendo-se aos sistemas de planeamento próprios. Esta medição simula o tratamento e requer sistemas específicos para a sua realização. Posteriormente procede-se a uma comparação do que foi medido com o planeado, de modo a verificar se existem erros no plano e se este pode ser ou não aprovado para o tratamento. Como método de análise da distribuição de dose quer no plano medido quer no planeado, é utilizada a análise gama que combina dois critérios, o de diferença de dose e o de distância, para calcular as diferenças existentes entre a distribuição de dose desses dois planos. No entanto, têm-se verificado alguma incoerências e falta de precisão por parte desse método, questionando-se a sua capacidade para estimar a presença de efeitos negativos clinicamente relevantes e erros no plano de tratamento do paciente.

Na Fundação Champalimaud, o processo de controlo de qualidade específico a cada paciente em IMRT é realizado diariamente, utilizando a análise gama como método de avaliação da distribuição de dose e o ArcCHECK, desenvolvido pela *Sun Nuclear Corporation*, como sistema de medição de dose.

Este estudo foi efetuado de modo a melhorar o processo de controlo de qualidade realizado na Fundação Champalimaud. Esse consistiu no teste de um software, 3DVH, também desenvolvido

pela *Sun Nuclear Corporation*, que permite avaliar a distribuição de dose recorrendo à análise com DVH, *Dose Volume Histogram*, o método promissor e que pretende substituir a análise gama no processo de controlo de qualidade. DVH consiste num gráfico que relaciona a dose entregue por volume (em percentagem) de cada estrutura analisada.

Para cumprir o principal objetivo deste estudo, foram feitos dois testes: um com campos quadrados abertos, e o segundo com planos de tratamento de pacientes. Seis planos de pacientes foram usados, cinco de cancro da mama e um de cancro da próstata. Todos os planos foram calculados no sistema de planeamento, Monaco.

Em ambos os testes foram usados planos com erros, ou seja, foram introduzidos erros nas folhas e nas unidades monitor (uma medida de calibração do acelerador associada à dose). Os primeiros alteram a posição das folhas, abrindo ou fechando as mesmas, tendo em conta o erro introduzido. Já os segundos erros alteram a quantidade de unidades monitor entregues no tratamento, reduzindo ou aumentando o seu número, tendo também em conta o erro introduzido. Relativamente aos erros nas folhas, foram introduzidos erros sistemáticos e aleatórios. Os primeiros consistem na mudança sistemática e simétrica da posição das folhas, ou seja, todas fecham ou todas abrem. Nos erros aleatórios as folham movem-se aleatoriamente, não se sabendo *a priori* que posição essas podem tomar. Foram introduzidos erros sistemáticos de ±0.5, ±1, ±2 e ±3 mm e erros aleatórios com desvio padrão de 1, 2, 3, 4 e 5 mm. Relativamente aos erros nas unidades monitor, foram introduzidos erros sistemáticos de ±2 e ±4%.

De modo a perceber se os softwares estão a efetuar as análises de uma forma precisa e se os sistemas de medição estão a adquirir dose de uma forma eficaz, foram realizadas predições para ambos os testes. No teste com campos quadrados abertos, ou seja, com planos mais simples, foi possível realizar as predições tanto para os dados dos erros nas folhas como para os dados dos erros nas unidades monitor. Enquanto que, para o teste com planos de pacientes apenas foram feitas predições para os dados dos erros nas unidades monitor, pois estes planos são mais complexos na forma como o plano é irradiado.

As medições de todos os planos com e sem erros foram efetuadas recorrendo-se ao acelerador *Synergy*, da *Elekta*, e aos sistemas de aquisição de informação dosimétrica, ArcCHECK e EPID (*Electronic Portal Imaging Device*). Utilizou-se o ArcCHECK, pois é o sistema utilizado na fundação e o que fornece os dados de medição compatíveis e necessários para realizar a análise em 3DVH. No caso do EPID, este, nós últimos anos, tem mostrado grandes capacidades dosimétricas e muitas vantagens por ser um sistema fisicamente ligado ao acelerador e já integrante no processo de controlo de qualidade em alguns institutos. Na fundação encontra-se em investigação, na tentativa de ser implementado, por isso também entrou para este estudo, de modo a ser comparado com o ArcCHECK.

As análises gama e com DVH foram feitas recorrendo-se aos específicos softwares de cada sistema de medição, PreDose, pdapp e pdDVH que usam os dados provenientes das medições com EPID e SNC e 3DVH que usam os dados provenientes das medições com ArcCHECK.

Os resultados relativos aos testes feitos com campos quadrados abertos mostraram que os sistemas foram capazes de detetar a presença dos erros nas unidades monitor tanto através da análise gama, como da análise usando DVH. No caso da deteção dos erros nas folhas, o 3DVH mostrou reduzidas capacidades para o fazer, ao contrário dos softwares de análise respetivos

ao EPID, tanto para a análise gama como para a análise usando DVH. Foram observadas algumas faltas de correlação entre a análise gama e a análise com DVH. Percebeu-se ainda que os erros maiores causam também maiores perturbações, neste caso, menores *gamma passing rate*, parâmetro de análise calculado pela análise gama, maiores desvios entre os DVHs de referência e os de medição e maiores valores de diferença de dose média. Pelas análises dos DVHs também se conseguiu perceber com maior clareza em que estruturas os efeitos eram mais evidentes e que os erros negativos causavam uma redução da dose entregue ao paciente e os positivos um aumento dessa mesma dose.

No caso dos resultados obtidos a partir dos testes com planos de pacientes, esses também mostraram algumas faltas de correlação entre a análise gama e a análise com DVH. Nestes testes a análise com DVH apenas foi realizada com o 3DVH, pois não foi possível realizar medições com erros em planos de pacientes. Nestes testes o 3DVH mostrou-se bastante eficaz em ambas as análises, destacando-se principalmente na análise com DVH, pois fornece bastante informação relativa à distribuição de dose no paciente. No entanto, devido aos resultados menos bons na deteção de erros nas folhas, as suas análises podem não ser as mais seguras. No caso na deteção de erros nas unidades monitor, tal como no teste dos campos quadrados, o 3DVH conseguiu detetar os erros em aproximadamente todos os planos analisados.

Em suma, o 3DVH parece ser uma boa opção a implementar no processo de controlo de qualidade da Fundação Champalimaud, tendo em conta que é um software compatível com o sistema de medição usado, essencialmente para efetuar a análise com DVH, a qual mostrou ser clinicamente mais eficiente e relevante do que a análise gama. No entanto, o 3DVH necessita de algumas melhorias. As faltas de correlação visíveis entre a análise com DVH e a análise gama mostram que este último método pode esconder erros relevantes, enquanto o tratamento é aprovado pelo mesmo. Como mencionado anteriormente, a análise com DVH, principalmente no 3DVH, fornece muita informação relevante e permite ter uma melhor noção das zonas afetadas pelos erros e com que intensidade estas são perturbadas, analisando valores específicos de dose, como por exemplo, a dose máxima, a dose média, a dose que afetou 95% do volume, entre outros. Pretende-se ainda perceber quais são os melhores valores de restrição de dose a analisar. O EPID também se mostrou muito eficiente e eficaz na deteção dos erros, e quando este for clinicamente aceite, poderá ser a melhor opção para realizar a controlo de qualidade especifica a cada paciente em IMRT, tendo em conta a sua geometria (está acoplado ao acelerador) e resolução.

Palavras-chave: Controlo de Qualidade em IMRT, Análise gama, Análise DVH, ArcCHECK, EPID

Abstract

In the last years, great developments in radiotherapy took place both in technology and in treatment techniques. An example of this is the Intensity-Modulated Radiation Therapy (IMRT), whose emergence changed the way treatment planning is performed. As a consequence, patient-specific quality assurance (QA) became essential in the treatment planning. This makes sure that the treatment is carried out as planned and it assures the quality of the treatment and safety of the patient. The QA consists in comparing the planned and measured dose distributions. Gamma analysis is the most common mathematical method used for dose comparison. It compares two dose distributions, reference dose and evaluated dose, by combining dose and distance criteria. However, gamma analysis has demonstrated incoherencies, poor accuracy in estimating the errors and poor correlation with clinically relevant dose deviations.

This study was performed in order to improve the patient-specific QA process carried out in Champalimaud Foundation. It consisted in testing a new software, 3DVH, that uses an alternative, Dose Volume Histogram (DVH) analysis to compare measured and planned doses. This method intends to replace the gamma analysis in QA.

To this end, two tests were performed, the first with open square fields plans and the second with patient plans. In both tests, MLC and MU errors were introduced in the plans, changing the leaves positions and the monitor units quantity used for the treatment, respectively. The measurements were carried out with the The ArcCHECK and the Electronic Portal Imaging Device (EPID) to measure the dose distribution. ArcCHECK is the device used in Champalimaud Foundation for QA measurements, and the EPID is the device that has been demonstrating accurate dosimetric capabilities and is currently in research in Champalimaud Foundation. The analysis was made using specific software: PreDose, pdapp and pdDVH for the EPID data, and commercial SNC and 3DVH for the ArcCHECK data. Thus, the reference and the measured dose distributions were compared using both gamma analysis and DVH analysis, and the results were compared with predictions previously calculated, in order to verify if there is a correlation between both methods and to test the accuracy of the systems to detect the errors.

In the square fields test, unlike 3DVH, EPID showed more sensitivity to estimate the effects of the MLC errors in the plans, mainly in the DVH analysis. All the systems detected the presence of the MU errors in the gamma and in the DVH analysis. Lack of correlation was observed between the gamma analysis and the DVH analysis, i.e. the gamma analysis can provide wrong results and hide relevant errors, while the treatment is approved. On the other hand, the DVH analysis provides more and clinically relevant information about the effect of the errors in the structures.

In the patient plans, the DVH analysis was just performed by the 3DVH and it showed significant accuracy in its performance for detecting MU errors. For MLC errors, its results are not

very reliable, due to the lesser results obtained in the square fields test. All the systems detected the presence of the errors in the gamma analysis. However, a lack of correlation between the DVH analysis and gamma analysis was also observed.

This study proved that the gamma analysis is a limited method, with incoherencies and that it is not a good method to estimate effects of the errors. On the other hand, the DVH analysis showed accuracy and efficiency in dose distribution evaluation, providing general (of all treatment) and individual (of each structure) clinically relevant information. Thus, 3DVH is a good system to be implemented for the DVH analysis. However, should EPID be clinically accepted, it is the best option, taking into account its geometry, performance and resolution.

Key-words: Patient-specific IMRT QA, gamma analysis, DVH analysis, ArcCHECK, EPID

Contents

List of Abbreviations

2D Two-dimensional
3D Three-dimensional
3D-CRT 3D Conformal Radiotherapy
%GP Gamma Passing Rate
AC Attenuation Correction
AP Anterior-Posterior
a-Si EPID Amorphous-Silicon EPID
CFRT Conformal Radiotherapy
cm Centimetres
cGy Centigray
CMF Contribution Modifying Function
CP Control Point
CT Computed Tomography
CTV Clinical Target Volume
DICOM Digital Imaging and Communication in Medicine
DTA Distance-to-Agreement
DVH Dose-Volume Histogram
EPID Electronic Portal Imaging Device
FF Flattening Filter
FFF Flattening Filter Free
GTV Gross Target Volume
Gy Gray
H& N Head and Neck
IC Ionization Chamber
IMRT Intensity-Modulated Radiation Therapy
ITV Internal Target Volume
ISQL Inverse Square Law
LINAC Linear Accelerator
LL Lateral Left
LR Lateral Right
MeV Mega Electron Volt
MLC Multileaf Collimator
mm Millimiters
MRI Magnetic Resonance Imaging

MU Monitor Unit
MV MegaVolt
PA Posterior-Anterior
PDP Planned Dose Perturbation
PET Positron Emission Tomography
PMMA Polymethylmethacrylate
PTV Planning Target Volume
QA Quality Assurance
ROI Regions of Interest
RT Radiotherapy
RTP Radiotherapy Treatment Planning
SD Standard Deviation
SPECT Single-Photon Emission Computed Tomography
SSD Source-Surface Distance
TFI Thin Film Transistors
TPS Treatment Planning System
VMAT Volumetric-Modulated Arc Therapy
VOI Volume of Interest

List of Figures

List of Tables

CHAPTER 1

Introduction

Cancer remains among the leading causes of death worldwide. According to recent statistical studies, this disease appears as the second main cause of death after cardiovascular disease, causing 8.2 million deaths globally with 14.9 million new cases in 2013 [1]. This disease, also defined as malignant tumours and neoplasms, is the rapid appearing and growth of abnormal cells, with unlimited proliferative potential, that grow beyond their usual boundaries and spread to other organs, creating metastases [2]. In Europe, in 2012, there was an estimate of 3.45 million new cases of cancer and 1.75 million deaths from cancer. In Portugal, in the same year, 491.8 hundred cases of cancer were reported, 241.1 hundred of which resulted in death [3].

Radiotherapy (RT) appeared in order to reduce the number of cancer deaths, being one of the major treatment methods for cancer, along with surgery and chemotherapy. The aim of radiotherapy is to, noninvasively, stop the proliferation of the cancer cells, preventing its continuous spread along the body. This is achieved by radiating the tumour tissue, i.e. the target region, with high-energy radiation. It has been assured that the surrounding normal healthy tissue will be spared as much as possible to prevent damage in the body. Irradiation is done by using external beam radiotherapy (EBRT) or brachytherapy, which will be explained in more detail later on. The effect caused in the tissue depends on the types of the types of radiation particle beams used, each of which have different interactions with the tissue. Megavoltage X-rays (photons), electrons and protons are the most commonly radiation types used [4, 5, 6].

RT was developed in the beginning of the century XX and has been subject to a number of technological innovations. Despite the fact that radiotherapy is one of the most used treatments of cancer, it is not perfect and complications may happen, such as healthy tissue affected or overdose administered. The research evolved aiming to prevent and overcome these problems, rendering the treatment more efficient and accurate.

This growth and development of radiotherapy was achieved by the rapid advance of new, high precision and improved technology, significantly changing the way radiotherapy is planned and carried out. In the image field, various procedures have been used (computed tomography, positron emission tomography, magnetic resonance imaging, ultrasonography), which are helpful for the treatment and which also belong the radiation therapy planning process. New and more sophisticated planning software has also been coming about. Consequently, there was a significant development of complex and accurate treatment planning procedures. In case of

delivered dose techniques of external beam radiotherapy, a growing interest in hypofractionated treatments was observed. These types of treatment allow for a higher dose delivery per fraction, which therefore diminishes the number of fractions needed. Intensity-Modulated Radiation Therapy (IMRT) and Volumetric-Modulated Arc Therapy (VMAT) are the most recently used techniques. They make use of multileaf collimators (MLC) which improve the efficiency of treatment delivery, replacing conventional blocking [7]. The Electronic Portal Imaging Device (EPID) was also an important technological innovation, because it allows to obtain easily and rapidly information about dose delivery in two or, preferably, three dimensions [5]. All these enhancements in radiotherapy imply a new way to perform Quality Assurance (QA) process, which evaluates the accuracy of the treatment and consequently the dose delivery in the patient with as few errors as possible. It consists in comparing a calculated dose distribution, using treatment planning system (TPS), to a measured dose distribution in a phantom, applying the patient plan to the phantom [6, 8].

Our project intends to improve the way patient-specific IMRT QA is performed. In the Champalimaud Foundation, the QA is carried out with a phantom, ArcCHECK, and gamma analysis, as the metric tool, to perform dose distribution comparisons. However, this metric tool shows some inconsistencies in its performance. Thus, the commercial 3DVH software was developed, which allows to carry out patient-specific QA by analysing dose per organ volume with Dose Volume Histogram (DVH), a more efficient and informative method for the patient's dose delivery analysis. The main goal of this project is to test this method and software with ArcCHECK, as well as the promising device to perform quality assurance in pre-treatment, the aforementioned EPID. This test has been carried out comparing measured and planned doses distributions using gamma analysis and DVH analysis, in order to verify whether or not there is a correlation between both methods. Square field plans and plans from breast and prostate were used to measure dose distribution. MLC and monitor unit (MU) errors were introduced in the plans in order to check the accuracy of both systems, ArcCHECK and EPID, to calculate DVHs, comparing these plans with error-free plans.

This dissertation describes the project developed in Foundation Champalimaud during nine months. It is divided in five chapters, in which all the information regarding the evaluation and implementation test of the 3DVH is presented. Chapter 1 is a general introduction to the dissertation, where the project and its aim and contents are presented. Chapter 2 reports the background of the project, presenting some concepts about some techniques of radiotherapy and previous studies and approaches regarding QA in IMRT. Chapter 3 describes the systems, software, methods and procedures used in this work to acquire and analyse the dose data. Chapter 4 shows the main results obtained and their specific discussion. Finally, Chapter 5 summarizes the main conclusions of the project and possible future work.

CHAPTER 2

Background

2.1 Radiotherapy

2.1.1 Principles of Radiotherapy

Radiotherapy, or radiation therapy, is one of the major treatments used in cancer treatment, being one of the three main therapies used. In surgery the tumour is removed; in chemotherapy chemical substances are introduced in the blood flow to eliminate the cancer cells; and in radiotherapy the tumour cells are killed using ionizing radiation. Depending on the cancer, it is possible to combine different therapies, in order to improve the treatment, or to use only one therapy.

The main goal of radiotherapy is to deliver a radiation dose to the tumour while sparing the normal tissue and possible surrounding organs at risk (OAR). The ionization radiation causes irreparable genetic damages in the tumour cells, killing them directly or causing cell apoptosis. In other words, when damages in the DNA structure of a cell occur, its reproduction is interrupted, causing cancer cells to die and, subsequently, the tumour stops growing. When the radiation dose is delivered to the patient's tissue, the absorbed dose varies while beam penetrates in depth. This variation depends on many parameters, such as beam energy, depth, field size and source distance [9].

Each cancer has inherently different radiation sensitivity, determining how to proceed in dose delivery process. Therefore, there are two types of radiation delivery, external beam radiotherapy and brachytherapy. The first one is regularly used and utilises high energy beams of ionization radiation of photons, electrons or protons to destroy the tumour cells inside the human body. The dose is delivered by a linear accelerator, which can generate radiation beams from different angles by rotating the gantry. Photon therapy is used in deep tumours, being able to penetrate deep into the body while sparing the skin; electron therapy is used for superficial treatments, providing a high dose to a few centimetres depth from the skin surface avoiding dose delivery beyond that; and proton therapy delivers energy with extreme precision, therefore limiting unwanted dose. The external beam radiotherapy method will inevitably cause damage of surrounding healthy tissue beyond tumour tissue. In order to overcome this negative point, several strategies are applied in clinical practice, improving the treatment as much as possible. As to the second type

of radiation delivery, brachytherapy, sealed radiation sources are temporarily or permanently placed into the tumour. As the sources are very close to the damaged tissue, their reach is limited, so the dose is delivered to the tumour in a precise way, sparing surrounding tissues. However, this method is invasive and less homogeneous, being specially used for smaller tumours [10, 11].

The ionising radiation, when interacting with the human tissue, causes some damage. There are physical effects, when radiation absorption in tissues leads to ionization and excitation; chemical effects result in breakage of chemical bonds and in generation of free radicals, because damaged atoms and molecules will react with other cellular components; biological effects lead to enzymatic reactions that act on residual chemical damage and the damage in the DNA that is not repaired and it leads to cell death; finally there are also clinical effects regarding delivered radiation process [11].

2.1.2 External Megavolt Photon Beam Radiotherapy Treatment

External megavolt photon beam radiotherapy is one of the most frequently used techniques to dose delivery treatment, as previously described (subsection 2.1.1). It uses photons of high energies to treat deep-seated tumours. Photons are produced by linear accelerators (LINACs). Electrons are generated and accelerated to high kinetic energies from 4 to 25 MeV using non-conservative microwave RF fields, in the LINAC, and then they collide with a tungsten target and lose kinetic energy, resulting in photon beam. It can be used for treatment after its additional collimation and optional filtering [6, 12]. A typical LINAC, represented in Figure 2.1, is composed of gantry, stand, modulator cabinet, treatment couch and control console. However, there are significant differences between commercial machines, depending on the goal of the treatment made using the respective system [12, 13].

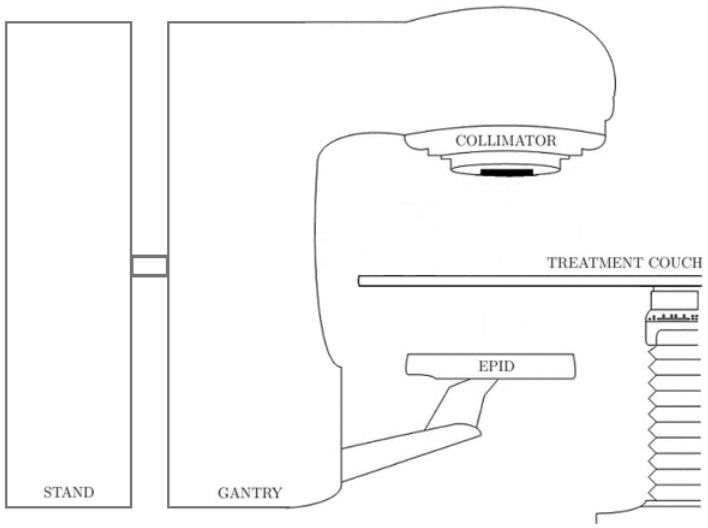

Figure 2.1: Illustration of LINAC setup and its components. The intern components are not illustrated in the figure. Adapted from [14].

The gantry is responsible for delivering the photon energy beam to a patient's tumour, rotating around him. It is composed of an electron gun, where the electrons are produced and then injected into the accelerator structure; of an accelerator structure, where the electrons are

accelerated; and of a treatment head, which is composed of certain components (bending magnet, primary and second collimators, flattening filter (FF) and scattering foil) designed to shape and monitor the treatment beam, obtaining a more uniform beam. As to the stand, it contains the set of systems (klystron or magnetron, waveguide, circulator and water-cooling system) that drives the linear accelerator, generating and guiding the electromagnetic waves to the accelerator guides. The modulator cabinet contains components that distribute and monitor primary electrical power and high-voltage pulses to the klystron or magnetron. The control console is responsible to monitor and to control the LINAC [13].

A major limitation to the efficacy of radiotherapy treatment is the production of undesirable complications caused by the irradiation of healthy tissue. Many organs are sensitive to radiation damage, thus special attention must be given and there must be alternatives to overcome this drawback. Beam shaping is a prerequisite and one of the options to take into account, in order to obtain dose distributions that conform to the tumour volume while sparing neighbouring health tissue. A conventional treatment machine shapes X-ray fields through a set of two pairs (upper (Y) and lower (X)) of dense metal collimators, jaws (or second collimator), built into the machine that produces rectangular beams, limiting the size of the treatment field. The jaws can open from 0 cm to the maximum field size of about 40 cm, or a little less. MLC is the most recent component of LINAC for beam shaping, replacing beam blocks on account of the several inherent disadvantages they presented, such as their manufactore, handling and storage is labour intensive and resource consuming. The MLC is located inside the LINAC, between both upper and lower jaws, and it consists typically of a set of 80 to 160 metallic leaves arranged in pairs with 0.25 to 1.0 cm wide. MLC movements are tracked by Y and X jaws in a horizontal and vertical direction, respectively. They can be positioned individually to shape the beam aperture to conform to the tumour, blocking some fraction of the radiation beam, in order to reduce the dose delivered to surrounding healthy tissue [6, 7].

The photon beam ia a bremsstrahlung beam. As such, its distribution in the MeV energy range demonstrates both an energy and intensity variation of the primary photon fluence with emission angle. To compensate for this effect, there are some accelerators with FF placed in the treatment head, located between the primary collimator and ion chamber, although this configuration can vary with the manufacture. FF modifies the distribution of photons, providing an almost uniform dose distribution at specific treatment depth, as shown in Figure 2.2. These filters consist of conical shaped pieces of metal, typically made of materials such as iron, copper or tungsten, and are specific to each particular energy [15, 16]. FF was important to compensate dose distribution effects. However, FF scatter photons are one of the major sources of radiation scatter in the treatment head and can lead to higher doses outside the treatment field [16, 17]. In response to this, advanced treatment techniques, such as IMRT and VMAT, where varying fluence pattern across the beam is delivered, have stimulated the increasing interest in operating linear accelerators in a flatting filter free (FFF) mode. Its inverse planning tools are able to handle unflattened beams. Besides reducing radiation scatter, removal of the flattening filter contributes to the increase of the dose rate, which is beneficial for the patient due to a reduction of the treatment duration, as well as of the leaf transmission, leakage radiation and out of field doses. Removing FF also provides improved accuracy in dose calculations [17].

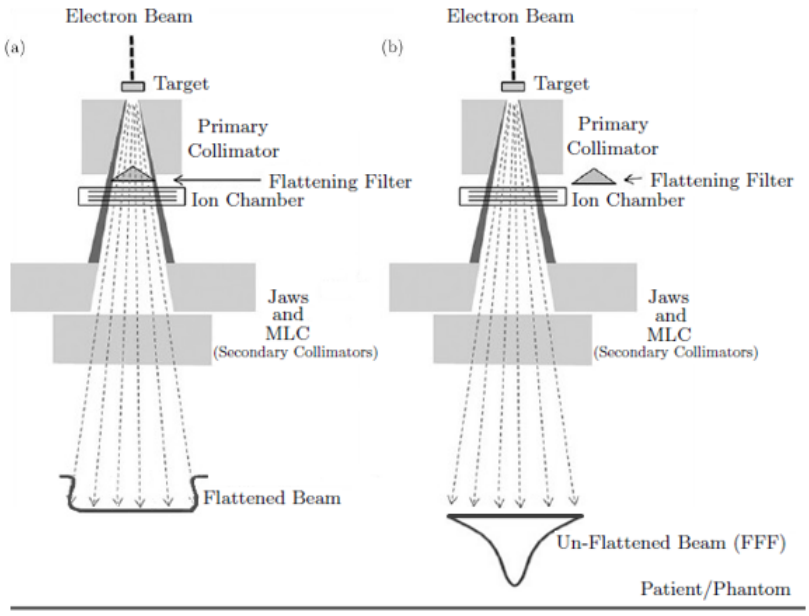

Figure 2.2: Illustration of radiotherapy treatment with (a) and without (b) flattening filter, respectively, and beams differences. Adapted from [18].

The EPID is another important component of modern LINACs. It allows to obtain images from the high energetic MV photon beam that exits from the patient during treatments. These images can be used for patient set-up verification or detection of organ motion and also for dosimetric verification of treatment, which is called portal dosimetry [6].

The treatment is often performed in a fractioned schedule, where the total dose is delivered, normally in 30 to 40 fractions, five times a week, typically lasting 5 to 8 weeks with a small (1.8 to 2 Gy) dose per fraction [12, 19]. However, with the improved accuracy in the way how radiotherapy is performed, a new mode to deliver dose to the patient was developed, hypofractionation. This delivers dose in a smaller number of fractions than in a conventional treatment. So the method can also deliver higher fraction doses, commonly measuring between 2 Gy and 8 Gy, as compared with conventional radiotherapy. Thus, this process exposes a tumour to a higher dose of radiation in a shorter period of time, sparing surrounding tissues, shortening the time of treatment and increasing its efficiency in destroying tumour cells [20, 21].

2.2 Dose Delivery Techniques

2.2.1 Conventional and Three-dimensional Conformal Radiotherapy

In the last years, progress was made in the way treatment is performed using radiation, in the devices and equipment used and in the treatment planning, the main goal being the reduction of the dose delivered to the normal tissue. Conventional radiotherapy defines the area to be treated in relation to bony landmarks. Multiple overlapping beams are then used to create a brick-shaped central region of high dose distribution. This method is simple and quick, but results in the irradiation of significant healthy tissue volume [22].

Three-dimensional Conformal Radiotherapy (3D-CRT) was then implemented, with the introduction of CT scanning, which improved the accuracy of defining and differentiating both

the tumour and organs at risk. In this technique, the beams of radiation used in treatment are shaped to match the tumour, allowing accurate dose conformity to irregular shapes. As its name indicates, this technique is based on 3D anatomic information, 3D target localisation, 3D treatment planning and 3D dose delivery techniques. 3D-CRT uses the image targeting information from CT, or other imaging techniques, to focus precisely on the tumour avoiding the healthy surrounding tissue, improving conformity of the radiation. Thus, it is possible to use higher levels of radiation in treatment, while sparing as much as possible the normal tissue. However, in order to treat with these high doses, it is necessary to further reduce the target volume irradiated. This would only be possible with the introduction of IMRT [12, 22, 23].

The treatment planning of the 3D-CRT is achieved with standard forward planning techniques, which design uniform intensity beams shaped to the geometrical projection of the target. In this planning process, beam arrangements are tested by trial and error, until a satisfactory dose distribution is produced. This is done manually, not via mathematical algorithms and computer software [12, 13].

Figure 2.3 shows the difference between three therapies.

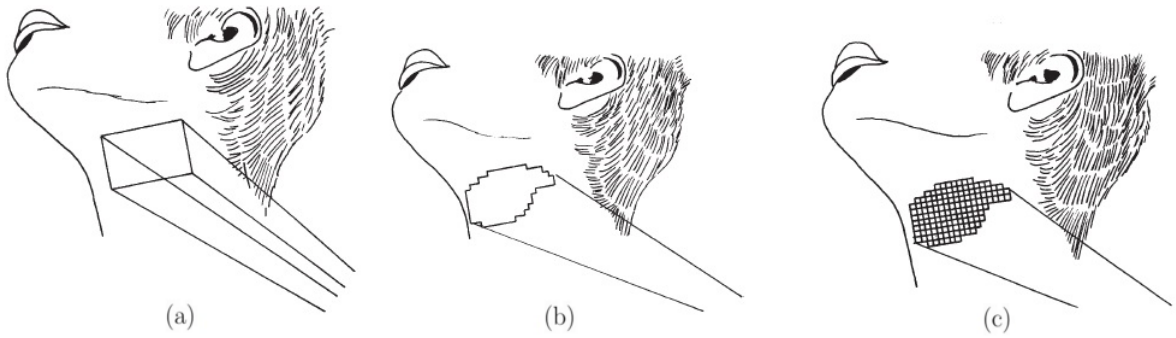

Figure 2.3: Illustration of the three therapies and their differences: (a) conventional radiotherapy, where dose is delivered using brick-shaped fields with additional blocks and wedges, (b) three-dimensional conformal radiotherapy with multileaf collimator, but without intensity-modulation, and (c) intensity-modulated radiation therapy with multileaf collimator and intensity-modulation with shaped field [24].

2.2.2 Intensity-Modulated Radiation Therapy

Intensity-modulated radiation therapy is one of the most important advances in radiotherapy of the last decades, being one of the results of the great developments in technology and health science. It is the advanced form of three-dimensional conformal radiotherapy. There is an extensive and ongoing world-wide research on the applications and improvements of this technique [22]. The introduction of IMRT changes the way how treatment planning occurs. Here inverse planning is used (to be further exposed), which utilises, in addition to beam shaping, intensity modulated beams to improve target dose homogeneity and to spare organs at risk [12].

An ideal radiotherapy treatment should deliver a high dose of radiation to the tumour tissue, causing minimal damage to the surrounding tissue. Intensity modulation with treatment beams can deliver radiation more precisely to the tumour, allowing more normal tissue to be spared than other techniques. This provides the possibility of both reducing toxicity and increasing the delivered dose to the target volume, improving tumour control. Comparing to 3D-CRT, IMRT differs in the existence of non-uniform intensity of the radiation and in the appearance of com-

puterised inverse planning [22]. It was put forward in 1982 by Brahme *et al.* [25]; it describes how a rotational technique with a simple idealised fluence modulation can irradiate uniform dose. In 1988 Brahme [26] developed a concept of creating fluence profiles from the required dose distributions. These approaches were also important for the introduction of the inverse planning concept, where, unlike in forward-planning approach, the starting point is the required dose distribution and the goal is to find a non-uniform fluence map that can produce it [24, 27].

The goal of IMRT is to shape the radiation dose to avoid or reduce exposure of healthy tissue and limit side effects of treatment while delivering a therapeutic dose to the cancer. This is possible because it allows the modulation of the intensity or fluence of each radiation beam, so each field can have one or many areas of high intensity radiation and any number of lower-intensity areas within the same field. Thus, it allows a greater control of the dose distribution in the target. The beam is manipulated so that when all the radiation delivery is considered, the dose conforms closely to the tumour or target volume within the patient. Unlike in conventional radiotherapy, IMRT is a fixed-beam treatment and uses MLC to modify both shape of the beams and the intensity distribution within each beam, instead of using blocks and wedges. With the introduction of MLC in the treatment, conforming the radiation to the target shape became significantly easier, more than with 3D-CRT. These leaves can move smoothly in and out of the treatment field during a short period of time [23, 28, 29].

There are two types of IMRT, the step-and-shoot IMRT, or segmented MLC IMRT (SMLC-IMRT), and the dynamic MLC IMRT (DMLC-IMRT), both presented in Figure 2.4. In the first one the leaves remain fixed during irradiation and the beam is turned off between consecutive MLC shapes. Which means, for each beam orientation, several different MLC-shaped fields are created and a modulated field intensity is achieved by summing all the fields. In the second one, the leaves are in continuous motion while the beam is on, moving in and out of the field to create the desired dose distribution. The intended intensity of radiation to the specified point is obtained due to existence of variation of the speed and distance between leaves [22, 29].

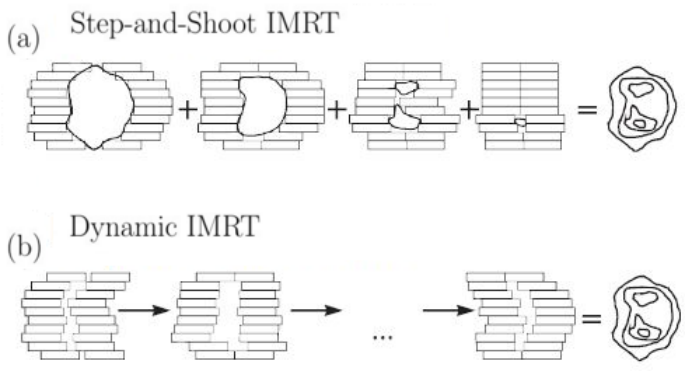

Figure 2.4: Illustration of two types of IMRT: (a) Step-and Shoot IMRT and (b) Dynamic IMRT. These methods use MLCs to create intensity distributions. In the first one, the beam is off during leaf motion, whereas in the second one radiation is delivered during leaf motion. Adapted from [29].

Thus, this technique can improve target conformity and it also can increase normal tissue sparing and can enable dose escalation. However, IMRT presents some drawbacks, such as the fact that it increases time needed for target and organ outlining, it needs extensive quality as-

surance process, it increases machine treatment time, as well as planning time and total body irradiation dose [22, 29].

The emergence of this technique has also changed the way treatment planning is performed. Before IMRT, radiation treatment was performed employing a forward planning process, during which the beams were manually set by physicists, choosing its number, shape and orientation and the wedges were also configured, in order to calculate dose distribution. In the case of the IMRT, inverse planning is used. It automates IMRT with an optimisation computer program, which determines the position, shape and intensity of the radiation beams in order to produce the required, ideal and most favourable 3D dose delivery, specifying the plan in terms of the tumour dose and normal structure dose limits. The computer system adjusts the beam intensities to find a configuration that best matches the required treatment plan. This process does not dependent as much on the geometric parameters as it does on the specification of volumes of tumour targets and sensitive structures, as well as on their dose constraints [22, 23, 24, 28].

2.2.3 Volumetric-Modulated Arc Therapy

Volumetric-modulated arc therapy is a recent and widely used method of delivering intensity modulated fields. It is a singular technique of IMRT, developed from the Intensity Arc Modulated Therapy (IMAT) that allows a treatment to be delivered in one or more dynamically modulated arcs. IMAT, proposed in 1995 by Yu [30, 24, 31], is similar to VMAT in that radiation is delivered while the gantry rotates around the patient and in every gantry rotation one intensity level is delivered from all angles. However, in the IMAT the dose rate and gantry speed are held constant, meaning it is not possible to change rate dose in each arc, which happens in the VMAT. Intensity modulation is achieved by delivering radiation over multiple gantry arcs. To increase dose level resolution, it is necessary to increase the number of arcs, which increases the treatment time [23, 27, 29].

VMAT differs from IMRT, as it is possible to see in Figure 2.5, in the fact that the radiation is delivered while the gantry rotates around the patient in one or more 360° maximum gantry rotation arcs, making it a faster method than IMRT. The dose is shaped using three important variables: MLC shape, gantry rotation speed and dose rate [27, 29].

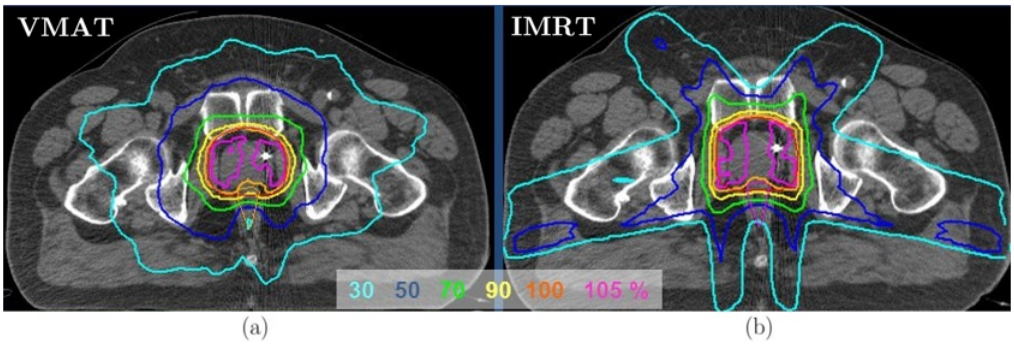

Figure 2.5: Illustration of image acquisition of treatment using (a) VMAT and (b) IMRT therapies. In the first one, it is possible to see the dose delivery while the gantry rotates and, in the second one, the dose delivery field by field [32].

2.3 Main Radiotherapy steps

In order to provide a better treatment for the patient, there are several factors to take into account and some procedures to follow. The main steps in radiotherapy, presented in Figure 2.6, are: evaluation consultation, patient positioning and immobilisation, image acquisition, target volume definition and organ delineation, dose planning, quality assurance, treatment delivery and clinical monitoring. There are some significant differences between planning and treatment delivery processes.

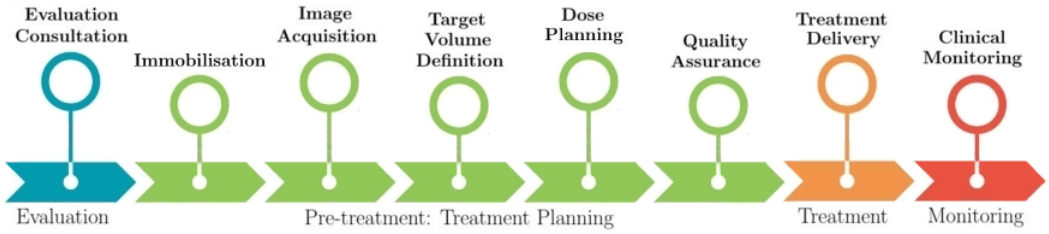

Figure 2.6: Schematic representation of the main steps in Radiotherapy.

2.3.1 Evaluation

The first step in radiotherapy is to make an evaluation of the patient, in order to understand the disease stage and define which treatment will be used and its aim. Afterwards, it is necessary to obtain images of the patient and delineate the targets and normal tissues on those images.

2.3.2 Pre-treatment: Treatment Planning

Pre-treatment consists in a set of processes carried out before treatment, in order to guarantee and provide the best treatment possible for the patient. It includes procedures such as immobilisation of the patient, image acquisition, target volume definition, dose prescription and quality assurance.

Immobilisation

It is necessary and important to the accuracy of the treatment that the position and anatomy of the patient coincide exactly with the geometry images acquired during the planning [9].

The treatment position depends on the location of the tumour. Several individual immobilisation techniques are used, such as simple immobilisation accessories (of members, of neck, amongst others) and of the thermoplastic masks. All these techniques allow to choose the best and most comfortable position for the patient. Skin marks are created on the patient for repositioning in the treatment. The position and immobilisation of the patient is, therefore, important during all the treatment process [9].

Imaging Acquisition

Imaging acquisition process allows for volume delineation of target organs and organs at risk, identifying the tumour and the normal tissues to be avoided. The image is acquired for each patient during the treatment position step.

There are many types of imaging acquisition. Computed tomography (CT) was the primary and standard imaging modality used for target delineation and dose calculation. However, other imaging modalities such as magnetic resonance imaging (MRI), positron emission tomography (PET) and Single-Photon Emission Computed Tomography (SPECT) can also be used. CT is widely and easily available, geometrically accurate and provides quantitative values, Hounsfield numbers, which are converted into electron density, relatively to water. This information is necessary for planning algorithms to calculate dose with organ heterogeneity correction. The main limitation of CT is that it cannot always identify the tumour adequately. Thus, other imaging modalities are needed to give additional information. MRI provides better anatomical visualisation than CT, because of its excellent soft tissue contrast. However, it cannot be used directly for radiotherapy planning due to geometric distortion and lack of electron density information. PET and SPECT are functional imaging techniques, providing valuable and additional information about patient and tumour physiology rather than anatomy. These imaging modalities use nuclear tracers to assess the microscopic environment and to define significantly proliferative areas within the tumour, tracking the distribution of a substance within the tumour cells. The nuclear tracers used depend on what will be measured. However, these techniques have poor spatial resolution and also do not provide electron density information, therefore they need to be combined with and matched to CT imaging for radiotherapy planning [9, 22, 24].

Target Volume Definition

Delineation of target volumes (safety margins) should be performed during treatment planning, in order to minimise the effect of geometrical uncertainties during treatment. The main volumes to be considered in the treatment plan are reported by the International Commission on Radiation Units and Measurements [33, 34], illustrated in Figure 2.7.

The gross tumour volume (GTV) is the gross demonstrable extent and location of the tumour; the clinical target volume (CTV) includes the damaged tissue, which means GTV plus the area directly surrounding it, which may contain subclinical malignant disease. This volume is the main target to be eliminated in the treatment, in order to achieve the aim of the therapy, the cure; and the planning target volume (PTV) is the CTV after geometric expansion, including uncertainties in the planning and treatment process, in order to ensure that the prescribed dose is actually absorbed in the CTV. It is also important to take into account other treatment plan components, such as the organs at risk, which are the normal tissues that can suffer radiation damage during treatment; the planning organ-at-risk volume, which is analogous to the PTV, but applies to normal tissues; and the remaining volume at risk, which consists of non-contoured parts of the patient. All these components are important to create the treatment plan of the patient.

The treatment is then planned so that the PTV receives the required tumour dose and the dose limits are defined for the organs at risk. The beam geometry is also designed and the dose distribution is calculated and evaluated [10, 23].

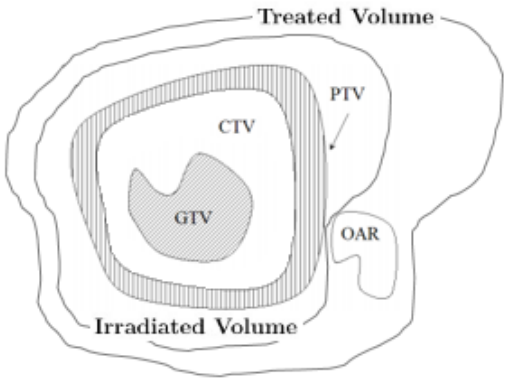

Figure 2.7: Illustration of the volumes delineation as defined by ICRU 50 and 62 reports. Adapted from [12].

Dose Planning

The patient's body is not homogeneous, which means each organ presents a different dose distribution and a different sensibility to the radiation. The dose planning step is used to obtain the beam shapes and dose distributions correspondent to each structure previously delimitated. This is done in order to maximise tumour control and minimise normal tissues complications [9, 12].

The treatment planning system generates the patient plan according to the best and most adequate technique to the treatment and target volume delineation. It uses three-dimensional (3D) imaging information of a patient to model the position and shape of both tumour and healthy tissue. Therefore, an optimum beam configuration, including photon beam energies, field sizes, shielding beam directions and relative weighting, can be determined and heterogeneities can be corrected, using specific calculation algorithms. Monte Carlo, which is the most accurate tool, simules the interaction of millions of photons with matter, using basic physics interactions. It also utilizes probability distribution significantly close to reality [6, 35]. Other algorithms faster than Monte Carlo model treatment beams use measurements of different beams. For every algorithm, the quality of the dose representation is strongly dependent on the parameters used. At the end, all beam parameters, which are needed to set up the linear accelerator, are defined and a 3D dose distribution inside the patient is obtained. The TPS also allows to simulate the treatment, used in quality assurance, in order to predict how it should occur, affecting the healthy tissue as little as possible [6, 9, 35].

As described above, as far as IMRT is concerned, the treatment planning takes into account the inverse planning, in which the clinician defines, at the beginning of planning, the tumour and OARs, the beam configuration and the radiation dose that he wants to deliver to the target tissue with an optimisation computer program. On the other hand, the 3D-CRT uses the forward planning, in which dose distributions in the relevant target volumes and OARs are evaluated at the end of the planning process, as also described above [36].

Once the plan is conceived, the patient-specific QA is performed to ensure its accuracy and approval. After approval, the data is transferred to the treatment machine.

State of the Art: Patient-specific QA of IMRT

The next and last step of pre-treatment is quality assurance. It is one of the three very important requirements in a radiotherapy treatment, which are an accurate delivery system, a treatment planning system and, finally, the QA process. The latter guarantees that the prescribed treatment is accurate and according to the planned and clinically acceptable error tolerances. The complexity of the dose delivery and the resulting distributions require the performance of measurements, in order to verify the accuracy of the calculated dose distributions. Looking back in time, the QA has been an integral part in clinical trials since 1972, while being part of the Radiation Oncology Committee for the original Cancer and Leukemia Group B [37]. However, when IMRT was proposed and implemented in many centres, a new clinical routine had to be adopted due to some particularities of the IMRT: complexity, need of higher accuracy, great potential for delivery errors and higher dose delivered [12]. The importance of carrying out a QA process to the IMRT equipment and to the patient's treatment planning has been discussed and emphasised in many papers, reports and books (e.g. report of the Intensity Modulated Radiation Therapy Collaborative Working Group (IMRTCWG) [38], Ezzell *et al.* [39], and others that will be mentioned further) [40]. On the one hand, this change on radiotherapy resulted from the emergence of new and better technology, devices, software and treatment techniques, modifying and improving the way processes occur; on the other, a very important goal is continually kept: reduced dose delivered to the patient.

There are two types of QA methods, machine QA and patient-specific QA. The first one is responsible for checking and assessing the machine characteristics and its performance, detecting mechanical errors and verifying if some parameters are on the baseline values. The second one, the patient-specific QA, should find transmission errors and computational dosimetry errors of the treatment planning. This type of QA assures the quality of each patient's treatment, ensuring a correct and accurate dose delivery to the patient and guaranteeing the treatment plan does not deviate from what was planned previously [28, 41]. Patient-specific QA, illustrated in Figure 2.8, can be performed by measuring the dose in a phantom using the patient plan, and comparing what was measured with the dose calculated by TPS. Afterwards, the evaluation of dose distributions is performed.

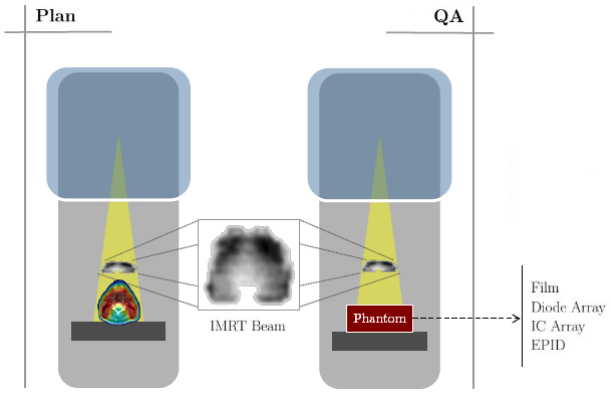

Figure 2.8: Illustration of the specific-patient QA of IMRT process. The process consists of the dose comparison between the plan of the treatment calculated by TPS and the same plan of the treatment measured with a film, diode array, IC array, EPID, among other systems. Adapted from [42].

The practice of IMRT QA is widespread, and there is no a standard and definite way to perform it, which means methods of IMRT QA vary from institution to institution [40, 43]. Nevertheless, there are several reports and papers which describe all this process in detail, reporting some briefings, rules and parameters to take into account and giving information about several devices used (e.g. Fraass *et al.* [44], report of the Intensity Modulated Radiation Therapy Collaborative Working Group [38], Ezzlle *et al.* [39], Low [45], Galvien *et al.* [46], Nelms *et al.* [43], report of ESTRO Booklet No. 9 [40], Low *et al.* [46]). For instance, Nelms *et al.* [43] carried out a survey about methods of IMRT QA in some institutions, even though only with users of an electronic two-dimensional diode array device. ESTRO Booklet No. 9 [40] shows examples of the way patient-specific IMRT QA is performed in many institutions where it is adopted.

Several ways of performing patient-specific IMRT QA have been suggested, for example, using ion chamber, films, diode arrays, electronic portal imaging device (EPID) and gel dosimetry to measure dose distributions in a phantom [41, 47]. These devices and methods are used as dosimeters and they have to be as accurate as possible in order to measure the dose distribution that can be compared with the calculations. This way, it is possible to detect and mitigate errors in TPS and in the delivery system, as previously said.

Ion chambers have been used from the beginning of IMRT dosimetry due to their excellent stability, linear response to absorbed dose and small directional dependence. They are waterproof and they have cylindrical symmetry. Ion chambers perform a point-dose measurement, verifying absolute dose distribution in a certain dose point [47]. However, they do not allow to obtain absolute dose distribution in all the plan that provides more information about it than just analysing a point-dose of the evaluated plan. Taking this factor into account, 2D ion chamber arrays were developed and they are less time-consuming, allowing fast analysis and immediate readout of dose distributions. A drawback is the separation between the ion chambers on the array, requiring interpolations of readings which limit the spatial resolution [28, 31].

MatriXX (Scanditronix Wellhofer, Germany) is an example of an ion chamber array based on a pixel-segment ionisation chamber (PXC) designed by Amerio *et al.* [48] and tested by Stasi *et al.* [49]. This array consists of 1020 cylindrical ion chambers, arranged in a 32×32 matrix, with a volume of 0.08 cm^3 and with a distance of 7.62 mm between chamber centres. It also has an active area of 24.4×24.4 cm^2. This device is adequate for planar dose measurements of absolute dose, and it is an device with both sufficiently high accuracy and speed for measurements in radiotherapy [27, 50].

Seven29™ (PTW, Freiburg, Germany) is another example of a two dimensional detector array described by Poppe *et al.* [51] and evaluated by Spezi *et al.* [52]. This device is the version 2 of 2D-ARRAY reported by Poppe *et al.* [51]. Version 1 has 256 (air-filled) ion chambers arranged in a 16×16 matrix covering an area of $\times$ 27 cm^2 and version 2 (Seven29™) has 729 (air-filled) ion chambers arranged in a 27×27 matrix also covering an area of 27×27 cm^2, both arrayed in a square pattern. The ion chambers from Seven29™ are equally spaced 1 cm centre to centre and each ion chamber has a size of $0.5 \times 0.5 \times 0.5$ cm^3, surrounded by a material called polymethylmethacrylate (PMMA). This detector is easy to use for daily IMRT QA, measuring the absolute dose. It reduces the workload when compared with conventional techniques and the dose distributions are acquired, shown and potentially processed quickly. For these reasons Seven29TM is

a dosimetrically accurate and sensitive tool for IMRT QA [47, 53]. However, it fails in the verification of gantry, collimator and couch angles and still do not correlate the measured composite dose distribution to the patient's anatomy [54].

Diode arrays are diodes arranged in a matrix (array) and they have also been one of the devices used for patient-specific IMRT QA, because they are more sensitive than ion chambers, they are easy to use and they provide QA results while measurements are being performed [55]. MapCHECK® (Sun Nuclear Corporation, Melbourne, FL) is one of the most popular commercially available arrays. It was first described as a prototype by Jursinic and Nelms [56] and evaluated by Létorneou *et al.* [57, 27]. This device contains 445 n-type diodes distributed over an area of 22 $\times$ 22 cm^2. The 10 $\times$ 10 cm^2 central area contains 221 diodes with 7 mm spacing, and the outer region surrounding the central grid contains 224 diodes with 14 mm spacing [27, 57]. This device can measure the absolute and relative dose distributions on a phantom, simplifying and reducing the IMRT QA workload, because it can eliminate some of the steps involved, for instance, in film dosimetry [55, 57].

Films are traditionally the device used since the beginning of IMRT dosimetry, evaluated for this process by Bucciolini *et al.* [58] and Ju *et al.* [59, 50]. Unlike ion chamber, film can be used to measure relative dose distribution in a plan that will be used to verify the treatment plan in a phantom [28]. There are two types of film used in patient-specific IMRT QA: radiographic and radiochromic film. The first one consists of a clear film base coated in an emulsion containing silver halide and it is not water-equivalent. There are several commercial radiographic films including Agfa, Fuji, Kodak, and Konica. Unlike radiographic film, the radiochromic film is nearly tissue-equivalent and EBT-2 is the only film commercially available with appropriate sensitivity [47]. The selection of the right film to use should be done based on the expected maximum dose to measure. Both types of films have high and good resolution. However, performing QA with film is a time-consuming process due to its calibration, scanning process, phantom setup and film analysis [60].

The two-dimensional detector arrays, as ion chamber and diodes arrays detectors, have gradually replaced film measurements due to their ease of use; simple setup; immediate achievement of the results after dose delivery; less time consumption; and their potential for increased efficiency of the measure, on grounds of their capability to provide a large number of dose measurements in a single irradiation per beam. They provide two-dimensional analysis of dose distribution. On the other hand, they can also provide three-dimensional analysis of dose distribution using specific reconstruction software that allows to analyse the dose distribution taking into account the three dimensions, obtaining more dose distribution information. However, they are planar dosimeters, i.e. they contain few detectors and its geometry is not the best for gantry rotation [47]. To overcome this drawback, there are the three-dimensional dosimeters, which make a more complete acquisition of IMRT dose distribution, providing also 2D and 3D dose distribution evaluation.

Delta^4 (ScandiDos AB, Uppsala, Sweden) is an available example of three dimensional detectors. More details about this system can be found in publications by Bedford *et al.* [61], Korreman *et al.* [62] and Sadagopan *et al.* [54], where it is possible to find descriptions and some assessments of this system [41]. This device shows a bi-planar detector geometry, consisting of a cylindrically

shaped PMMA phantom. It is composed by 1069 p-type cylindrical silicone diodes arranged in a rectangular matrix along two orthogonal planes (cross-sectional). The diodes have a volume of 0.04 mm^3 and are spaced 0.5 cm centre to centre in the central area ($6 \times 6\ \mathrm{cm}^2$) and 1 cm in the outer area ($20 \times 20\ \mathrm{cm}^2$) [61, 62, 63]. The detector planes are placed in an acrylic cylindrical phantom with 22 cm of diameter and 40 cm of length [64]. Its orthogonal shape provides full coverage of the cross section of any beam direction while dose measurements are done with the gantry rotating. Nevertheless, the device does not take into account all dose delivery angles, due to its cross shape [64]. IMRT QA, provided by Delta^4, is a complex, laborious and time consuming procedure [54, 61]. However, this detector has the necessary capacity of reproducibility and it is sufficiently accurate and stable to perform efficient patient-specific IMRT QA [54].

ArcCHECK® (Sun Nuclear Corporation, Melbourne, FL) is a competitive device created to resolve the need of rotational IMRT QA, due to its cylindrical shape. It was presented by Létourneau *et al.* [65] and Yan *et al.* [66] as a suited dosimeter for IMRT QA [67]. Thus, this detector is a cylindrical acrylic (water-equivalent) phantom with 1386 diodes. They are arranged on a helical grid to reduce the amount of detector overlap and to obtain more three dimensional view of the measured dose distribution as compared to a 2D array measurement [68][69]. This detector is suitable to accurately measure both relative and absolute doses and it allows measurements at arbitrary gantry angles with sufficient spatial resolution, although it still has low resolution [67]. It is also easy to set up and its performance is a less time consuming process.

The last two detectors described are also considered phantoms, which are constructed using either water or water-equivalent plastic, as acrylic. Water phantoms can be used when the beam is perpendicular to the phantom surface, and where great flexibility in detector positioning is desired. In case of water-equivalent plastic phantoms, they can be used with multiple detectors, as films, ion chamber, and rapid and efficient setup [47]. An example of this phantom Is OCTAVIUS® described by Van Esch et al.[70]. This octagonal polystyrene phantom is used with the ion chamber, described above, Seven29™ [41]. Its octagonal shape is advantageous as it allows easy positioning for measurements in multiple plans [70].

EPID is the promising device, which reliably and accurately measures absolute dose distribution. It has also replaced the traditional dosimetry devices in the clinic for plan verification in some institutes, because they have few measuring points and therefore a low spatial resolution.

van Elmpt *et al.* [71] made a detailed bibliographic review about the use of EPID in dosimetry and its applications, about several types of EPID that appeared since the beginning and about respective evaluated studies. EPID emerged, as a dosimetry device, in the late 1980s/early 1990s at Netherlands Cancer Institute, Amsterdam by Meertens and van Herk [72, 73, 74]. This detector was described as liquid-filled ionisation chamber EPID (Li-Fi EPID or SPLIC EPID) [75] and consisted of a matrix of 256 $\times$ 256 ionization chambers filled with an organic liquid (isooctane) over an area of 32 $\times$ 32 cm^2. It can convert measured dose-rate to absolute dose by recording a continuous readout of the monitor chamber signal of the LINAC during image acquisition, as well as by recording the number of monitor units delivered for the measurement dose image. The scintillation crystal-photodiode detector 'RTIM-AGE' is the second and non-commercial detector developed in the beginning of the 1990s at the Royal Marsden Hospital in London by Morton *et al.* [76] and was used for dose measurements. The following detector, Camera-based

EPID, consists of a fluorescent phosphor-screen with a metal plate on the top that converts high-energy photons into visible photons. The most common type of EPID available nowadays is the amorphous-silicon EPID (a-Si EPID) or flat-panel imager, described by Antonuk *et al.* [77, 78] in 1995. The detector consists of an X-ray converter, light detector and an electronic acquisition system for receiving and processing the resulting digital image. When the a-Si EPID emerged, the interest in EPID dosimetry increased especially due to its favourable characteristics, such as fast acquisition, ease in measurements at different angles, high resolution and contrast, digital format and analysis tools and potential for *in vivo* measurements and 3D dose verification. It also allows the measurements for any gantry angle, due to the fact that it is linked to the LINAC, following the gantry in each positon [71].

Finally, Gel-dosimetry, still in the development stage, is the method which guarantees high resolution, accuracy and precision. Two types of gels, polyacrylamide (PAG) and Fricke gels are used together with methods of dose-readout techniques, as magnetic resonance (MR) imaging and optical-computed-tomography (optical-CT). The first one consists of bis, acrylamide, nitrogen, and gelatine. It uses the mechanism of radiation-induced polymerisation of monomers, where small monomer molecules join together under the influence of the dose. The second one is first described by Gore *et al.* [79]. This gel is easy to produce and reliable. However, it has a drawback related with the fact that the radiation-induced ferric ions diffuse through the gel matrix, leading to the degradation and eventual loss of the recorded dose distribution [27, 45]. Gel-dosimetry allow to do 3D dose reconstruction, determining the dose distribution in all volume, obtaining a complete dose distribution information.

Several studies (e.g. Chandraraj *et al.* [80], Defoor *et al.* [64], Feygelman *et al.* [63], Fredh *et al.* [41], Hussein *et al.* [81], Li *et al.* [52]) were developed in order to compare many of the systems described above and test their capacity to accurately carry out specific-patient IMRT QA. For instance Fredh *et al.* [41] compared four measuring systems (Delta4, OCTAVIUS, COMPASS (MatriXX) and EpiqaTM (Epid)) intentionally introducing errors in the clinical plans. The systems are able to detect errors. Delta4 and Epiqa were more effective on the detection than the other two systems. Finally Feygelman *et al.* [63] compared ArcCHECK with Delta4 and also proved their ability to carried out QA IMRT.

After dose distribution acquisition via a detector and phantom, the dosimetric analysis must be carried out, where the calculated dose distribution is compared to the measured dose distribution. This analysis is done using one of these methods: dose difference, distance-to-agreement (DTA), gamma analysis and dose volume histogram.

The first one is a straightforward and intuitive method and consists of calculation point by point in dose domain of the absolute or relative difference of two (calculated and measured) dose distributions [82]. The second one was developed by Van Dyk *et al.* [83] and applied in a software tool to compare two-dimensional dose distribution by Harms *et al.* [84]. DTA measures the closest distance from a point in reference dose distribution to a point in evaluated dose distribution [82, 85]. Gamma analysis is the most common method used for IMRT two-dimensional dose distribution comparison, because it is very difficult to compare it via dose difference in low gradient region and via DTA in high gradient region. This happens due to the unsystematic presence of low and high gradient regions. Gamma analysis incorporates both dose difference and

DTA methods. It is, therefore, more sensitivity in these regions, faster and more accurate too, and produces a quantitative test based on both dose and spatial criteria [86]. Low *et al.* [87, 88] developed this method, which provides a numerical quality index, gamma value (γ), that serves as a measure of disagreement in the regions that fail the acceptance criteria and indicates the calculation quality in regions that pass.

Although gamma analysis is the most common tool used in dose distribution comparison, several recent studies demonstrate problems with important clinical implications when performing patient-specific QA based on the gamma index method. Nelms, Zhen and Tomé [89, 90] started to study the sensitivity and specificity of the gamma analysis. Their studies, as well as others, reached the following conclusions: lack of correlation between patient dose errors and gamma passing rates (%GP) for IMRT QA, which means, gamma analysis can hide the existence of errors in clinically relevant regions, taking into account points in clinically irrelevant regions [89]; lack of correlation between global gamma indices and clinical DVH metrics [90, 91, 92]; gamma method inability to guarantee the absence of clinically significant dose deviations [93, 94, 95]; and, finally, existence of poor accuracy, sensitivity and specificity of the standard gamma algorithm [96, 97].

Dose-Volume Histogram is the promising method to overtake the lacks that result from the use of gamma analysis, the former being a significant and powerful tool in treatment approval with three-dimensional dose distributions (3D). DVH was introduced by Drzymala *et al.* [98] and consists of a 2D graph, which summarises data of 3D dose distribution per volume for the patient's specific organ, providing some statistical information as well. 3DVH® (Sun Nuclear Corporation, Melbourne, FL) is an example of a pre-treatment software that creates DVH for each organ of a patient plan. It uses data from MapCHECK and ArcCHECK QA measurements to estimate the 3D dose delivered to a patient. Thus, it allows to compare delivered and planned patient DVH and also mean, minimum and maximum dose of regions of interest (ROI), using a computational algorithm named Planned Dose Perturbation (PDP™)[90, 99].

QA Measurements

- **ArcCHECK**

ArcCHECK (Sun Nuclear Corporation, Melbourne, FL) has been developed for routine IMRT QA, specifically for VMAT, due to its cylindrical shape. ArcCHECK is a cylindrical water-equivalent phantom with a three-dimensional array of diode detectors, arranged in a helical geometry, which provides consistent and highly sensitive measurements for all gantry angles, as visible in Figure 2.9. It can make both relative and absolute dose measurements in an efficient and accurate way. It also allows to obtain the two-dimensional dose distribution reconstruction as well as the three-dimensional dose distribution reconstruction with auxiliary software. Its interface is SNC Patient software, which is used to analyses the data measured on the QA. 3DVH is the software used to perform the 3D dose distribution analysis [67].

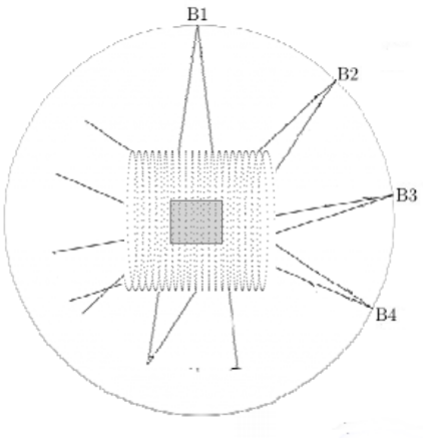

Figure 2.9: Representation of the dose distribution measurements using ArcCHECK for four gantry angles and its diodes helical matrix. Adapted from [100].

- **EPID Dosimetry**

EPID is the most recent and efficient device to measure dose distribution used in patient QA. It was originally designed for verification of patient position by analysing the portal image obtained. However, another capacity was put into practice: the ability to obtain dosimetric information for pre-treatment verification and *in vivo* dosimetry, due to the fact that EPID images contain dose information [71]. Thus, EPID converts portal dose image into dose distribution in a patient/phantom via a back-projection algorithm. The image is obtained via the generation of electrons by an incident MV photon beam, which means, pixel values in the EPID images are related with absolute dose values in the phantom or patient [5, 47, 60]. Thereby, back-projection algorithm, described by Wendling *et al.* [5], allows to compare the calculated dose distribution with the delivered dose distribution in the patient or phantom, enabling the two-dimensional dose reconstruction in the patient from portal images, and, as required, providing information for three-dimensional dose reconstruction [5]. EPID is attached to the LINAC and follows all the gantry rotation around the patient.

The amorphous silicon EPID is the device used mostly for EPID dosimetry. It consists of an X-ray converter, the light detector and the matrix of amorphous silicon detectors to receive and process the resulting digital image, as presented in Figure 2.10. The X-ray converter consists of a metal plate of copper placed on top of a detector scintillating phosphor screen that is typically made of terbium-doped gadolinium oxysulfide ($Gd_2O_2S:Tb$) or Cesium-iodide (CsI). The first layer, which acts as a build-up, produces Compton electrons from incident photons and absorbs scattered radiation that reduces the image contrast; and the second layer converts the photons into optical photons (light). This is detected by a matrix of pixels, being each pixel composed of photodiodes and thin film transistors (TFT). The photodiode absorbs visible light and the TFT's act like a switch to control the readout of the signal. In the end an image frame is obtained [101, 102]. In terms of dosimetric capabilities, the light signal measured at each pixel can be related to the dose distribution inside the phantom, which means, each pixel value in the portal image obtained by EPID measurements is related to dose values on the phantom. In other words, the measured grayscale portal image is converted into a portal dose image. From this portal dose image the energy fluence - the total energy of the photons passing through an area that exit the

LINAC - is extracted and the dose on the phantom/patient is calculated from here [4, 103].

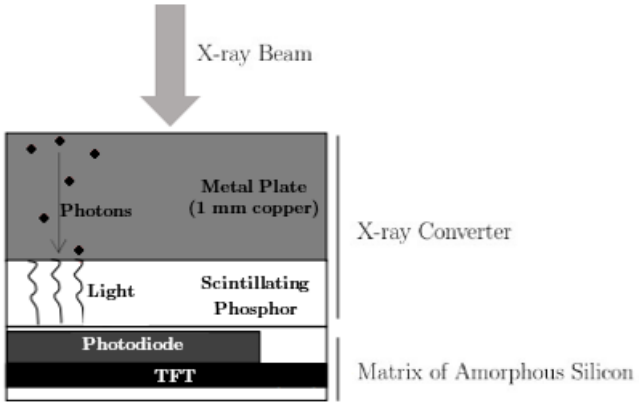

Figure 2.10: Illustration of EPID constituents and X-ray conversion. Adapted from 101.

In EPID dosimetry there are some factors to take into account: verification procedure can be classified according to whether or not they are performed during treatment, which means *in vivo* (with the patient) or outside of treatment (without patient). Dosimetry methods can be grouped according to whether or not beams have passed through an attenuation medium between the source and the detector (non-transmission dosimetry) or if the dose is reconstructed inside a phantom or a patient (transmission dosimetry) [71]. Also, it is important to take into account if the measurements and calculations are done and compared at the EPID level (forward-projection) or if the measurements data is projected into the patient/phantom, i.e. it is possible to reconstruct the dose in the patient/phantom level (back-projection). The last one can be used for *in vivo* dosimetry [5]. These factors are presented in Figure 2.11.

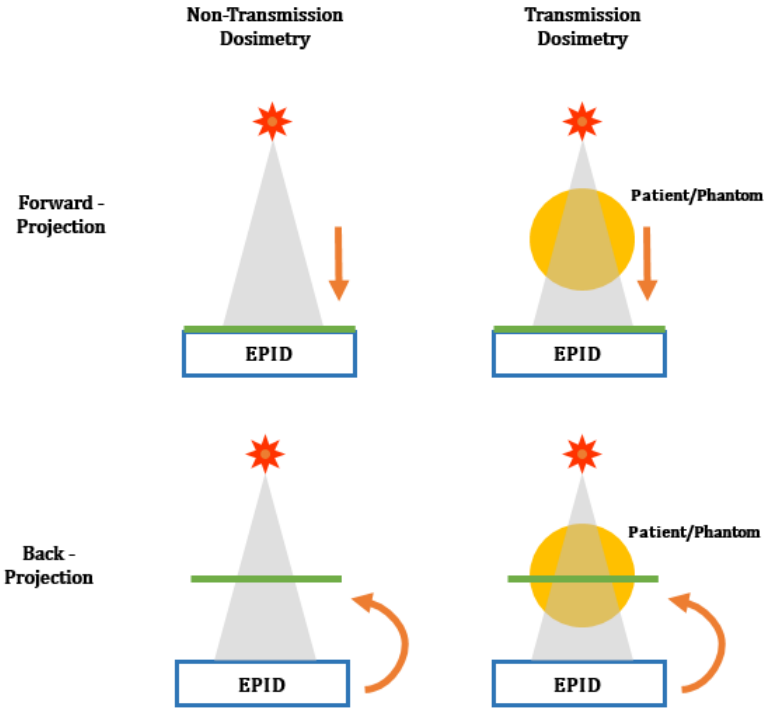

Figure 2.11: Two approaches of EPID Dosimetry, where in each it is possible to obtain the dose distribution at the EPID level (forward-projection) or at the patient/phantom level (back-projection). Adapted from [71]

Dose Distribution Evaluation Methods

After measurements it is necessary to decide if the plan is acceptable for the treatment, wherein the dose measured and calculated distributions are compared using quantitative and efficient methods. There are four important dose evaluation methods: Dose Difference, Distance-to-Agreement, Gamma Analysis and Dose-Volume Histogram [85].

- **Dose Difference**

As previously described, dose difference is a method of dose distribution evaluation and it is the most straightforward and intuitive method used. It consists in a point-by-point calculation of the difference between two dose distributions, the reference dose (D_r) and evaluated dose (D_e), in dose domain. This method allows to know how much two dose distributions disagree [82, 85].

The dose difference, ΔD, can be used to define an acceptance criterion, determining if the plan passes or fails. The most used common dose difference criterion is ΔD =3% of the maximum dose [88, 104]. This criterion can be used in low gradient regions, but it is inadequate in high gradient regions, because a small alignment error in the last mentioned region can translate into a big dose error, which means this method is not suited for this region [87, 105].

- **Distance-to-Agreement**

Distance-to-Agreement is another dose distribution evaluation tool that is based on the local dose gradient. It is described by the spatial distance between a point in the reference distribution and the closest point in the evaluated distribution that shows the same dose. DTA at a position ($\vec{r}_r$) is presented in the next equation 2.2:

$$DTA(\vec{r}_r) = min\{|\vec{r}_e - \vec{r}_r|\},\ \forall\{\vec{r}_e\},\ where\ D_e(\vec{r}_e) = D_r(\vec{r}_r), \tag{2.1}$$

$\vec{r}_r$ is the reference position and $\vec{r}_e$ is the evaluation position [85, 104].

The distance-to-agreement criterion, Δd, is the spatial tolerance and is also assumed as an acceptance criterion, determining if each point passes or fails this dose distribution evaluation test. The most common distance-do-agreement criterion is Δd =3 mm. This criterion does not work on low gradient region, but in high gradient region where it is more sensitive [85, 104, 105].

- **Gamma Analysis**

Gamma analysis is the most used dose method to compare two dose distributions, taking into account both dose and spatial differences between them. It provides a numerical quality index, gamma value (γ), that works as a measure of disagreement in the regions that fail the acceptance criteria and indicates the calculation quality in regions that pass. Thus, it represents the minimum multidimensional distance between the reference and the evaluated points in a space composed of both dose and physical distance coordinates. It is calculated based on the normalised percent dose difference (%Diff) and distance to agreement (DTA). The analysis procedure starts by normalising doses and spatial coordinates. The two dose distributions to be compared are assigned as reference ($D_r(\vec{r}_r)$) and evaluated ($D_e(\vec{r}_e)$) dose distributions. For each

point in the reference distribution, the normalised distance to each point in the evaluated distribution is measured, where the distance includes both normalised spatial and dose values. γ value is the closest approach (minimum distance) of the reference distribution, being unity when the closest approach of the reference distribution is in the unit sphere. The unit sphere indicates the region where the comparison test passes. Thus, if the reference distribution is inside the unit sphere, the γ test passes, otherwise it fails [47, 105].

For the vector position of the evaluated $(\vec{r}_e)$ and reference $(\vec{r}_r)$ points the γ is governed by the following two equations:

$$\gamma(\vec{r}_r) = min\{\Gamma(\vec{r}_e, \vec{r}_r)\}, \ \forall\{\vec{r}_e\}, \tag{2.2}$$

where

$$\Gamma(\vec{r}_e, \vec{r}_r) = \sqrt{\frac{r^2(\vec{r}_e, \vec{r}_r)}{(\Delta d)^2} + \frac{\delta^2(\vec{r}_e, \vec{r}_r)}{(\Delta D)^2}}, \tag{2.3}$$

where $r(\vec{r}_e, \vec{r}_r) = |\vec{r}_e - \vec{r}_r|$, is the spatial distance between the evaluated and the reference positions, $\delta(\vec{r}_e, \vec{r}_r) = D_e(\vec{r}_e) - D_r(\vec{r}_r)$, is the dose difference between the two positions analysed, ΔD is the acceptance dose difference criterion and Δd is the acceptance DTA criterion.

When

- $\gamma(\vec{r}_r) \leq 1$, the test passes;
- $\gamma(\vec{r}_r) > 1$, the test fails.

Figure 2.12 shows a schematic representation of the gamma analysis tool in 2D, denoted by an ellipse.

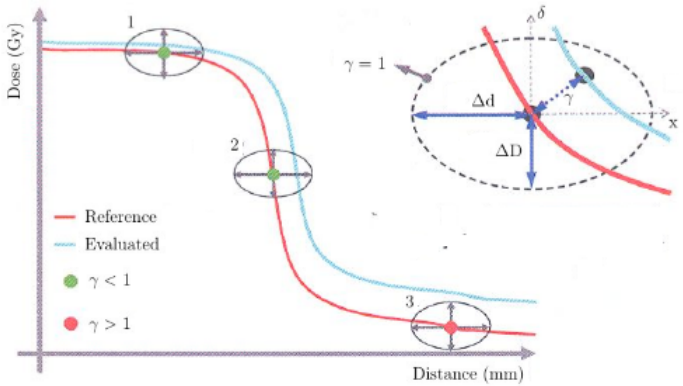

Figure 2.12: Graphic explication of the gamma method. The difference of reference data and the evaluated data are presented in a dose as function of distance graph. The gamma value limits are presented, being possible to see the dose (y axis) and distance difference (x axis), observing if these are large or in the limits imposed (ΔD, Δd respectively), which means, if the difference between both data is within the ellipse, the test passes, and if it is outside of the ellipse, the test fails. Adapted from [106].

There are three important parameters to take into account on gamma analysis: %Diff, DTA (already described) and dose threshold. This consists of the percentage value that rejects the dose points below the dose threshold chosen of the planned maximum dose. Finding the best value

for the three parameters is a somewhat complicated task: there has been no agreement as to the best values for the criteria [55]. This can also be a drawback of the method that can affect the analysis, in addition to the others previously described. However, some previous studies (report of the AAPM Task Group 119 [107], Both *et al.* [55] and Basran and Woo [108]) assert that 3% for %Diff and 3 mm for DTA are the most common criteria at 10% for dose threshold value and with an accepting threshold of gamma passing of 90% [55, 89].

- **Dose-Volume Histogram**

Dose-Volume Histogram is the promising tool to be implemented in quality assurance, being already a powerful tool used on planning treatment. It quantifies and summarises in a 2D graph the data of 3D dose distribution per volume for the patient's specific organ, providing some statistical information as well. It is very useful for assessing tumour volume coverage and also the dose delivered to healthy tissue surrounding the target, revealing the presence of hot spots in it [98, 109]. There are two types of DVH (Figure 2.13): differential (or direct) and cumulative (or integral) DVHs [12, 19]. The DVH is created by portioning the volume of interest into volume elements, called voxels, which are small enough in order to avoid dose variations on the voxel. The first type of DVH, differential DVH, is a histogram and represents the sum of the number of voxels with a particular dose, resulting in a plot of the absolute volume or the percentage of the total organ volume as a function of dose. The second type of DVH, cumulative DVH, is more popular than the other type and also shows the percentage or the absolute volume as a function of dose of a specific organ. However, herein is represented the volumes of the targets that receive at least the dose indicated in the differential DVH. In case of percentage volume as a function of dose, it starts at 100% of the volume for 0 Gy, since all the volume does not receive no dose [12, 19].

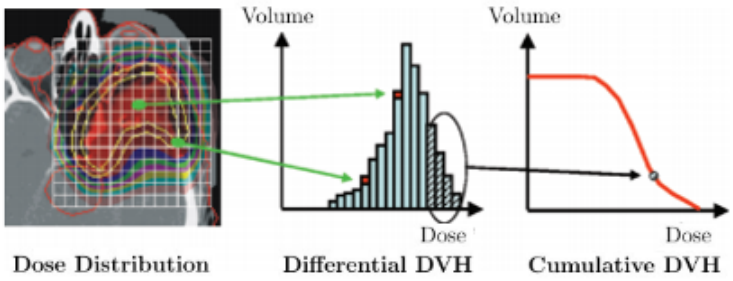

Figure 2.13: Illustration of the two types of DVH and how they are constructed. The two selected voxels in Dose Distribution (image on the left) are correspondent to a lower dose (the one on the edge) and a high dose (the one on the centre). Afterwards, they are represented in the Differential DVH (image in the centre) in a low and high dose bin according to the dose received by each voxel. In the Cumulative DVH (image on the right), the total volume of the structure that receives at least the given dose in the dose bin indicated in the differential DVH is represented [19].

There are some important parameters that can be derived directly from DVH and that agree with the recommendations from the ICRU Report 83 [110]:

- Dmin: the minimum absorbed dose by the target volume;
- Dmean: the mean absorbed dose by the target volume;
- Dmax: the maximum absorbed dose by the target volume;

- D98%: the near-minimum dose, i.e. the minimum absorbed dose that covers 98% of the volume;
- D50%: the median dose, i.e. the absorbed dose received by 50% of the volume;
- D2%: the near-maximum dose, i.e. the maximum absorbed dose in the target volume or minimum absorbed dose that covers 2% of the volume;
- and other points specific of some organs.

2.3.3 Treatment Delivery

Prior to each treatment, it is necessary that the patient is set up in the same position as he was for the planning scan to assure the radiation is delivered to the correct location. Several hardware and software are used in the treatment. The most common involve a linear accelerator (LINAC) with rotating gantry and moving MLCs.

As previously referred (subsection 2.1.2), the treatment is often performed in a fractioned schedule, where the total dose is delivered with a small (1.8 to 2 Gy) dose per fraction five times a week. Typically, the treatment lasts from 5 to 8 weeks [12, 19].

2.3.4 Clinical Monitoring

During the treatment and after, the patients are submitted to monitoring consultations. It allows the doctor to see the results of the treatment effects on the patient, in order to control the side effects and the tumour stage.

CHAPTER 3

Methods

Taking into account all the limitations of the gamma analysis described in the last chapter (subsubsection 2.3.2, it is necessary to find a better option to replace it. DVH seems to be the best option for the IMRT QA, instead of gamma analysis.

This study intends to show the accuracy and relevant information provided by the DVH analysis in the IMRT QA, testing a commercial software, 3DVH, intended to replace the gamma analysis used in dose evaluation, which is the method carried out in Champalimaud Foundation. The capacity of EPID dosimetry to calculate DVHs was also tested.

This chapter presents the main procedures and tools used in order to fulfil the goal of the study.

3.1 Overview of Dose Distributions Measurements and Analysis

This study, described in Figure 3.1, was performed using square fields plans and patient plans. The patient plans, planned previously in Monaco® (v.5.00.04, Elekta AB, Stockholm, Sweden), were irradiated with IMRT and VMAT using 6 MV and 10 MV photon beam and the square fields plans were irradiated with 6MV photon beams. All was measured using the linear accelerator of Elekta Synergy® LINAC (Elekta AB, Stockholm, Sweden) with 80 leaf MLC. The measurements were performed with the iViewGT™ EPID (Elekta AB, Stockholm, Sweden), attached to the LINAC, and ArcCHECK® (Model 1220, Sun Nuclear, Melbourne, FL), which is the device actually used for patient QA in Champalimaud Foundation. The dose distribution analysis was performed using 3DVH® (v.3.3, SunNuclear, Melbourne, FL), of ArcCHECK, and an in-house developed program, pdDVH, of EPID. They provide a 3D reconstruction of the dose distribution of the patient, calculating DVHs of each organ. The gamma analysis was performed by using the software specific for EPID and ArcCHECK, pdapp (v.R1.0 C003, NKI-AVL, Amsterdam, ND) and SNC Patient software (v.6.2.3, SunNuclear, Melbourne, FL) respectively. MLC and MU errors were introduced in the square field and patient plans to test the performance and accuracy of the systems, using an in-house developed program.

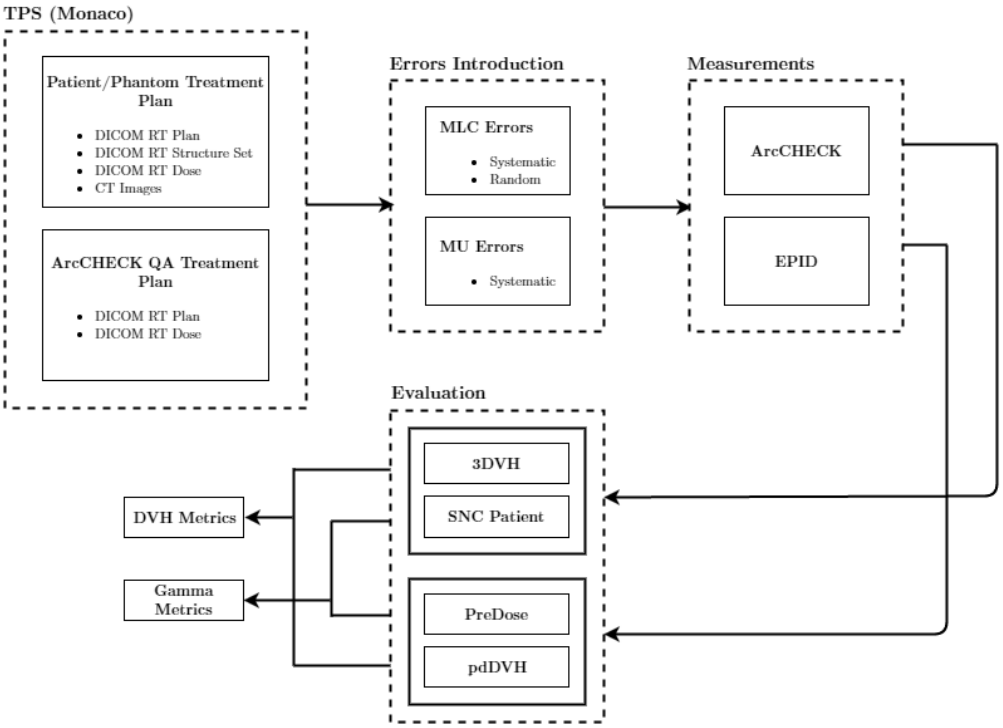

Figure 3.1: Schematic of the study workflow.

3.2 Square Fields tests

The tests using square fields were performed to evaluate if the dose distribution given by the programs is correct and also to better understand the errors interference when they are introduced in the plans. These tests were performed using a slab phantom of twenty slabs placed one over the other. This phantom is the SP34 model of slab phantom from Iba Dosimetry® (Schwarzenbuck, Germany). In this case, it consists of a set of twenty 10 mm thick and 30 $\times$ 30 $\times$ 30 cm^3 square-shaped slabs. The material composition is water equivalent with approximately 98% of white polystyrene, type RW3 and 2% of titanium oxide (TiO_2), and its density is 1.045 cm^3.

Three plans of a slab phantom were planned in Monaco, the treatment planning system associated to Elekta that uses the Monte Carlo and the Collapsed Cone algorithms to accurately perform the treatment planning. Each one contains three structures: a PTV, a cube and a cylinder. The PTV, a 10 $\times$ 10 $\times$ 10 cm^3 cube, intercepts the 6 $\times$ 6 $\times$ 6 cm^3 cube at point 1.5 cm of the latter. The PTV also intercepts the cylinder at point 1.5 cm of the latter. The cylinder presents a diameter and a height of 6 cm. Three plans were created: the first one (Figure 3.2 (a)) shows only one field that will be irradiated with the gantry at 0°, the anterior-posterior (AP) field; the second one (Figure 3.2 (b)) shows two fields at 0°, the anterior-posterior (AP) field, and 180°, the posterior-anterior (PA) field; and the last one (Figure 3.2 (c)) presents four fields at 0°, the anteroposterior field, 180°, the posterior-anterior (PA) field, 270°, the lateral right (LR) field, and 90°, the lateral left (LL) field. All the fields were created in order to encompass the PTV and they are conformal fields, which means, there is no dose modulation during treatment delivery. The structures and fields sizes were generated automatically by the Monaco, because it uses the inverse planning, described in the last chapter (subsection 2.2.2). Each plan was irradiated with

6 MV photon beam from Synergy LINAC and was delivered on the slab phantom. All the plan parameters are shown in Table 3.1.

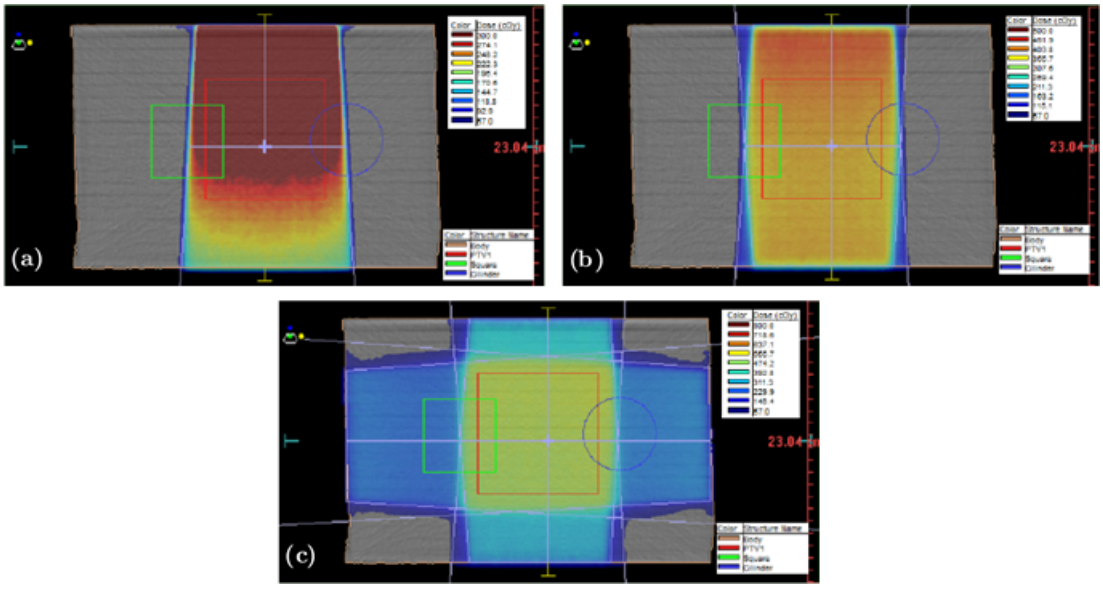

Figure 3.2: Representation of the plans with specific fields and structures created in the slab phantom at the transverse plan by the Monaco. On the left, (a) shows the first plan with just one field and the three structures created. The green one is the cube, the red one is the PTV and the blue one is the cylinder. On the right, (b) shows the second plan with two fields and also the three structures created and described previously. And on the centred, (c) shows the third plan with four fields and the three structures created.

Table 3.1: Characteristics of the three plans created for the patient ZZZ1 of a slab phantom.

Patients	Plan	Energy (MV)	Fields	Fraction Dose (Gy)	Monitor Units
ZZZ1 (AP)	Slab Phantom	6	1	3.44	412.8
ZZZ1 (APPA)	Slab Phantom	6	2	3.96	462.3
ZZZ1 (BOX)	Slab Phantom	6	4	5.1	656.7

For the planning, a CT of the slab phantom was necessary and previously acquired by the Philips CT system, Brilliance CT Big Bore (meter a Philips). The twenty slabs were placed on the table, one on top of the other, forming the phantom structure to be acquired, as shown in Figure 3.3.

Figure 3.3: Illustration of the CT acquisition of the slab phantom in the CT room.

The measurements with square fields were done with the leaf position and monitor unit errors as a perturbation in the plans. The measurements were performed with both ArcCHECK and EPID. For ArcCHECK measurements, the slab phantom was not used. For the EPID measurements, the slab phantom simulated the patient and was placed on the table, again twenty slabs one on top of the other, as shown in Figure 3.4.

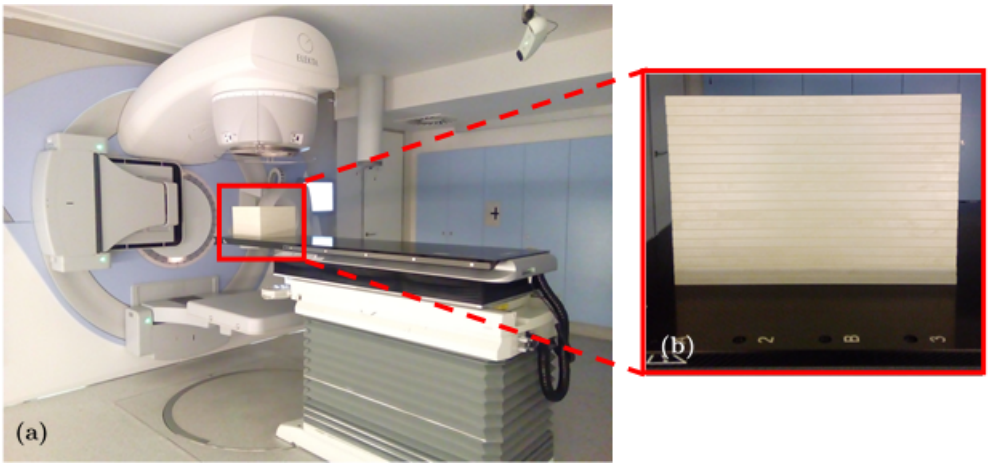

Figure 3.4: Illustration of the setup of the measurements in the slab phantom in the LINAC room (a) and the slab phantom (b).

The slab phantom was placed at the table so that isocentre was in the centre of the phantom. This gave the SSD (Source-Surface Distance) distances, each associated to an angle, as presented in Table 3.2. Each of these distances corresponds to the distance from the source of the treatment machine, the LINAC, to the surface of the phantom.

Table 3.2: SSD parameters applied in the measurements.

Plan	Angle (°)	SSD (cm)
1 field	0	90
2 fields	0	90
2 fields	180	90
4 fields	0	90
4 fields	90	83.5
4 fields	180	90
4 fields	270	86.7

The evaluation programs mentioned above were used to analyse the data, i.e. 3DVH, SNC Patient, PreDose, pdapp and pdDVH.

3.3 Patient Plans Specification

Six cancer patient plans (one prostate and five breast) were used in this study. They were previously planned and optimised using the Monaco treatment planning system and irradiated with IMRT and VMAT dose delivery techniques, using 6 MV and 10 MV photon beam. A list of patients and its respective parameters is shown in Table 3.3. These were the patient samples used

to test the accuracy of the systems used patient-specific QA and the interference of the errors in complex plans. PreDose, SNC Patient and 3DVH were the evaluation programs uses to perform the dose evaluation.

Table 3.3: Characteristics of the six patient plans used in this study.

Patients	Type	Plan	Energy (MV)	Fields	Arcs	#Fractions	Dose (Gy)	MU
ZZZ28210	IMRT	BreastL	6	7	___	15	3.2	576
ZZZ8363	VMAT	BreastR	6	___	2	15	2.7	985
ZZZ1295	VMAT	Prostate	10	___	1	28	2.5	608.8
ZZZ34486	IMRT	BreastR	6	7	___	15	3.2	618
ZZZ29113	IMRT	BreastL	6	7	___	15	3.2	320
ZZZ11603	VMAT	BreastR	6	___	2	15	3.2	919

3.4 Treatment Planning Files

As described above, all the plans were carried out with Monaco. During their planning the necessary files, which contains the information required for the treatment delivery and also for the QA measurements and evaluation, were generated. These files are in a DICOM format (Digital Imaging and Communications in Medicine). DICOM is a way of standardisation for communication of all systems and information necessary to the radiotherapy treatment. In other words, DICOM includes a file format definition and network communication protocol, allowing the transmission between any two entities that are capable of receiving image and patient data in DICOM format [111].

There are four important DICOM files used during this study:

- RT Image, which consists of the relevant images to radiotherapy acquired by CT;
- RT Structure Set, which contains information related to patient anatomy, such as structures, regions, points and volumes of interest for the treatment;
- RT Plan, which contains geometric and dosimetric data of the treatment, such as information about beam angles, collimator, couch and gantry angles;
- RT Dose, which contains dose data generated by the treatment planning system, Monaco.

3.5 Error Introduction

Multi leaf collimator and monitor units errors were introduced in the square fields and patient plans, in order to test the accuracy of the systems on the detection of the errors and how it is shown in gamma analysis and DVHs.

The errors were introduced in the patient plans using an in-house program, Modify RTP. This software uses the RTP file of each plan, where the errors are introduced. The RTP files from each original treatment plans were converted from RT plan DICOM file that was exported from the Monaco treatment planning system. After errors introduction, the files were imported to Monaco and converted into RT Plan files. RTP files contain all needed information for the Elekta LINAC, in order to deliver the treatment efficiently. It includes both basic patient information and treatment information, such as the patient's name and ID number, and the treatment name,

the control points (CP), gantry angles, leaves positions per CP and the number of monitor units, respectively. It organises the treatment information for each field of the plan. Control points define the MLC shapes at a fraction of the delivered monitor units.

3.5.1 Multi Leaf Collimator Errors

Systematic and random leaf position errors were introduced in the patient plans using an in-house program, modifying the RTP files, as described previously. When introducing systematic errors, the position of each leaf was changed systematically, which means the position of all leaves changes at the same value, ±3, ±2, ±1 and ±0.5 mm. The leaves position also changes in a symmetric way, which means the leaves move in opposite directions, either closing or opening. The negative errors correspond to leaves closing. The positive errors correspond to leaves opening. These effects are illustrated in Figure 3.5.

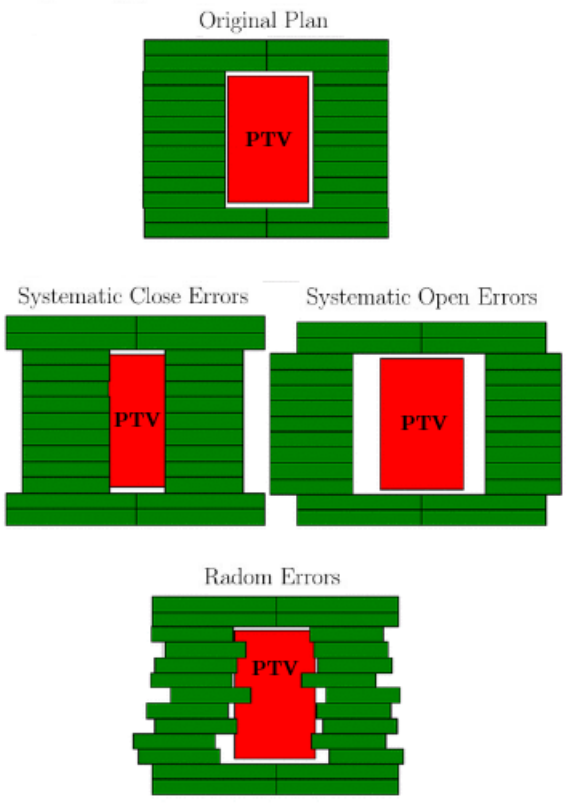

Figure 3.5: Illustration of the effect of the MLC errors on the leaf position of an original plan. Systematic errors, where negative errors cause the closing of the leaves and positive errors the opening of the leaves, and also random errors. Adapted from [112].

The introduction of random errors, with standard deviation varying from 1 to 5 mm, changed the position of each leaf randomly, as its name implies (Figure 3.5).

It is important to pay attention to the minimal leaf separation of the leaves when they are closed in negative systematic errors introduction. This value is defined as 0.6 cm. The program used shows for each field all the control points and for each control point a picture with the changes caused by the error in the leaves position. Figure 3.6 presents the interface used to introduce errors on the plan, with an example of systematic close errors introduced in a patient

plan.

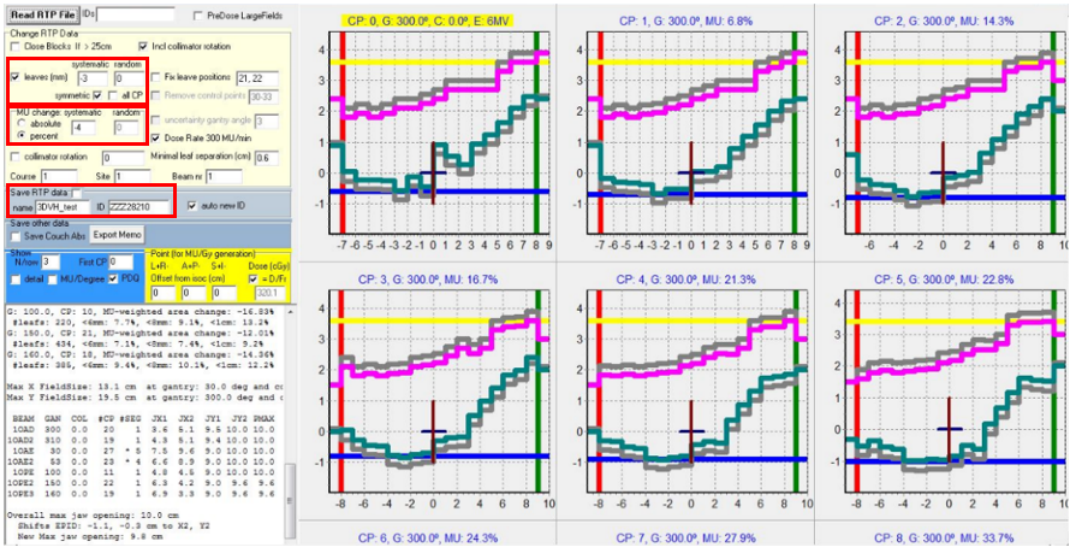

Figure 3.6: Illustration of the error introduction interface. It is an example of the change in the leaves position caused by systematic error of -3 mm, which means the leaves close 3 mm. The new leaf position is represented by the coloured leaves. In the interface it is possible to choose the patient, select the type of error to be introduced (in this case, MLC errors and MU errors are highlighted), see the control points and the plan information, and save the data. The example illustrated is from the error introduction process of a patient test.

A total of 14 modified RTP files were generated for each patient and for each square fields test: the original plan without MLC errors, eight plans with the different systematic errors (±3, ±2, ±1 and ±0.5 mm), and five plans with the different random errors (1, 2, 3, 4, 5 mm). They were imported, for future dose distributions measurements, into MOSAIQ® (v.2.41.01J0, Elekta AB, Stockholm, Sweden), which is the Elekta treatment management software. It contains all the information regarding the radiation oncology program, that is, all patient treatment information, and it is also used for the measurements.

3.5.2 Monitor Unit Errors

Monitor Unit errors were also introduced into the patient plans. MUs are used to measure the output of the machine (LINAC) to deliver accurate dose. By convention, one monitor unit equals 1cGy of absorbed dose in water under specific calibration conditions for the LINAC [113]. MU is a measurement of ionisation occurring in a treatment beam within the treatment head. The errors change the total MUs value defined to each plan with magnitudes of -4%, -2%, 2% and 4%. Systematic errors were the type of error chosen and consist in a constant percentage change in the MUs for each control point within the plan. The same in-house program, Modify RTP, was used. The interface is presented in Figure 3.6. In the end, a total of 5 modified RTP files were created for each patient and for each square fields test: another original plan file without errors and four plans with the different systematic errors. They were also imported to MOSAIQ for the measurements.

3.6 ArcCHECK Measurements

ArcCHECK is the device used daily on Champalimaud Foundation to perform the measurements of the patient-specific QA. After testing some devices, ArcCHECK was the chosen one, because its phantom geometry and its capability to detect the presence of errors are better than those of other devices and because it is easy to work with and set up.

3.6.1 ArcCHECK description

It consists of a 16 kg cylindrical acrylic phantom, which contains an array (21 cm in diameter and length) of 1386 diodes detectors (SunPoint®) with size of $0.8 \times 0.8\ \mathrm{mm}^2$ and arranged in a helical geometry (HeliGrid™) with 1 cm inter-detector spacing. The phantom has a length of 32.28 cm and it has an outer diameter of 26.59 cm and an inner cavity diameter of 15 cm, as shown in Figure 3.7. This cavity centre accommodates a PMMA plug, the CavityPlug™, with 1.183 $\mathrm{g/cm}^3$ of density, in order to eliminate the central cavity inhomogeneity. ArcCHECK also contains two inclinometers, one to measure the angle of rotation of the cylinder and one for angle of coronal angle (tilt); and a temperature sensor to measure the ambient temperature of the detector area [68, 114].

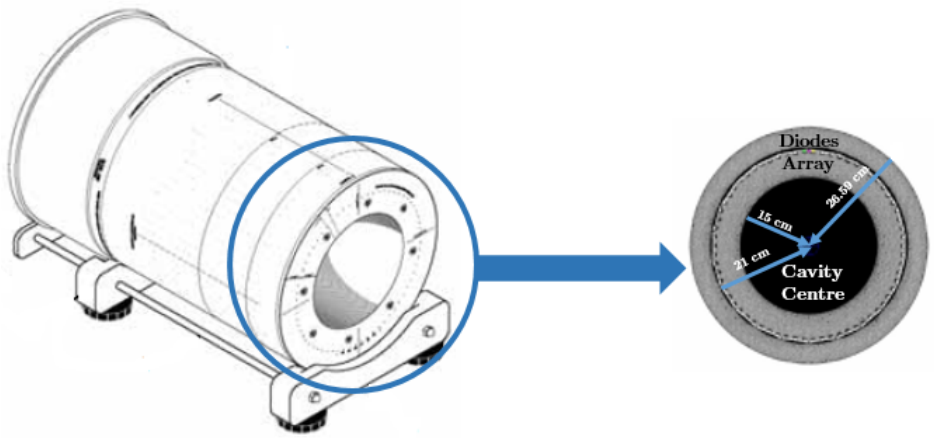

Figure 3.7: Illustration of the ArcCHECK device and its constituent divisions. Adapted from [115].

3.6.2 Calibration and Measurements

The measurements with ArcCHECK were done for both square fields plans and patient plans. This system is easy to set up, which is very important in QA process, in order to save as much time as possible.

There are some procedures to fulfil, when setting this device to the acquisitions. First of all, the ArcCHECK is placed on the table over a support, in the LINAC room. Afterwards, it is necessary to align the axis of the ArcCHECK, in order to position the device correctly. To do this it is necessary to resort to the laser to align the transverse axis, moving the device and the table until laser and device axis align. The coronal axis is aligned with the axis of a light field which is opened. The CavityPlug™ is placed inside the cavity centre and after this the device is connected to the exterior data interface through a cable. The data interface is supplied by a power. Outside the room, the device is connected to the computer that will acquire and save the data, using an

USB cable. Figure 3.8 presents the ArcCHECK cabling and Figure 3.9 presents the device setup in the LINAC room.

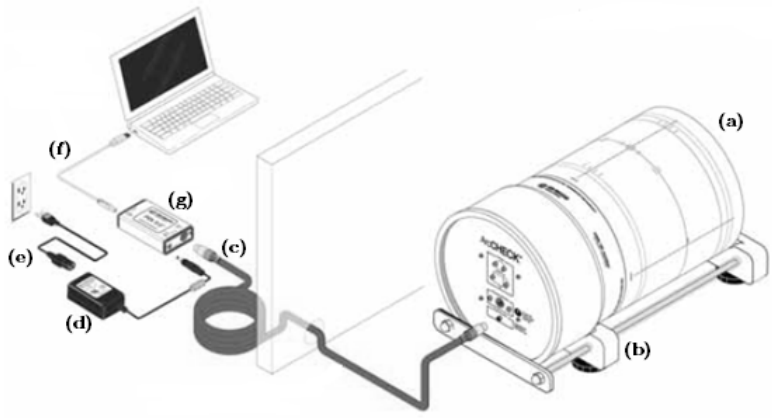

Figure 3.8: Illustration of the AcrCHECK setup. Device cabling and connection between interior and exterior of the LINAC room. (a) corresponds to the ArcCHECK phantom, (b) is the ArcCHECK support, (c) is the cable that connects the device to the exterior, (d) corresponds to the power supply, (e) is the line power cord, (f) is the USB cable that connects the device to the computer and finally (g) corresponds to power/data interface. Adapted from [115].

Every day, before any QA, ArcCHECK calibration is done for the energies 6 MV or/and 10 MV, depending on which is needed for the measurement. This process consists in calibrating the device for absolute dose using the SNC Patient software and allows for the correction of the ArcCHECK measurements for the output variations of the LINAC.

The LINAC system is in service mode, instead of treatment mode, and a 200 MU beam with a 10×10 cm field is defined, which will be delivered to the device at a gantry angle of 0°. In the SNC software the calibration option is selected, in order to do a measurement for each energy. In the end, the known dose value specific to each energy, 249.7 cGY to 6 MV and 261 cGy to 10 MV, is inserted in the SNC software. These values are obtained with the Monaco, creating an 10x10 cm^2 open field with 200 MU. Thus, the dose in the detectors is obtained theoretical.

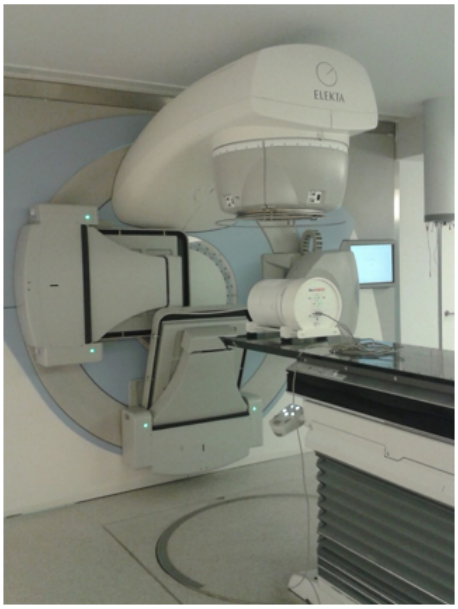

Figure 3.9: Illustration of the ArcCHECK setup in the LINAC room.

The measurements consist of simply selecting the patient and square field plans in the MOSAIQ and, with the LINAC on treatment mode, clicking the button 'beam-on', in order to deliver the dose to the device with gantry rotation. In the ArcCHECK software, it is just necessary to click the button 'start', so that the SNC acquires the dose data, and click the button 'stop' at the end of the measurement to save the data. The dose measurements from each sensor are updated every 50 ms, saving all measurement data as a function of time of absolute dose measurements. Each ArcCHECK measurement consists of the sum of all fields of the plan, which means, it is not done field by field. The data is saved in three file extensions, *.txt that integrates correction factors into the measurement and has the information about total dose in each detector; *.acm, which consists of a multi-frame (movie) file that contains data from each diode for each update; and *.acml, which is also a movie file and a binary format that contains calculated gantry angles and dose information as a function of time for each measurement. The last one is the required file for 3DVH software.

3.6.3 Dose Evaluation

After dose acquisition data, the dose evaluation was performed using the SNC Patient software. This software allows to do a two-dimensional dose analysis from ArcCHECK acquisitions for all gantry angles, as seen in Figure 3.10.

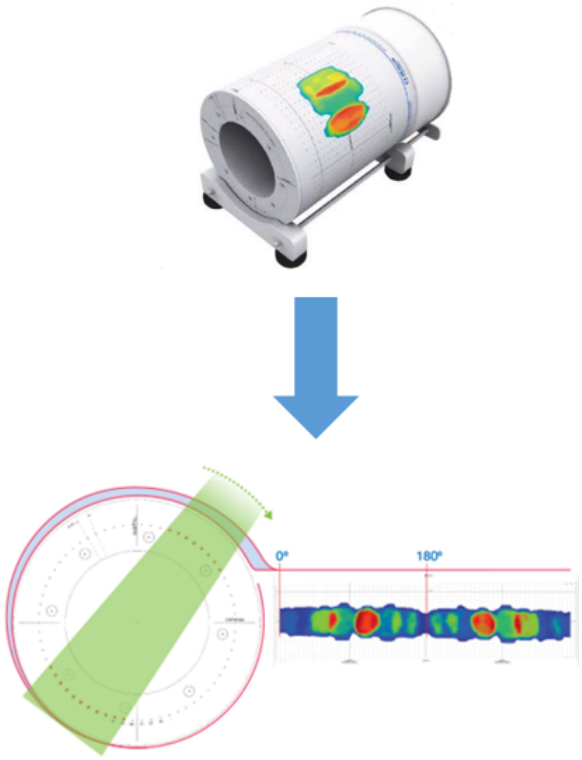

Figure 3.10: Illustration of dose distribution acquisition with ArcCHECK and the correspondent dose map obtained on the SNC Patient software. Adapted from [116].

ArcCHECK displays the unfolded 2D profiles from the cylindrical surface (Figure 3.10), being possible to see dose distribution throughout the entire arc delivery. It was possible to make an absolute dose comparison between the planned dose distribution calculated in the TPS and

the measured dose distribution acquired by the ArcCHECK using gamma analysis, described in the last chapter, at the acceptance criterion 3%/3 mm, which corresponds to 3% dose difference criterion and 3 mm distance-to-agreement criterion and with a threshold of 10%. The gamma analysis was carried out taking into account the number of the diodes which satisfied specific tolerances of dose differences between calculations and measurements relative to the maximum value on the calculated dose map (%Diff) and DTA criterion. Only the diodes with the dose values larger than 10% of the maximum value on the dose map were included in the analysis, because it was the threshold chosen, as presented above; 3% dose difference as a criterion used means that only the values that show 3% or lower of dose difference are taken into account; and 3 mm distance-to-agreement criterion means that the values corresponding to the space between the reference and the measured points with the same dose values are considered if it is 3 mm or lower. These gamma analysis requirements are illustrated in Figure 2.12. The patient plan was considered acceptable if the gamma passing rate was $\geq$ 90%. This method just gives information about dose distribution along the plan, only showing the points/detectors that fail and pass and also 2D gamma passing rate value, but nothing about the dose distribution along each organ volume and dose constraints. The points in the plan that fail are highlighted in red for high dose and in blue for low dose.

This evaluation was performed comparing the measured data, which appears on the left-hand side of the analysis window, as shown in Figure 3.11, with the planned data on the right-hand side of the analysis window. The measured data is the ArcCHECK acquisition and the planned data corresponds to the QA plan calculated in Monaco for the ArcCHECK measurements. It consists in a plan with the same volumes created in the patient plan, but in this case, they were generated in a structure. which was virtually created with the density and length of the ArcCHECK. SunNuclear advised not to use the CT of the device, due to existence of image artefacts caused by the diodes.

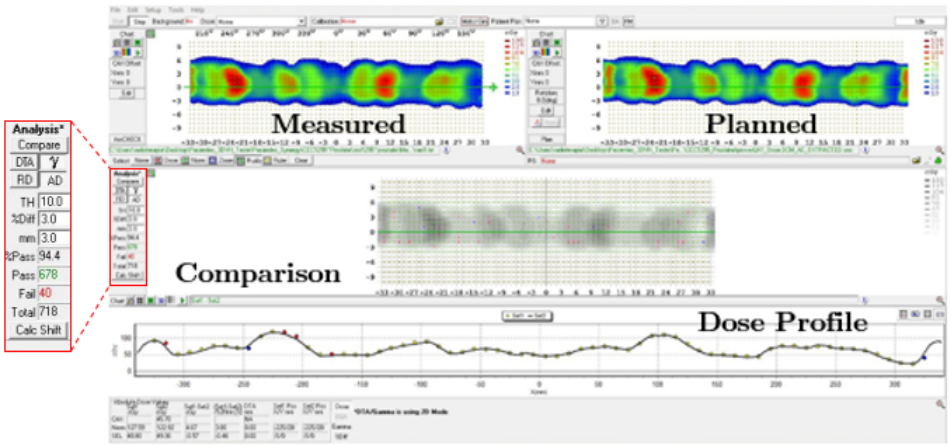

Figure 3.11: Illustration of the ArcCHECK interface. It is possible to see the measured data (left side), the planned data (right side) and the result, compared data, which is the gamma dose map. It is also possible to obtain the dose profile for X and Y axis and dose statistic (above). The highlighted buttons on the left are selected for the gamma analysis for absolute dose option. The example illustrated is from the analysis of a patient test.

3.7 EPID Measurements

3.7.1 EPID Description

The EPID used in this study is a flat panel from Elekta, designed as iViewGT™ and based on the amorphous silicon detector type of XRD1640 (PerkinElmer Optoelectronics, Fremont, CA, USA) that is coupled to the LINAC gantry. This panel has a detection area of 41×41 cm^2 that consists of 1024×1024 detector elements, pixels, with a sampling aperture (pixel size) of 0.4×0.4 mm^2. Its active area is composed of 1 mm thick copper plate and 0.54 mm thick terbium-doped gadolinium oxysulphide ($Gd_2O_2S : Tb$) screen, which is fixed at 160 cm from the target of the LINAC. The entire panel elements are enclosed in a cover made of high-density polystyrene and acrylonitrile butadiene styrene, presenting a thickness of 10 cm [101].

Figure 3.12 illustrates the general iViewGT™ a-Si EPID constitution described above, the its external and internal components and the iViewGTTM a-Si EPID coupled to the LINAC in the treatment room.

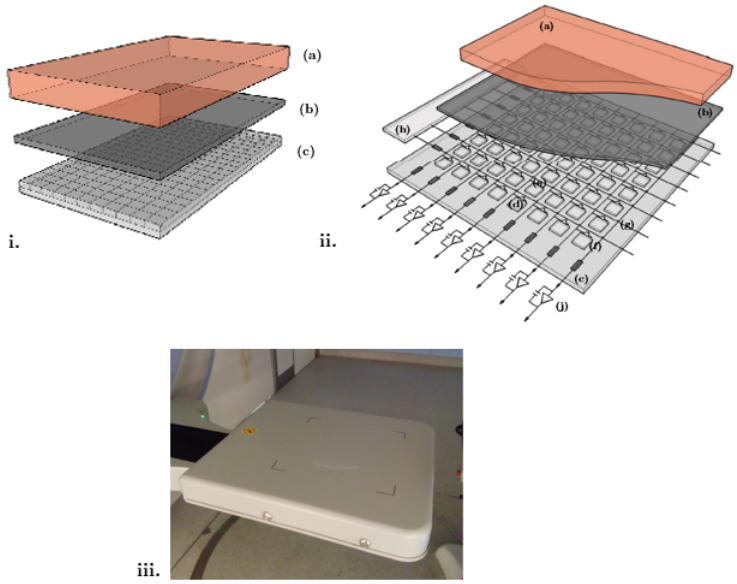

Figure 3.12: Illustration of the iViewGT™ a-Si EPID external (i) and internal elements (ii) and the same coupled to the LINAC in the treatment room (iii). (a) corresponds to the copper metal plate, which, with the scintillating phosphor screen (b), acts as an x-ray converter to optical photons detected by the active matrix array in order to be converted in image (c), where each pixel is composed of a-Si photodiode (d) and TFTs (e). (f) is the data line, which controls the readout of the charge of each TFT's along a column, and (g) the gate control line that allows the signal conduction of TFT's along a row; (h) corresponds to the preamplifiers, which joined to the control gantry circuitry (j) are the external electronics that amplify, process and digitize the imaging signal. Each data line is connected to a preamplifier. Adapted from [101].

3.7.2 Measurements

The measurements with EPID were performed both for the square fields plans and for the patient plans. They allowed to obtain the necessary data to the dose evaluation software: PreDose, pdapp and pdDVH. The first two software allow to do a two-dimensional dose analysis from EPID acquisition through gamma analysis, and the last one allows to do a three-dimensional dose analysis from EPID acquisition through DVH analysis.

The EPID is very easy to set up (Figure 3.13). One simply needs to open the panel, which is already mounted in the LINAC gantry. The detector is connected to the computer with the iViewGT (v.R3.4, Elekta AB, Stockholm, Sweden) acquisition software that provides the synchronization between the EPID and the LINAC.

Figure 3.13: Illustration of the iViewGT™ a-Si EPID setup in the LINAC room.

For the measurements, it was necessary to have the LINAC on treatment mode and to select the plan to measure on the MOSAIQ. The iViewGT had also to be open, in order to acquire and save the data. The data was acquired field by field. For square fields and VMAT patient plans, the measurements were made with rotation of the gantry. However, in IMRT plans and in case of open images acquisition, an override of the gantry on 0° was done, because, as there is no attenuation medium and the EPID follows the beam source during all the treatment, the gantry can be on the same angle during the measurement.

Two types of measurements were done with EPID: the first one without any attenuation medium (patient/phantom) to obtain the so called open images, which are used in PreDose and also in pdapp for both the square fields and the patient tests; and the second one with the slab phantom, which is used in pdapp for the square fields test. Both software are described after.

The iViewGT software projects an image with a limited size. It scales the pixel and the field dimensions to 0.25 $\times$ 0.25 mm^2 and 25.6 $\times$ 25.6 cm^2 respectively, avoiding the acquisition and computing of patients with big fields, because points outside of 25.6 cm square cannot be accurately computed, due to the fluence measurement to be not done for those points. The obtained image is a sum of frames for each segment of the field during the beam delivery. The integrated pixel value (IPV) for each segment is obtaining using the following equation:

$$Integrated\,pixel\,value = \frac{65535 - RawPixelvalue}{PSF}, \tag{3.1}$$

where the number 65535 is the 16-bit offset and PSF is the pixel scaling factor, which is reported by the software for each segment. PSF, when divided into the pixel values of a corresponding image, produces the dose result for the beam delivered. The acquired data is saved on a database [117, 118].

A succinct explanation of the image acquisition was done above. These captured images

contain dose information and for the QA process it is necessary to obtain these values of the dose distribution in the main structures. These values are acquired by converting the image in dose information. The grayscale image is then converted into a portal dose image, by assessing the intensity of the EPID image pixels. The portal dose image has fluence distribution data that is used as input of a dose algorithm, for instance back-projection algorithm, to reconstruct a dose distribution for the patient.

3.7.3 Dose Evaluation

The dose distribution in the data acquired by the EPID was evaluated by three software: pdapp PreDose and pdDVH.

pdapp

pdapp is a software developed by the Netherlands Cancer Institute-Antoni van Leeuwenhoek Hospital in Amsterdam and used in Champalimaud Foundation for research. This software is mainly used for *in vivo* measurements with the patient. It always requires an attenuation medium for the dose calculation. This software allows to perform the specific-patient QA comparing the planned data with the measurements data performed with the phantom/patient. For this comparison open images, the images previously acquired without any attenuation medium, are also taken into account. It provides three types of analysis: beam 2D analysis, beam 3D analysis and fraction. The first one consists in analysing the 2D dose distribution field by field in a plane through isocentre; the second one the 3D dose distribution field by field as well; and the last one consists in analysing the 3D dose distribution per fraction (sum of all 3D beams). The latter is the most frequently performed and necessary for pdDVH. The former two are more used in case of doubt, because it allows to see what is happening in each field. A summary of gamma analysis is shown, containing the gamma passing rate value, the gamma means and the dose difference between the reference dose distribution and the measured dose distribution.

Figure 3.14 shows the interface of this software, where it is possible to see, on the left-hand side, the measurement data, field by field. The first data fraction, which stands out from the others, corresponds to the open imagens and the other corresponds to the phantom/patient measurements. It is also possible to observe the 3D planned and measured dose distribution, respectively, in a CT of the phantom/patient. Under the images, the difference dose map is observed, related to the gamma analysis. If the gamma value presents a lower value ($<$ -1), the point shows a blue colour and corresponds to an underdose. On the other hand, if the gamma value presents a higher value ($>$ 1), the point shows a red colour, corresponding to an overdose. On the right-hand side it is possible to observe the gamma analysis summary (described above) field by field or the total evaluation, depending on what is intended.

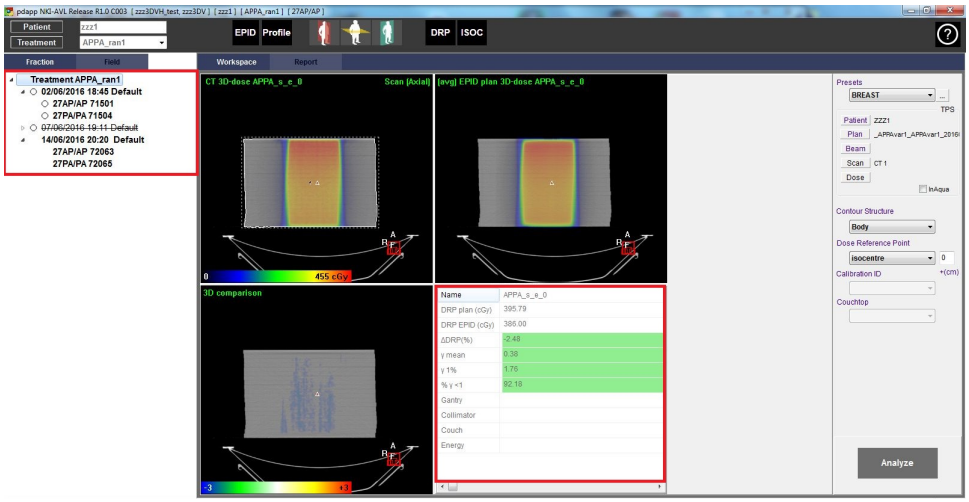

Figure 3.14: Illustration of the pdapp interface used to analyse the planned and measured data acquired by the EPID. The example illustrated is from a 2 field analysis of squared field test.

The comparison between the planned and measured dose distribution in a phantom or patient is done using the back-projection algorithm. It allows to reconstruct the dose distribution in the patient/phantom, projecting in them the measurements done by EPID and the information obtained from portal image acquired (Figure 2.11). There are some factors to take into account, such as the dose-response of the EPID, the lateral scatter within the EPID, the scatter from the phantom or patient to the EPID, the attenuation of the beam by the phantom or patient, the distance from the radiation source to the EPID plane and to the dose-reconstruction plane, and finally, the scatter within the phantom or patient. The detailed description of the algorithm was done by Wendling *et al.* [5]. However, it is important to retain some equations that illustrate the factors described above.

It is necessary to correlate the EPID pixel values with the dose values. As a reference data, to fit some parameters, ionization chamber measurements are used. They were performed with the IC placed in the centre of a phantom with 20 cm of thickness, in order to measure the dose in the isocentre. This is done for the reference field size 10×10 cm^2. The EPID images were acquired and the intensity of the EPID image pixels provided dose information.

The dose D_{ij}^{EPID} at a certain pixel ij of the EPID consists in the sum of the portal dose PD_{ij}^{EPID} of the radiation reaching the EPID directly with the scatter Sc_{ij}^{EPID} within the EPID, described by the following equation:

$$D_{ij}^{EPID} = PD_{ij}^{EPID} + Sc_{ij}^{EPID}. \tag{3.2}$$

Firstly, it is important to relate dose values with pixel values, i.e. to determine the dose-response function f_{DR} of the EPID,

$$PV_{ij}^{EPID} = f_{DR}(D_{ij}^{EPID}), \tag{3.3}$$

where PV_{ij}^{EPID} is the time integrated pixel value at a certain pixel ij of the EPID. It is assumed that f_{DR} is equal for all pixels of the EPID.

The scatter component is given by the convolution of the portal dose PD_{ij}^{EPID} with a scatter

kernel $\widetilde{K}_{ij}^{EPID}$.

Another important factor is the existing scatter from the patient to EPID. In this case the portal dose image PD^{EPID} behind a patient includes this component, $Sc_{ij}^{patient \to EPID}$, being described by the following equation

$$PD_{ij}^{EPID} = Pr_{ij}^{EPID} + Sc_{ij}^{patient \to EPID}, \tag{3.4}$$

where $Pr_{ij}^{EPID}$is the primary portal dose that results from radiation coming directly from the head of the LINAC. In order to estimate the scatter contributions, it is necessary to calculate the total transmission T^{total}. The latter is obtained dividing the portal dose image with a patient in the beam path by the portal dose image without a patient in the beam path (open image), as described by the following expression,

$$T_{ij}^{total} = \frac{PD_{ij}^{EPID,with\ patient}}{PD_{ij}^{EPID,without\ patient}}. \tag{3.5}$$

The scatter contribution is then obtained by replacing the Equation 3.4 in Equation 3.5, appearing a new component, $T_{ij}^{primary}$ that consists in the primary transmission, that is, the transmission when no scatter from the patient can reach the EPID, as observed in Equation 3.6.

$$T_{ij}^{total} = \frac{Pr_{ij}^{EPID,with\ patient} + Sc_{ij}^{patient \to EPID}}{PD_{ij}^{EPID,without\ patient}} = T_{ij}^{primary} + \frac{Sc_{ij}^{patient \to EPID}}{PD_{ij}^{EPID,without\ patient}}. \tag{3.6}$$

It is important to refer that the T^{total} depends on field size, but $T^{primary}$ has to be field size independent by definition. This allows to estimate the scatter contributions. T_{ij}^{total} is experimentally obtained as a function of field size, fs, by irradiating a phantom of a reference thikness, 20 cm, with square fields of different sizes. It is given by the following expression,

$$T_{ij}^{primary}(fs^2) \approx \lim_{fs \to 0} T_{ij}^{total}(fs^2). \tag{3.7}$$

Another required parameter is the total dose D^{mid} in the patient. D^{mid} consists in the sum of the primary dose Pr^{mid} with the scattered dose Sc^{mid} within the patient, as demonstrated in the Equation 3.8.

$$D_{ij}^{mid} = Pr_{ij}^{mid} + Sc_{ij}^{mid}. \tag{3.8}$$

To calculate the primary dose, the Inverse Square Law (ISQL) and an attenuation correction (AC) are used, joined to the primary dose of the EPID, as seen on the Equation 3.9,

$$Pr_{ij}^{mid} = Pr_{ij}^{EPID} \times ISQL \times AC = Pr_{ij}^{EPID} \times (\frac{d_{resconst}}{d_{EPID}})^{-2} \times \frac{1}{\sqrt{T_{ij}^{primary}}}, \tag{3.9}$$

where $d_{reconst}$ is the distance of the reconstruction surface from the accelerator target; d_{EPID} is the distance of the EPID from the accelerator target, which is 160 cm; and AC is related with

the $T^{primary}$, which is calculated by the following expression,

$$T_{ij}^{primary} = \exp(\mu_{AC} \times t_{ij}). \tag{3.10}$$

For dose reconstruction, the attenuation has to been corrected to the radiological path length along a ray through the patient.

In the end, a three dimensional dose distribution can be obtained for simple fields, by reconstructing the dose in different planes from the target, that is, by changing the $d_{reconst}$ for each gantry angle. This dose can be compared direcly with the planned patient/phantom dose.

PreDose

PreDose is an in-house software, still under development, that allows to perform specific-patient QA comparing the planned data with measured data, too. It is based on forward-projection, because the comparison between planned and measured data is done at the EPID level. However, instead of using the measured data with a phantom or patient and the open images, only the latter are used. The open images measurements required for the software are illustrated in (Figure 2.11). In this case, instead of measuring the dose at the patient level, by the back-projection way, it is measured at the EPID level (PD^{EPID}). This 2D dose image is estimated in the first steps of the previously mentioned back-projection algorithm (subsubsection 3.7.3), in which the expression for EPID level calculation is described, more specifically in Equation 3.2.

Using the Monaco treatment planning system, a QA plan is calculated using a 2 cm slab phantom, simulating the copper plate of the EPID, overriding the slab phantom density by the copper plate density, which is 7 $\mathrm{g/cm^3}$.

Figure 3.15 illustrates the interface of this software where it is possible to see some EPID images and the dose distribution in the planned and the measured dose map, the gamma dose map, the dose profiles, all the settings and the box with the analysis data output.

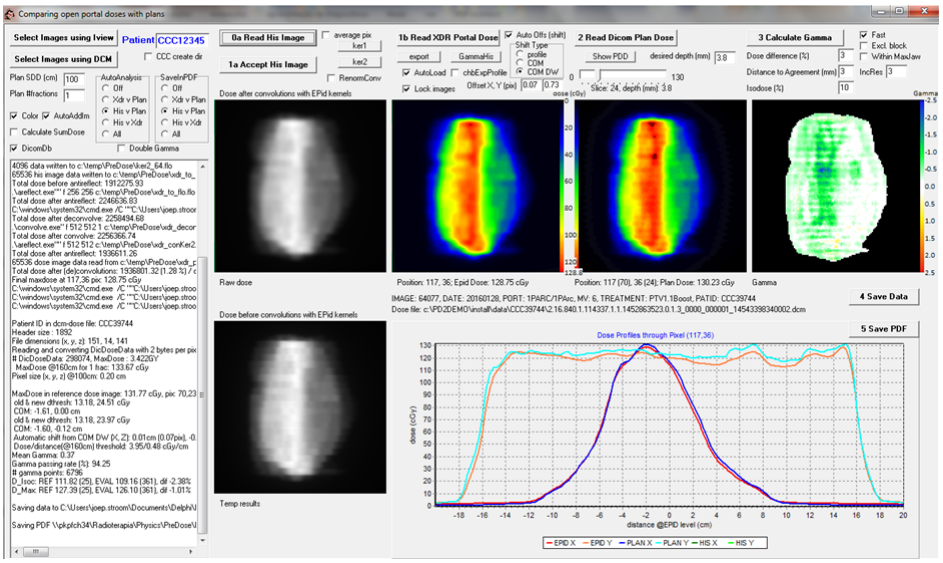

Figure 3.15: Illustration of the PreDose interface.

The gamma analysis was also performed to all square fields and patient plans with PreDose,

in order to be compared with the other systems. Hence, it was carried out to 3%/3 mm criterion, 3% of dose threshold for MLC errors analysis and 10% of dose threshold for MU errors analysis, with 90% as acceptable criterion.

pdDVH

pdDVH (v.1.3) is another in-house software that calculates DVHs using dose data from pdapp or DICOM RT dose. To obtain the DVHs, the following is necessary: reading the DICOM RT Structure file of the calculated plan, the DICOM RT Dose file or the pdapp dose file and selecting for which structure the DVH will be performed. The 3D pdapp was generated when the fraction analysis is performed. Having these files, the software associates the dose values obtained to the respective structure and calculates the DHV. With the DVH, it is possible to calculate the measured dose distribution and to compare it to the reference dose distribution along each constituent structure. It is also possible to calculate the respective dose statistics.

Figure 3.16 shows its interface where it is possible to see the dose distribution along the plan in analysis, the structures constituents of the plan and its respective DVH. Also it is possible to obtain and see the dose statistics of each structure.

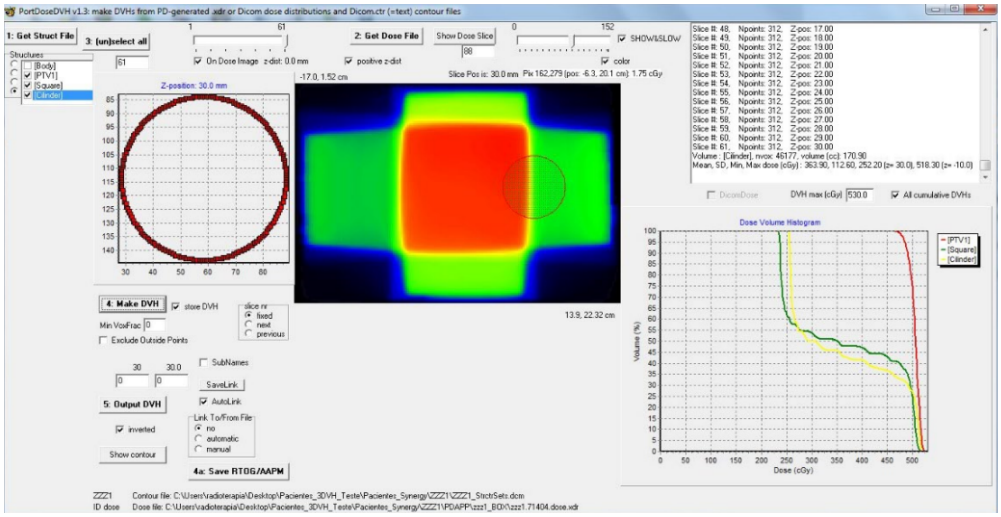

Figure 3.16: Illustration of the pdDVH interface, where it is possible to see all its analysis options. The example illustrated is from a 4 field analysis of the cylinder in square field test.

These analyses were just done to square fields test. The pdDVH uses the dose data from pdapp. In the case of the square fields, the measurements with the slab phantom were carried out with EPID in order to be used in pdapp, joined to planned data with slab phantom CT. In case of patient plans, the *in vivo* measurements with errors were not possible to be acquired.

3.8 3DVH Analysis

3DVH allows to obtain DVHs of the main structures that are important to the treatment and that should be analysed during the QA process. DVH would be a better dose evaluation method, still to be implemented clinically to improve the patient-specific QA of IMRT. It can replace gamma analysis, the conventional metric that is limited in sensitivity and specificity. 3DVH provides

clinically relevant metrics, such as the DVH – which enables the dose analysis per region of interest – and other dose points of interest, to obtain a three-dimensional evaluation of the dose distribution. It consists of an interface that offers a user-friendly way to analyse the plans and the dose distribution in important structures, giving both quantitative and qualitative information.

Having the necessary files from TPS and ArcCHECK measurements, 3DVH allows to compare the planned dose with the measured dose through DVH and gamma analysis. 3DVH uses the TPS and ArcCHECK data and creates a new plan perturbed by the errors caused by the differences between measured dose and calculated dose. This perturbation is done by using an algorithm called "Planned Dose Perturbation" (PDP™). Figure 3.17 shows the main steps in 3DVH analysis.

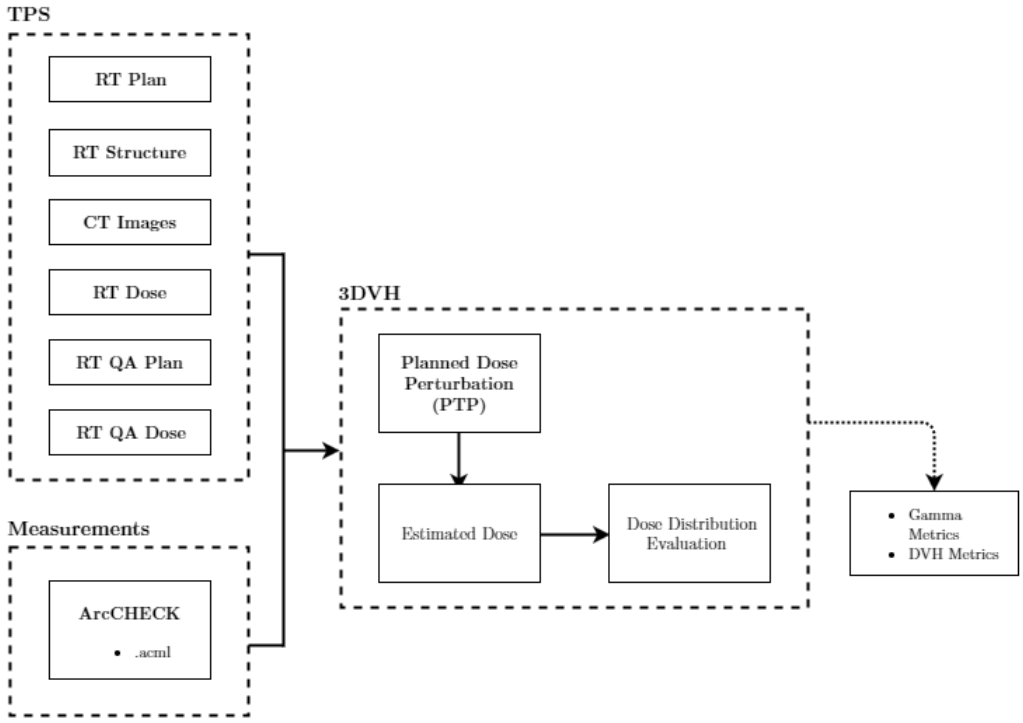

Figure 3.17: Schematic of the main steps and files and equipment used in 3DVH analysis.

3.8.1 Planned Dose Perturbation Algorithm

The PDP algorithm (Figure 3.18) utilises the measured data and compares it to the planned treatment plan data. It is used in 3DVH to perturb the treatment plan with the errors and differences between the planned and measured data, originating a correct dose map with the failed hot and cold points. This analysis and correction are done voxel-by-voxel. The perturbation allows to obtain a new and correct dose reconstruction that displays the estimated dose to the patient. The perturbation can be described as a back-projection of the measured errors into the original treatment plan, changing each dose voxel of this plan according to the dose differences detected between TPS and ArcCHECK [28].

It does not introduce new sources of error. The variations introduced are just the inaccuracies existing in the treatment plan that were detected. The plan is altered only if and where dose differences are detected. These discrepancies represent the inaccuracies of the TPS dose

calculation algorithm and of the LINAC. Thus, voxel-by-voxel in both plans are compared, and the plan is perturbed if some dose difference was detected with ArcCHECK.

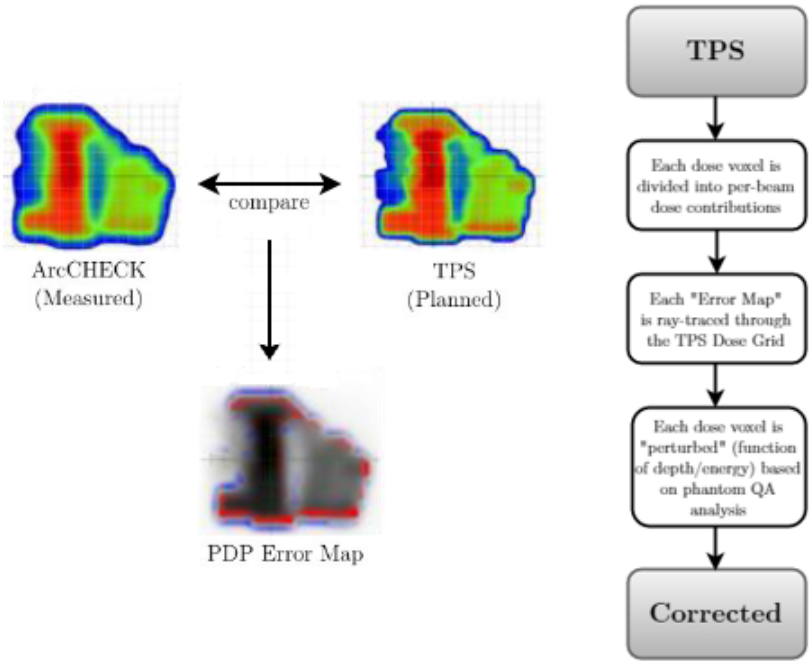

Figure 3.18: Illustration of the PDP algorithm. Both measured and planned dose distribution maps are observed. They are compared voxel-by-voxel and where a dose difference is detected, a perturbation is introduced, originating a new dose map with all these perturbations. Adapted from [100].

The algorithm is explained in detail in Zhen *et al.* [90]. The absolute dose planes are superimposed producing error masks. The absolute dose differences and local percentage errors are stored in the error masks, which are afterwards used in the perturbation. The local percentage difference (measured-calculated QA dose) error mask is described for the $i-th$ beam as

$$\Delta QAdose(i,j)^{i}_{QAdepth,distance}$$

.

Having both TPS and QA RT plan, the treatment beams are associated with their corresponding QA dose pair. PDP derives the per-voxel dose contribution from each beam. Thus, for the $i-th$ beam, the contribution by a dose voxel (x,y,z), $Dose^{i}_{xyz}$, is estimated using a physics-based energy deposition model. Having been portioned into per-beam contributions, each dose voxel in the 3D grid can be perturbed using the PDP algorithm. The error mask is modified (depending on the depth in patient/phantom and distance to the voxel from the source) by a contribution modifying function (CMF) and applied to the dose contribution of the beam i. The CMF computes the contribution of voxel dose from each beam and modifies the errors from the specific phantom geometry to the patient. For the $i-th$ beam and single voxel (xyz) this perturbation can be described as:

$$PDP^{i}_{xyz} = \Delta QAdose(i,j)^{i}_{QAdepth,distance}$$

$$\times CMF(depth^1_{xyz}, distance^1_{xyz})$$
$$\times QAdose(i,j)^i_{QAdepth,distance} \times Dose^i_{xyz},$$

where PDP^i_{xyz} is the perturbation for i beam and single voxel, $\Delta QAdose(i,j)^i_{QAdepth,distance}$ is the local percentage difference, CMF is the contribution modifying function, depending the depth and distance, $QAdose(i,j)^i_{QAdepth,distance}$ is the errors mask, which depends the depth and distance, and $Dose^i_{xyz}$ is the dose voxel contribution.

When the total dose perturbation is accumulated over all voxels, it can be used to perturb the TPS dose grid. The total perturbation is therefore described by

$$PDP^{plan}_{volume} = \sum_{xyz}\sum_{i} PDP^i_{xyz}. \tag{3.11}$$

This perturbation can then be applied to the TPS dose grid to generate the new dose grid, which is corrected by the errors detected corresponding to the differences between measured and planned dose distribution [90].

3.8.2 Interface description

As described previously (subsubsectio 3.8.1), 3DVH uses the PDP algorithm to accurately estimate the DVH and other important metrics utilising the ArcCHECK QA data as inputs.

As described in Figure 3.17, the inputs of the 3DVH correspondent to the planned data are 4 DICOM files imported from TPS, RT Plan, RT Structures, CT Images and RT Dose. As to measured data, 3DVH uses the measured ArcCHECK file (*.acml). The software also uses the RT Dose and the RT Plan of the ArcCHECK. This allows to perform correspondences between the planned and measured data, through the coordinates from each TPS and ArcCHECK files, being possible to estimate the dose on the patient/phantom geometry. The CT images are an optional set of files, because, as the software compares voxel-by-voxel of the planned and measured plans, it does not use the CT information, which is the organs density. Thus, this file is just illustrative for the analysis. However, despite the fact that the CT file is optional, the heterogeneities of the patient are taken into account, because the planned doses vary based on tissue heterogeneities, which means, dose deposition is directly related to tissue density. After input insertion, the calculation is carried out, taking from 3 to 5 minutes, depending on if the plan is an IMRT or a VMAT planning, respectively.

When calculation ends, the dose distribution analysis can be carried out. It is possible to perform the gamma analysis, to analyse the ROIs, obtaining their DVH and their statistics, and to analyse the dose distribution beam by beam.

Figure 3.19 shows an illustration of the 3DVH interface. It is possible to observe the dose distribution of the individual data (reference or measured) and of the comparison data in the sagittal, coronal and axial planes of the patient/phantom. On the left-hand side are the structure colours, quick statistics option and gamma analysis calculation. It is also possible to see the histogram of the pass and fail points and the number of these points, where the green, blue and red colours in the histogram indicate matching, underestimated and overestimated doses, respectively, between treatment plan and measurements. The software provides many analyses.

In the tabs, it is possible to choose the 3D Dose tab, previously described; DVH analysis, where both cumulative and differential DVH for each structure are shown and can be imported and saved; anatomy structure analysis, where it is possible to do an analysis structure by structure, obtaining the individual gamma passing rate and pass and fail points to each structure; BEV tab, where it is possible to analyse each beam and its dose profiles; and 4D workspace, which provides a simulation of the treatment.

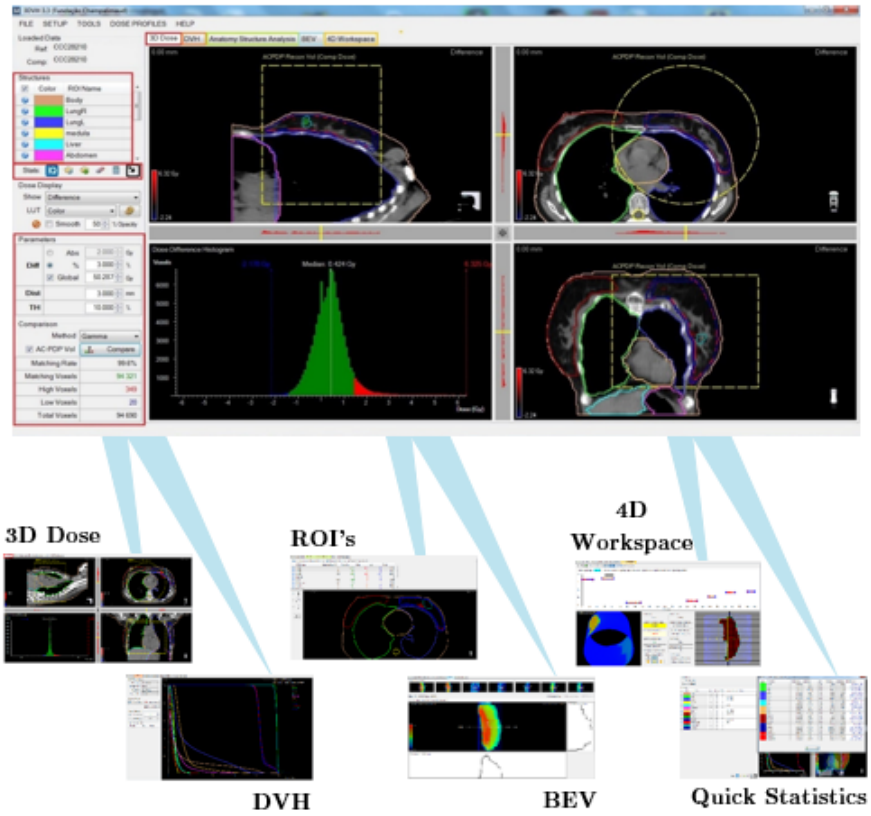

Figure 3.19: Illustration of the 3DVH interface and respective analysis options. 3D Dose, DVH, Anatomy Structure Analysis (ROI's), BEV and 4D Workspace tabs are presented. The quick statistics section is presented, too. The example illustrated is from the analysis from a patient's test.

All the square fields and patient plans were analysed using the 3DVH. As described above, it was possible to perform the dose distribution analysis, to obtain the gamma analysis and to obtain the DVH for the main structures and its statics values. as well. Values such as mean dose, maximum dose, minimum dose and some other dose constraints values, which are specific for each type of cancer, are the examples of the statics values that can be obtained. Once more, the gamma analysis was performed for 3%/3 mm criteria, 50% of dose threshold and with 90% as acceptable criterion.

CHAPTER 4

Results and Discussion

The present chapter presents the data analysis and their discussion. Due to the large data obtained, only the most important and relevant data regarding the square field and patient tests are presented.

This chapter is divided in two main sections:

- Square Fields Test;
- Patients Test.

Each section contains subsections where gamma analysis and DVH analysis are presented and discussed for MLC errors and MU errors.

4.1 Square Fields Test

The first results presented regard a simple case of open square fields without patient heterogeneities, that allows theoretical predictions and understanding if the systems are precise on the data evaluation. This is done comparing the data obtained with predictions previously calculated. Data, with MLC and MU errors and without any error, were acquired by ArcCHECK and EPID, and analysed using their respective software and 3DVH. The evaluation consisted of gamma analysis and DVH analysis. Figure 4.1 shows the dose distribution for each square fields cases, 1 field (Figure 4.1 (a)), 2 fields (Figure 4.1 (b)) and 4 fields (Figure 4.1 (c)), obtained by 3DVH and where some differences are observed between the three plans, related with dose distribution. The last plans show more homogeneity than the others.

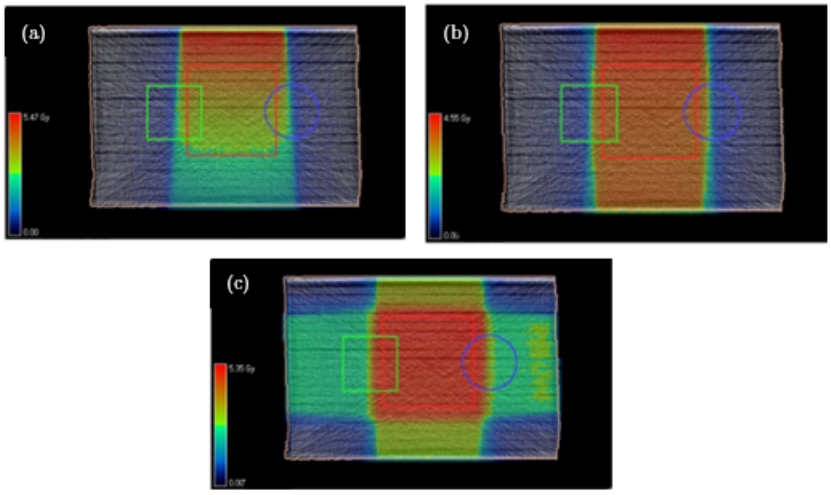

Figure 4.1: Illustration of the dose distribution in the three cases of the patient ZZZ1 slab phantom: (a) 1 field, (b) 2 fields and (c) 4 fields, obtained from 3DVH.

4.1.1 Comparison of Gamma Criterion

Gamma analysis is the most common dose evaluation method used. Gamma passing rate, the percentage of points that satisfies the condition γ<1, was calculated using specific software corresponding to the measurements systems used. SNC (referred as ArcCHECK in the tables and graphs), 3DVH and PreDose were the software used to obtain gamma analysis for all square fields plans, in order to test the accuracy of the method and the systems. This analysis was performed for both MLC and MU errors, using the 3%/3mm criteria, 10% of dose threshold for 2D gamma analysis performed by SNC and PreDose, and 3%/3mm criteria, 50% of dose threshold for 3D gamma analysis performed by 3DVH, and 90% as the clinically acceptance threshold. In the case of MLC errors, 3%/3mm criteria, 3% of dose threshold for PreDose were used, because with 10% no differences were observed. The dose thresholds are different, because, in 3D gamma analysis more points are considered comparing with 2D gamma analysis. Consequently, for 3D gamma analysis, a dose threshold that exclude more points than the threshold used for 2D gamma analysis is used. Also, the systems of dose measuring and evaluation are different and can apply the gamma analysis algorithm in a different way.

MLC Errors

As described previously, the MLC errors change the leaf positions, i.e. they open or close some millimetres. The errors will influence the area that is irradiated and the dose that is delivered to the structure, affecting mainly the edge of the field. In Table 4.1 the mean of the gamma passing rates and its specific standard deviation (SD) corresponding to all cases for all MLC errors, obtained by 3DVH, SNC of ArcCHECK and PreDose are presented.

Table 4.1: Mean and standard deviation of the Gamma Passing Rate (%γ<1) for the three square fields cases tested for both systematic (sys) and random (ran) MLC errors.

%γ<1	3DVH	ArcCHECK	PreDose
Errors (mm)	**Mean ± SD**	**Mean ± SD**	**Mean ± SD**
sys -3	96.6 ± 1.9	90.5 ± 4.3	86.0 ± 4.2
sys -2	97.2 ± 0.7	93.9 ± 3.7	90.3 ± 3.2
sys -1	98.6 ± 0.5	98.2 ± 1.7	95.1 ± 3.0
sys -0.5	98.3 ± 0.9	98.9 ± 1.0	97.2 ± 1.0
0	99.2 ± 0.2	99.2 ± 0.7	98.3 ± 0.1
sys 0.5	98.9 ± 0.5	98.5 ± 1.6	98.2 ± 0.2
sys 1	99.1 ± 0.1	97.6 ± 1.7	97.5 ± 0.5
sys 2	98.7 ± 0.3	92.9 ± 3.6	96.3 ± 0.5
sys 3	98.3 ± 0.9	88.1 ± 5.2	91.6 ± 0.1
ran 1	98.9 ± 0.4	98.2 ± 1.7	97.6 ± 0.8
ran 2	98.5 ± 0.2	96.1 ± 1,9	96.1 ± 0.8
ran 3	98.0 ± 0.4	94.0 ± 2.3	93.5 ± 0.2
ran 4	94.5 ± 4.6	91.2 ± 3.0	90.6 ± 1.8
ran5	94.4 ± 2.6	90.6 ± 3.9	90.2 ± 0.5

Looking at Table 4.1, it is possible to see the effects of the MLC errors in all the plans of the square fields test, analysing the mean of the %GP for each error. In theory, when leaves open or close systematically, the evaluation system detects the error, and the gamma value will be worse than the value obtained for the plan without errors. Thus, the larger the error, the smaller the gamma passing rate. So, a symmetry between the negative errors and positive errors should be seen. This happens, because when the leaves are closed or opened the dose distribution along the structure is different comparatively with planned plan. Thus, when the gamma method calculates the dose difference in space, this difference is detected and reflected on the gamma passing rate.

For systematic errors, the ArcCHECK results show that the system can detect the errors. As expected, the larger errors cause more damage than the smaller. A symmetry between the negative and positive errors is approximately observed. However, the positive errors present worse gamma passing rate than the negative.

For PreDose data, the system presents more sensibility in the detection of negative errors, so a great asymmetry between the positive and negative errors is seen. This can be justified by the dose threshold used, which is related with the maximum planned dose. Despite being low, which includes the dose values that causes underdose, affecting the %GP obtained, the dose values obtained when the leaves are opened are outside the threshold, not affecting so much the %GP. PreDose already detects less dose than it is supposed in the reference situation, possibly the leaves callibration results in slightly more closed leaves. So, the errors that open the leaves, i.e. the positive errors, sometimes can correct the dose delivery system and not cause many effects or even improve the %GP. The %GP from PreDose results are also worse than the ArcCHECK results, because it takes into account the output variations of the LINAC, unlike ArcCHECK, which corrects for output variations every day. This effect can also contribute to the asymmetry seen.

The 3DVH results are very flat. They are also very different from ArcCHECK results, despite using ArcCHECK data, not detecting very well the presence of the errors. This can be justified

by five reasons:

1. The gamma analysis is not a good and accurate dose distribution evaluation method, which can be proven if the DVHs of these plans present differences between measurements and reference. This evaluation is carried out below;

2. The plans used consist of open square fields, which means, the MLC does not act so much, comparing with an IMRT plan, for example. Thus, the errors on MLC may not be very significant and relevant in these plans;

3. The ArcCHECK software performs a 2D gamma analysis, whereas 3DVH performs a 3D gamma analysis. In 3D analysis more points will be considered leading to smaller gamma values;

4. The criteria used. It is complicated to choose the dose threshold. As gamma analysis with 3DVH is considered 3D gamma analysis, it is better to choose a high dose threshold in order to exclude the larger number of low dose points, which will decrease the %GP. However, too high thresholds can exclude the points affected by the errors. Also the DTA (3 mm) criterion used can affect the results, because it is near to the error values introduced;

5. The gaps between the diodes of ArcCHECK. Their distance is 1 cm, which is larger than the errors introduced.

In the case of random errors, the results are better and the relation between errors and gamma passing rate is observed for all systems. However, the 3DVH results do not change that much. The ArcCHECK presents values smaller than 3DVH.

In the following Figure 4.2, this relation between the errors, systematic and random, and gamma passing rate, and all the effects described are more clearly seen, but now just for the case of 4 fields, because it is the plan with better homogeneity in the PTV, as it is possible to see in Figure 4.1. Thus, it can show better the inferences of the MLC errors. It is also possible to compare the %GP corresponding to PreDose ArcCHECK and 3DVH.

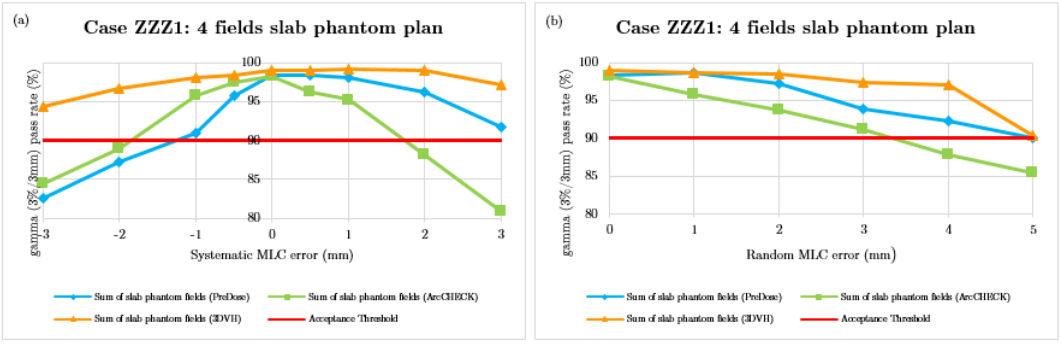

Figure 4.2: Gamma Passing Rates as function of MLC errors for the case of the patient ZZZ1, 4 fields slab phantom plan for 3%/3mm criteria with 10% dose threshold for ArcCHECK, 3%/3mm criteria with 3% dose threshold for PreDose and 3%/3mm criteria with 50% dose threshold for 3DVH. The %GP acceptance threshold is 90%. (a) corresponds to Systematic MLC errors and (b) corresponds to Random MLC errors.

Looking at Figure 4.2 (a) corresponding to systematic errors, it is possible to observe the relation between errors and gamma passing rate referred above and seen in Table 4.1.

3DVH does not detect systemaic errors, because the %GP are very similar for all the errors. ArcCHECK and PreDose show capacity to detect these errors, because high errors show worse %GP than low errors as expected. However, the %GP are above or very close of the acceptance criteria and PreDose shows a great asymmetry between the negative and positive errors.

For random errors (Figure 4.2 (b)), all the systems detect their presence, 3DVH included. Once more, high errors show %GP worse than the low. However, it is difficult to predict the effect of these errors in the plans, because the leaves moves randomly.

MU Errors

The MU errors affect linearly the dose that is delivered to the patient. Unlike the MLC errors, MU errors perturb all the field equally. Table 4.2 presents the mean of gamma passing rate and its standard deviation obtained by 3DVH, SNC and PreDose for all square fields cases and for each MU error. The measurement without errors was repeated for the MU error measurements, because they were done several months after the MLC measurements. The difference between the two reference measurements is possibly due to the output variations of the LINAC, for which PreDose does not correct (but ArcCHECK does), or due to slight changes in LINAC/MLC settings after the LINAC maintenance.

Table 4.2: Mean and standard deviation of the Gamma Passing Rate (%γ<1) for the three square fields cases tested for MU errors.

%γ<1	3DVH	ArcCHECK	PreDose
Errors (%)	**Mean ± SD**	**Mean ± SD**	**Mean ± SD**
-4	79.4 ± 6.2	96.6 ± 1.6	63.1 ± 8.0
-2	98.9 ± 0.4	98.5 ± 1.3	98.1 ± 0.3
0	96.9 ± 1.4	96.0 ± 3.4	97.2 ± 1.1
2	78.7 ± 4.4	83.9 ± 11.3	68.2 ± 6.9
4	40.8 ± 1.3	58.4 ± 29.1	43.1 ± 6.2

From Table 4.2 it is possible to observe that the dose is directly and more affected by the change of the MUs, because they are directly related with the delivered dose: MU errors affect the whole field and MLC errors only affect the edge of the field.

As expected, the negative errors reduce the dose delivered and the positive errors increase the dose delivered. As in the MLC errors, the larger the error, the worse the gamma passing rate. This effect is seen for all systems. However, the positive errors cause more perturbation than the negative errors, which means, theres is an asymmetry between the negative and positive errors.

Figure 4.3 presents more clearly the relation between the errors and the gamma passing rate obtained just for the case with 4 fields plans as in the MLC analysis. Once more, it is possible to compare the data of 3DVH, ArcCHECK and EPID and determine which is more sensitive to detect the errors.

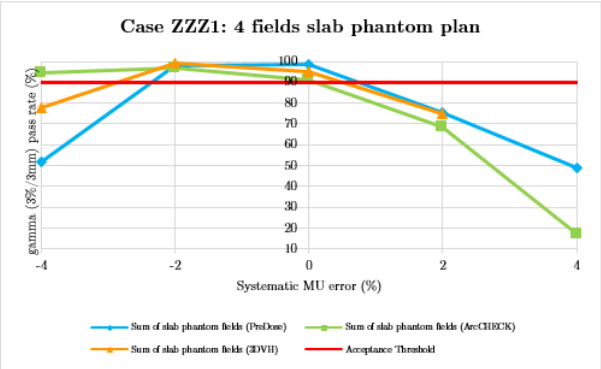

Figure 4.3: Gamma Passing Rates as function of MU errors for the case of the patient ZZZ1, 4 fields slab phantom plan. The analysis was done for 3%/3mm criteria and 10% of dose threshold for PreDose and ArcCHECK; and for 3%/3mm criteria and 50% of dose threshold for 3DVH, with 90% as acceptance threshold

Figure 4.3 shows that, as seen in Table 4.2, the larger errors cause more perturbation than the smaller and an asymmetry in all systems results is also observed, which means, the positive errors presented smaller %GP than the negative errors. In this case, a MU increase affects more the dose delivered than when the MU decreases. This asymmetry shows that the negative error of -2% is above the acceptance criteria, unlike the positive error of 2%. Taking into account the way gamma analysis works, the dose thresholds eliminate the smaller dose values of the planned dose map. Thus, the negative errors, which reduce the dose delivered might not be included in the analysis as the positive errors will, because they are out of the region analysed by gamma metric, resulting the asymmetry observed. Again, the asymmetry in the PreDose might be caused by the output variations of the LINAC, as previously described (subsubsection 4.1.1). The ArcCHECK and 3DVH results are also different due to the different threshold used, as mentioned above (subsubsection 4.1.1).

The gamma passing rate value of 4% was not obtained in 3DVH, because the software crashed: 3DVH cannot handle too large dose deviations (also observed in ArcCHECK results). This is a limitation of the system.

4.1.2 Analysis of DVHs

DVHs give clinically relevant 3D information of dose distribution in a structure and it is the another option for dose evaluation. 3DVH and pdDVH (referred as EPID in the figures and graphs) were the software used to calculate DVHs, using data from ArcCHECK and EPID measurements, respectively.

As many DVHs were obtained, only the relevant ones of MLC errors (systematic of -3 and 3 mm and random of 1 and 5 mm) and of MUs errors (systematic of -4 and 4%) will be presented in the following sections, and just for the case of 4 fields.

MLC Errors

The effect of MLC errors were detected in the DVH of each structure. These errors affect mainly the volumes in the DVHs of the structures, so Tables 4.3 and 4.4 present the predictions previously calculated of the reduction and increase of the volume percentage of each structure for all MLC systematic errors and for all cases obtained by 3DVH and by pdDVH, respectively.

The predictions were done just for systematic errors, because the effects of the random errors are harder to predict, since the leaves move randomly. The systematic errors that affect the positions of the leaves, closing or opening them symmetrically, will affect mainly the edge of the fields. Consequently, in cube and cylinder structures more effects are expected than in PTV, for which any perturbation is not expected. Therefore, the predictions were only calculated for cube and cylinder. With these predictions is easier to understand if the systems detect accurately the presence of the errors in the plans.

Table 4.3: Predictions and measurements of the effect of MLC errors in the volume of 50% for the three square fields cases obtained by 3DVH. The first column corresponds to the predictions, the second column corresponds to the difference between the reference volume (50%) and the measured volume (V_{meas}), and the last column shows the difference between the second and the first columns.

Errors (mm)	$\Delta V_{pred}(\%)$		$\Delta V_{meas}(\%)$		Difference (%)	
	Cube	Cylinder	Cube	Cylinder	Cube	Cylinder
Case ZZZ1: Slab Phantom 1 field plan						
-3	-5.0	-6.4	-0.5	-0.3	4.5	6.1
-2	-3.3	-4.2	-0.4	-0.2	2.9	4.0
-1	-1.6	-2.1	-0.3	-0.1	1.3	2.0
-0.5	-0.8	-1.1	-0.3	0.0	0.5	1.1
0	0.0	0.0	0.0	0.0	0.0	0.0
0.5	0.8	1.1	0.0	0.0	-0.8	-1.1
1	1.7	2.1	-0.1	0.1	-1.8	-2.0
2	3.3	4.2	0.0	0.1	-3.3	-4.1
3	5.0	6.4	0.7	0.2	-4.3	-6.2
Case ZZZ1: Slab Phantom 2 fields plan						
-3	-5.0	-6.4	0.0	0.0	5.0	6.4
-2	-3.3	-4.2	-0.7	-0.5	2.6	3.7
-1	-1.6	-2.1	-0.4	-0.4	1.2	1.7
-0.5	-0.8	-1.1	-0.3	-0.3	0.5	0.8
0	0.0	0.0	0.0	0.0	0.0	0.0
0.5	0.8	1.1	0.0	0.0	-0.8	-1.1
1	1.7	2.1	0.0	0.4	-1.7	-1.7
2	3.3	4.2	0.0	1.5	-3.3	-2.8
3	5.0	6.4	0.0	1.7	-5.0	-4.7
Case ZZZ1: Slab Phantom 4 fields plan						
-3	-5.0	-6.4	-0.1	-0.5	4.9	5.9
-2	-3.3	-4.2	0.0	-0.6	3.3	3.6
-1	-1.6	-2.1	0.0	-0.5	1.6	1.6
-0.5	-0.8	-1.1	0.0	-0.6	0.8	0.5
0	0.0	0.0	0.0	0.0	0.0	0.0
0.5	0.8	1.1	0.0	-0.2	-0.8	-1.3
1	1.7	2.1	0.0	-0.3	-1.7	-2.4
2	3.3	4.2	0.0	0.5	-3.3	-3.7
3	5.0	6.4	0.0	2.0	-5.0	-4.4

Table 4.4: Predictions and measurements of the effect of MLC errors in the volume of 50% for the three square fields cases obtained by EPID. The first column corresponds to the predictions, the second column corresponds to the difference between the reference volume (50%) and the measured volume (V_{meas}), and the last column shows the difference between the second and the first columns.

Errors (mm)	$\Delta V_{pred}(\%)$		$\Delta V_{meas}(\%)$		Difference (%)	
	Cube	Cylinder	Cube	Cylinder	Cube	Cylinder
Case ZZZ1: Slab Phantom 1 field plan						
-3	-5.0	-6.4	-4.2	-5.6	0.8	0.8
-2	-3.3	-4.2	-3.1	-3.2	0.2	1.0
-1	-1.6	-2.1	-1.4	-1.6	0.2	0.5
-0.5	-0.8	-1.1	-0.4	-1.0	0.4	0.1
0	0.0	0.0	0.0	0.0	0.0	0.0
0.5	0.8	1.1	0.4	1.2	-0.4	0.1
1	1.7	2.1	1.3	2.0	-0.4	-0.1
2	3.3	4.2	2.6	5.1	-0.7	0.9
3	5.0	6.4	6.6	5.2	1.6	-1.2
Case ZZZ1: Slab Phantom 2 fields plan						
-3	-5.0	-6.4	-5.0	-7.1	0.0	-0.7
-2	-3.3	-4.2	-2.4	-5.0	0.9	-0.8
-1	-1.6	-2.1	-0.6	-4.1	1.0	-2.0
-0.5	-0.8	-1.1	0.7	-2.5	1.5	-1.4
0	0.0	0.0	0.0	0.0	0.0	0.0
0.5	0.8	1.1	1.0	-0.3	0.2	-1.4
1	1.7	2.1	1.9	0.1	0.2	-2.0
2	3.3	4.2	4.3	3.1	1.0	-1.1
3	5.0	6.4	4.9	4.4	-0.1	-2.0
Case ZZZ1: Slab Phantom 4 fields plan						
-3	-5.0	-6.4	-5.7	-6.4	-0.7	0.0
-2	-3.3	-4.2	-5.1	-4.1	-1.8	0.1
-1	-1.6	-2.1	-2.1	-2.2	-0.5	-0.1
-0.5	-0.8	-1.1	-2.4	-1.3	-1.6	-0.2
0	0.0	0.0	0.0	0.0	0.0	0.0
0.5	0.8	+1.1	-0.8	0.1	-1.6	-1.0
1	1.7	2.1	1.0	0.8	-0.7	-1.3
2	3.3	4.2	1.9	4.4	-1.4	0.2
3	5.0	6.4	4.4	5.6	-0.6	-0.8

In Tables 4.3 and 4.4, the predictions are the expected changes in the percentage of the volume that receives high dose (e.g. >2 Gy, so V(2Gy) in the DVH). For the cube, these predictions correspond to the size of the MLC error (E_{MLC}) divided by the length of the cube L (6 cm):

$$\Delta V_{pred}(\%) = E_{MLC}/L. \tag{4.1}$$

So, for a -3 mm MLC error, $\Delta V_{pred}(\%) = -3/60 = -5\%$. For the cylinder, we approximated the prediction by:

$$\Delta V_{pred}(\%) = (4/\pi) \times E_{MLC}/L, \tag{4.2}$$

with L = 6 cm, because we considered the 50% volume for the analysis.

The following steps were taken to estimate the measured volume $\Delta V_{meas}(\%)$ from the DVHs:

1. We took the dose corresponding to the 50% volume in the reference DVH, i.e. $D_{ref}(50\%)$;
2. We determined the volume corresponding to this in the error DVHs, so $V_{meas}(D_{ref}(50\%))$;
3. The measure volume change is then: $\Delta V_{meas}(\%) = V_{meas}(D_{ref}(50\%)) - 50\%$.

The 50% volume was chosen, because it is approximately the volume of cube and cylinder that is receiving the high dose, as observed in Figure 4.1.

Analysing Tables 4.3 and 4.4, it is possible to see that the 3DVH was not efficient in detecting the errors. Very little deviation is seen in all the results. This could be explained by ArcCHECK having a 1 cm gap between the diodes, which size is larger than the error values introduced, affecting the acquisition and detection of the errors. On the other hand, the pdDVH detects the errors, and many of the measured results are close to the predictions for all plans and for both structures. Some differences between the predictions and measurements observed in EPID results exist probably because EPID takes into account the output variations of the LINAC.

There is also a lack of correlation between the gamma analysis and the DVHs analysis of EPID systems. In gamma analysis the system does not detect the presence of the positive errors very well. However, in DVHs analysis they are detected.

In the following figures (Figures 4.4 to 4.8), these effects are shown on the DVHs, but just for the systematic errors of -3 and 3 mm and for the random errors of 1 and 5 mm for the plan of 4 fields. We also compared the DVH from Monaco, which is the reference, with the error-free measured DVHs obtained from 3DVH and pdDVH (Figure 4.4). Figures 4.5 to 4.8 correspond to the comparison between error-free, measured reference, and measured plans with introduced errors. The first evaluation is done to see the usual errors of the clinical system, and the second evaluation allows to see only the effect of the introduced errors.

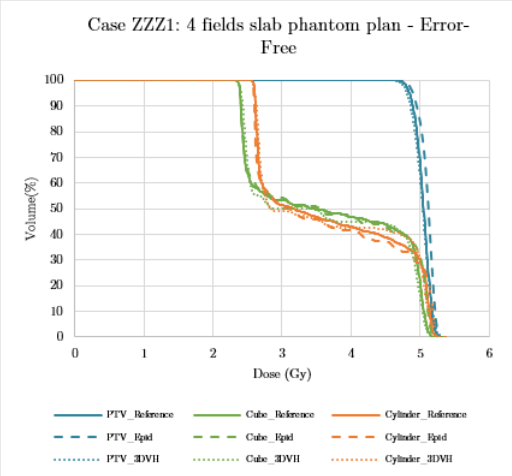

Figure 4.4: DVH of the structures, PTV, Cube and Cylinder of the case ZZZ1, 4 fields slab phantom plan, error-free. The reference data, obtained by Monaco, is compared with the measured data without errors, acquired by the EPID and ArcCHECK and analysed with pdDVH and 3DVH respectively.

By comparing the EPID and ArcCHECK measurements without errors with the reference obtained by Monaco, small deviations, mainly in cube and cylinder, are observed. This deviation

can be related with the variation in the dose delivery, measurement, LINAC output, and planning systems.

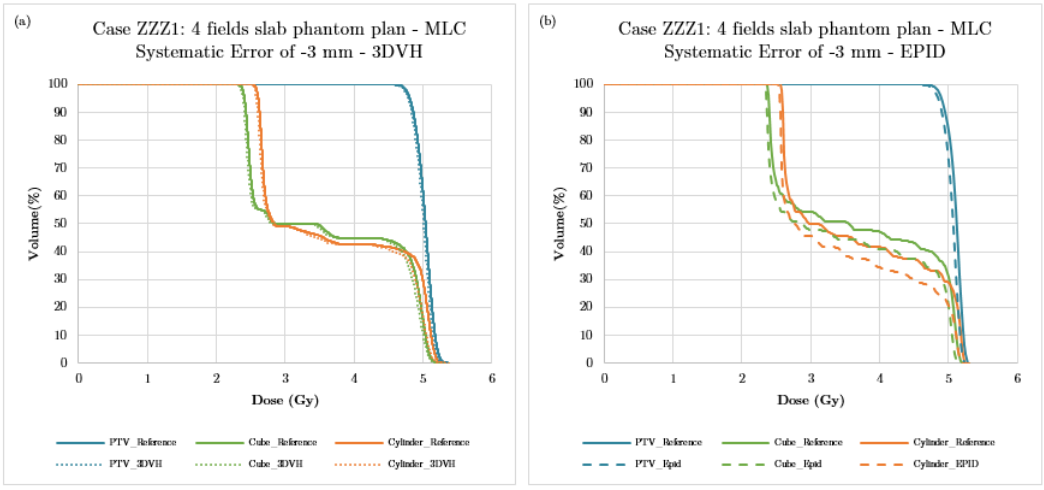

Figure 4.5: DVH of the structures, PTV, Cube and Cylinder of the case ZZZ1, 4 fields slab phantom plan, MLC Systematic Error of -3 mm analysed with 3DVH and pdDVH. The reference data, i.e. measurements without errors, is compared with the measured data with MLC systematic errors of -3 mm, acquired by the ArcCHECK and by the EPID. (a) corresponds to 3DVH analysis and (b) corresponds to pdDVH analysis.

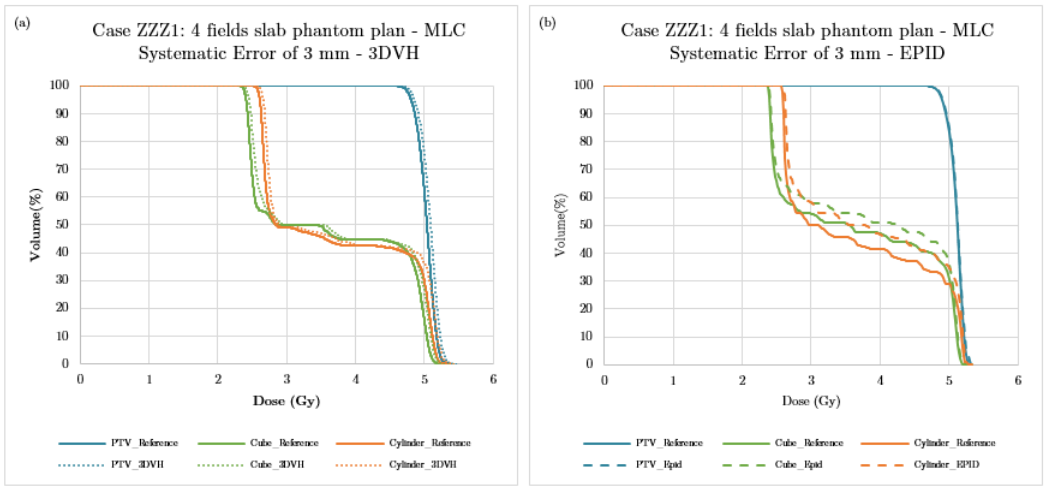

Figure 4.6: DVH of the structures, PTV, Cube and Cylinder of the case ZZZ1, 4 fields slab phantom plan, MLC Systematic Error of 3 mm analysed with 3DVH and pdDVH. The reference data, i.e. measurements without errors, is compared with the measured data with MLC systematic errors of 3 mm, acquired by the ArcCHECK and by the EPID. (a) corresponds to 3DVH analysis and (b) corresponds to pdDVH analysis.

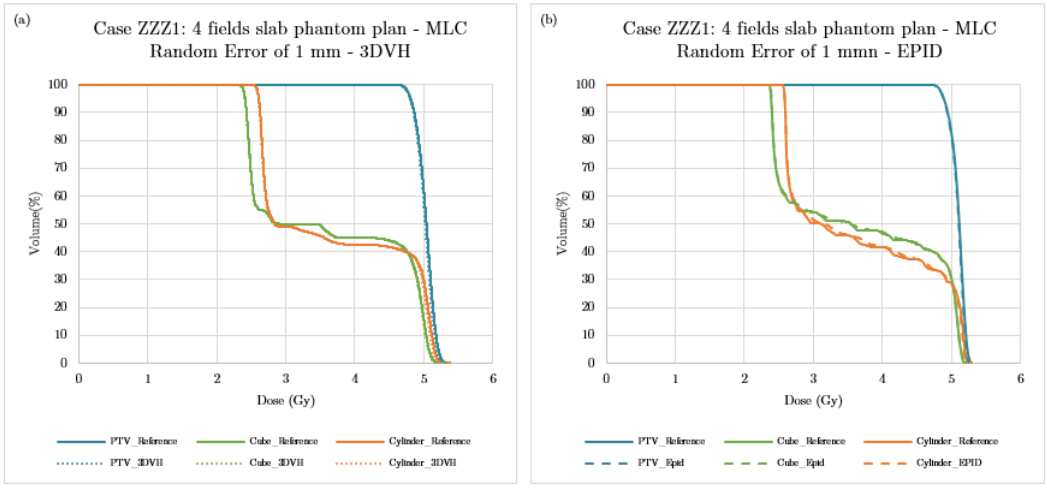

Figure 4.7: DVH of the structures, PTV, Cube and Cylinder of the case ZZZ1, 4 fields slab phantom plan, MLC Random Error of 1 mm analysed with 3DVH and pdDVH. The reference data, i.e. measurements without errors, is compared with the measured data with MLC random errors of 1 mm, acquired by the ArcCHECK and by the EPID. (a) corresponds to 3DVH analysis and (b) corresponds to pdDVH analysis.

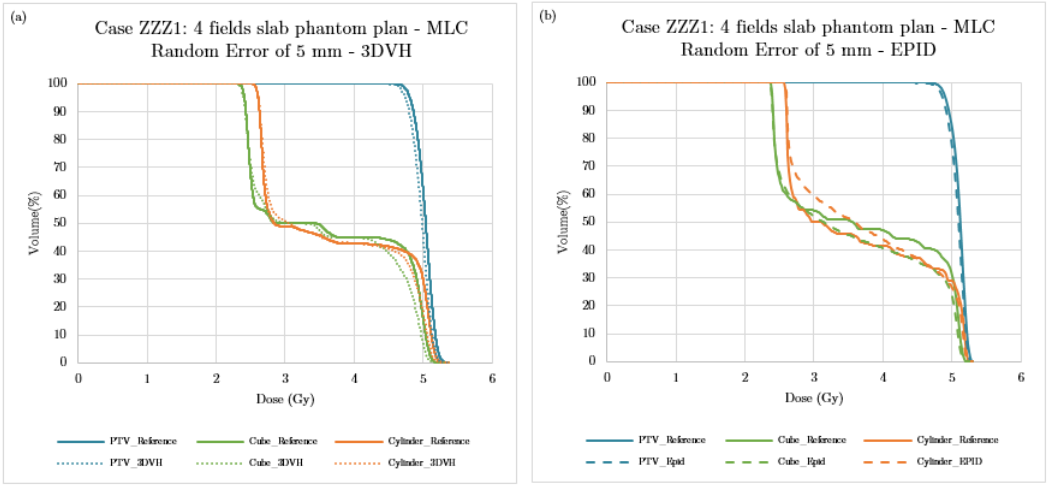

Figure 4.8: DVH of the structures, PTV, Cube and Cylinder of the case ZZZ1, 4 fields slab phantom plan, MLC Random Error of 5 mm analysed with 3DVH and pdDVH. The reference data, i.e. measurements without errors, is compared with the measured data with MLC random errors of 5 mm, acquired by the ArcCHECK and by the EPID. (a) corresponds to 3DVH analysis and (b) corresponds to pdDVH analysis

Looking at the DVHs of PTV, it is possible to see that there is not a great difference in both errors cases. When the leaves open, the field is a bit bigger than PTV, which means, it covers all the PTV area. So the opening of the leaves will just affect the surrounding PTV area, i.e. the cube and cylinder structures. When the leaves close, the same effect on the PTV is seen. Despite the the fact that the leaves closing may affect the area of distribution of the PTV, the margin between the field and the PTV can be bigger than the MLC error. Thus, as any significant difference is not detected between the reference and the measured, the leaves may not be closed enough to include the PTV and may not affect its dose distribution.

In theory, for cube and cylinder structure, the systematic errors will affect how the dose is delivered to them by reducing or increasing of their volumes. The negative errors will reduce the space that receives dose, that is, they will reduce the cube and cylinder volumes. The reduction of

the volume increases with the larger errors. On the other hand, the positive errors will increase the space that receives the dose, raising the volumes with the larger errors as well. In these structures, when the dose is delivered, firstly, there is no dose in the volume; after, the dose will increase until approximately 50% of the volume is irradiated with high dose, because this volume is in the area irradiated by the field, as observed in the DVHs and in Figure 4.1 (c). Thus, when the leaves close, the DVH line moves down, because less volume is affected and when the leaves open, the DVH line moves up, because more volume is irradiated.

Comparing the DVHs of systematic errors of – 3 mm (Figure 4.5) with the ones of systematic errors of 3 mm (Figure 4.6) for cube and cylinder, it is possible to see that the effects, described above, were more detected by the pdDVH, than in the 3DVH, which does not the detect a presence of the errors, as also previously seen in Tables 4.3 and 4.4. The DVHs of cylinder present more deviations than the ones obtained for the cube, as expected.

In terms of the random errors, the DVHs presented are for random errors of 1 mm and 5 mm and it is observed that both systems detect the presence of these errors for all cases. However, the pdDVH detects better the existence of the errors than 3DVH. It is hard to predict the effect of these in the volumes, because the leaves move randomly. However, it is possible to claim that larger errors cause larger consequences of the dose distribution, comparing the DVHs of random errors of 1 mm (Figure 4.7) with the ones of random errors of 5 mm (Figure 4.8). As in the systematic errors, it is observed more effects of the errors in the cylinder than in the cube, principally in the DVH of random error of 5 mm.

DVHs from reference, pdDVH and 3DVH of cube and cylinder present fluctuations, related to dose calculation by the software.

MU Errors

The effect of the MU errors was also analysed by DVH of each structure of each square field case 1 field plan, 2 fields plan and 4 fields plan.

As for MLC errors, in Figure 4.9 we compared the Monaco DVH with the ones obtained from 3DVH and pdDVH without errors. Figures 4.10 and 4.11 present the deviations caused by the MU errors in each structure between the reference, which is the measured data without errors, and the measured data with errors. As in the MLC errors analysis, having the measured data without errors as reference allows to take into account only the errors introduced, excluding the common errors originated by the planning and treatment systems.

Therefore, Figures 4.9 to 4.11 show the effects on the DVHs obtained respectively for without errors and -4% and 2% (3DVH does no calculate for error of 4%) of MUs errors, just for the case of 4 fields.

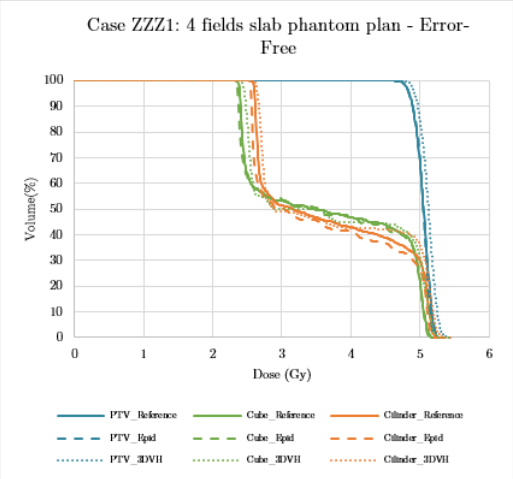

Figure 4.9: DVH of the structures, PTV, Cube and Cylinder of the case ZZZ1, 4 fields slab phantom plan, error-free. The reference data, obtained by Monaco, is compared with the measured data without errors, acquired by the EPID and ArcCHECK and analysed with pdDVH and 3DVH respectively.

Once again, there is no large deviations between the Monaco reference and the measured plans without errors. Just the common caused by the planning and delivered systems.

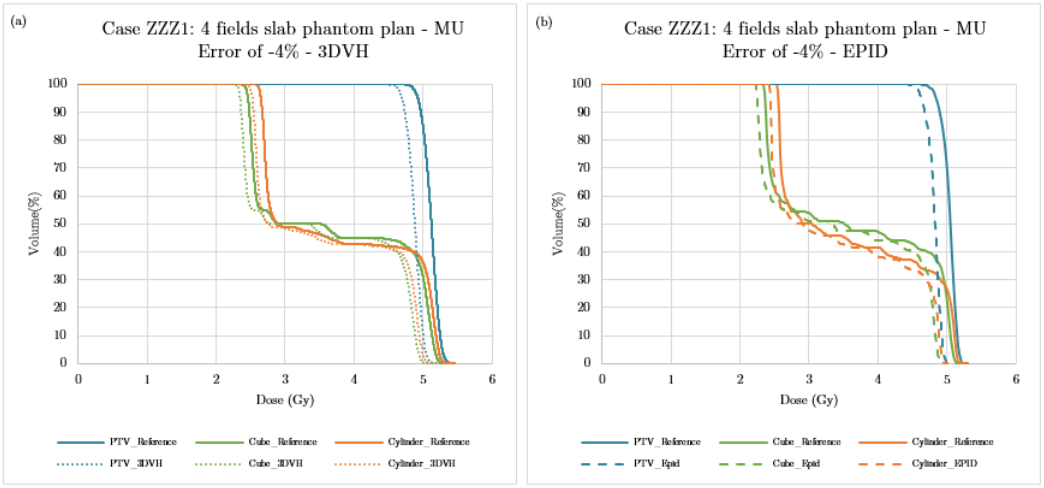

Figure 4.10: DVH of the structures, PTV, Cube and Cylinder of the case ZZZ1, 4 fields slab phantom plan, MU Error of -4% analysed with 3DVH and pdDVH. The reference data, i.e. measurements without errors, is compared with the measured data with MU errors of -4%, acquired by the ArcCHECK and by the EPID. (a) corresponds to 3DVH analysis and (b) corresponds to pdDVH analysis.

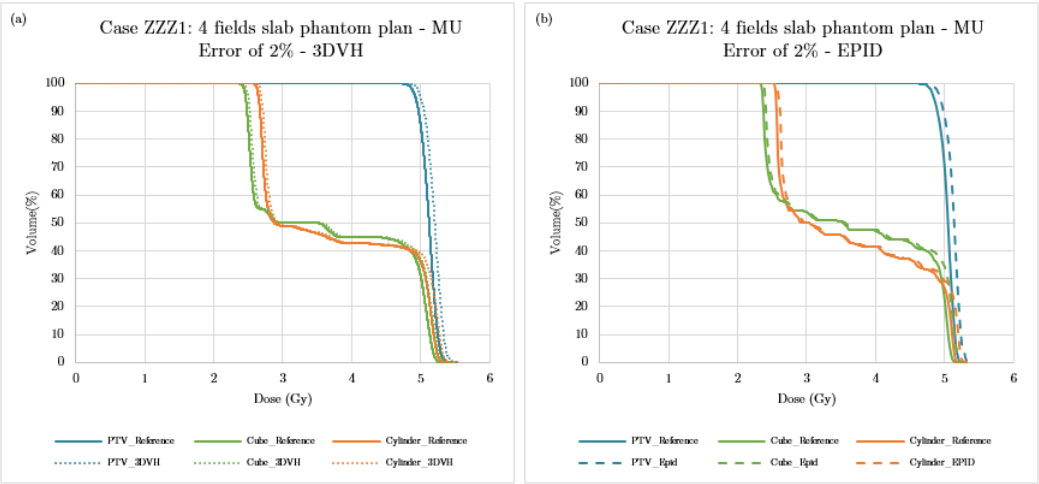

Figure 4.11: DVH of the structures, PTV, Cube and Cylinder of the case ZZZ1, 4 fields slab phantom plan, MU Error of 2% analysed with 3DVH and pdDVH. The reference data, i.e. measurements without errors, is compared with the measured data with MU errors of 2%, acquired by the ArcCHECK and by the EPID. (a) corresponds to 3DVH analysis and (b) corresponds to pdDVH analysis.

It is expected that MU errors affect all the structures in the same way, unlike the MLC errors, because with MU errors, whole the field is affected instead of only its edges. Despite half of the volume of cube and cylinder is affected by the field, these errors interfere the dose delivered to each structure, reducing or increasing it.

Observing the PTV DVHs in Figures 4.10 and 4.11, several differences between the reference and the measured are seen. The DVHs of the other structures also show variations mainly after 50%, because just approximately 50% of the volume of cube and cylinder structures receives dose, as seen in Figure4.1 (c). Looking at the negative errors, the moving of the DVH to the left is observed, because, as described above, the negative errors decrease the dose distribution. Looking at the positive errors, the opposite movement is observed. As expected, the DVH moves to the right, because the positive errors increase the dose distribution. These movements increase to the larger errors. Both the systems detect the presence of the errors, presenting many similarities in the deviations between the reference DVHs and the calculated DVHs.

4.1.3 Comparison of Relative Mean Dose Difference

In this subsection, the evaluation of the relative mean dose difference is made. The mean dose difference is the difference between the measured mean dose and the reference mean dose, and it is an important dose constraint to be evaluated and obtained by DVH analysis. Mean doses were provided by the 3DVH (ArcCHECK) and by pdDVH (EPID).

MLC Errors

The MLC errors effects are also detected in the mean dose difference results. Figures 4.12, 4.13 and 4.14 show these effects of systematic (a) and random (b) MLC errors in the case ZZZ1 of 1 field, 2 fields and 4 fields, respectively, comparing the mean dose difference detected by 3DVH and pdDVH.

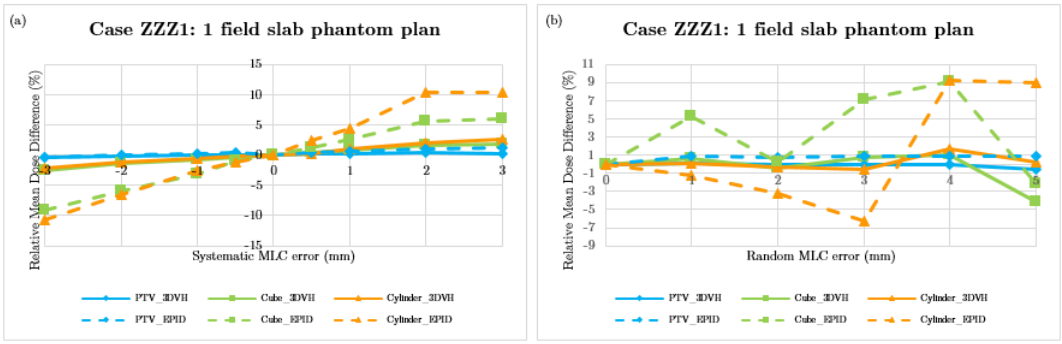

Figure 4.12: Relative Mean Dose Difference of PTV, Cube and Cylinder of the case ZZZ1, 1 field slab phantom plan. The data obtained by 3DVH is compared with the data from EPID obtained by pdDVH for the (a) Systematic MLC Errors and the (b) Random MLC Errors.

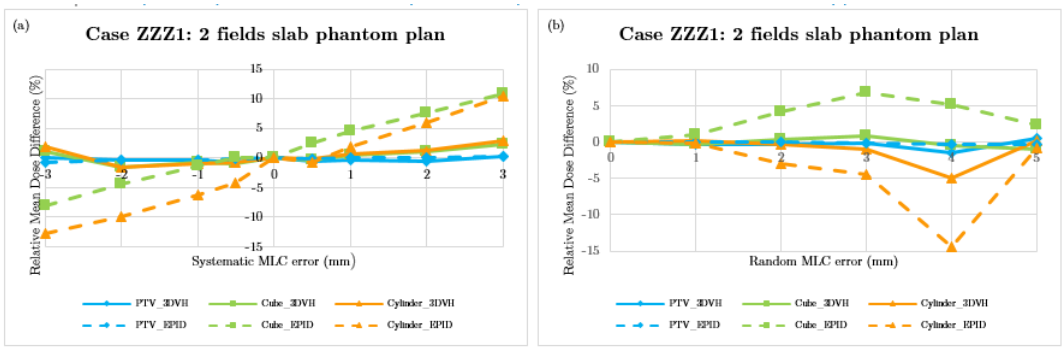

Figure 4.13: Relative Mean Dose Difference of PTV, Cube and Cylinder of the case ZZZ1, 2 fields slab phantom plan. The data obtained by 3DVH is compared with the data from EPID obtained by pdDVH for the (a) Systematic MLC Errors and the (b) Random MLC Errors.

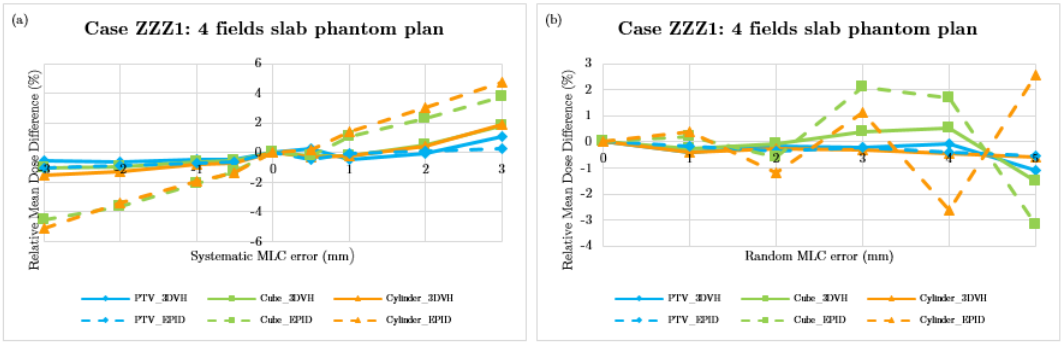

Figure 4.14: Relative Mean Dose Difference of PTV, Cube and Cylinder of the case ZZZ1, 4 fields slab phantom plan. The data obtained by 3DVH is compared with the data from EPID obtained by pdDVH for the (a) Systematic MLC Errors and the (b) Random MLC Errors.

Looking at Figures 4.12 (a), 4.13 (a) and 4.14 (a), the relation between the systematic MLC errors and the relative mean dose for the three structures, PTV, cube and the cylinder is seen. As expected, the pdDVH is more sensitive in detecting the errors than 3DVH. As seen previously in the DVHs, pdDVH can detect the perturbations caused by the MLC, showing now a linear straight that proves that the larger the errors, the larger the mean dose differences. On the other hand, the 3DVH does not detect very well the perturbation caused by the errors, as also seen in the DVHs. Its curves are very flat and near zero for PTV and near approximately ±2% for cube

and cylinder for all cases. In pdDVH results, more variations in cube and cylinder than in PTV are observed, as seen in DVH and as expected. The relative mean dose difference obtained for PTV are very close to the zero and constant. Comparing the cube and cylinder, the latter is more affected than the former, because, as previously described, the cylinder has smaller volume than the cube, so any perturbation on the cylinder causes more damage than in the cube. However, the difference is not so high as predicted, mainly for the last case. For the pdDVH results, a symmetry between the negative and positive errors is seen, that is, the negative errors cause the same impact than the positive, presenting approximately the same mean dose difference values. The negative errors cause underdose, so the mean dose difference may be negative, and as the positive errors cause overdose, the mean dose difference may be positive. In the most results, mainly in the EPID results, this is confirmed.

Figures 4.12 (b), 4.13 (b) and 4.14 (b) show the relation between the random MLC errors and the relative mean dose for the three structures for all cases. However, the relation the larger the error, the larger the perturbations is not observed. Comparing the random error of 1 mm and random error of 5 mm the relation is observed, as seen in the DVH. However, comparing all the errors, many fluctuations in the mean dose difference values are seen, which means, it is complicated to understand which interferences the changed of the leaves position causes in the plans, when they move randomly. Despite larger errors will open more the leaves than the smaller errors, they also can close them, resulting in an equilibrium, and not causing many changes.

The pdDVH is also more sensitive in detect random MLC errors than 3DVH. In cube and cylinder, variations are observed, as expected, and in PTV many interferences of the errors are not observed, mainly in the pdDVH data, as also expected. In 3DVH data there is no significant variations in all structures.

Comparing dose difference analysis with gamma analysis, no correlation between them is seen. Gamma analysis results present approximately a proportionality between the errors and the %GP, whereas dose difference analysis present results with no relation between each other.

MU Errors

The MU error effects can also be detected in the mean dose difference. It is expected that the errors increase or decrease the mean dose linearly, so 2 and 4%. In this case the relative mean dose will also show if the deviations between reference and measured detected by the systems are equal to the errors introduced.

Figure 4.15, 4.16 and 4.17 show the effects of systematic MU errors described for 1 field, 2 fields and 4 fields, respectively, comparing the relative mean dose difference obtained by 3DVH and pdDVH.

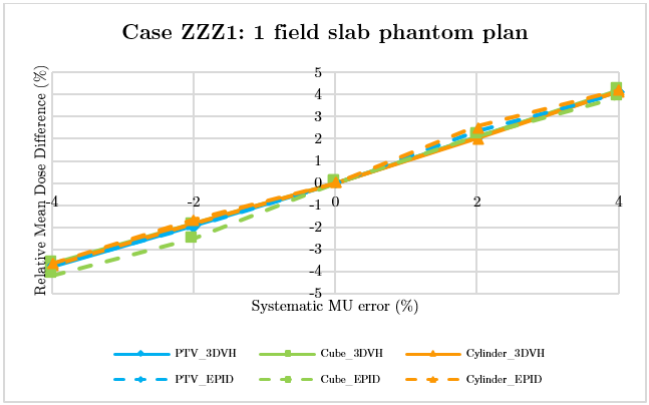

Figure 4.15: Relative Mean Dose Difference of PTV, Cube and Cylinder of the case ZZZ1, 1 field slab phantom plan. The data obtained by 3DVH is compared with the data from EPID obtained by pdDVH for the Systematic MU Errors.

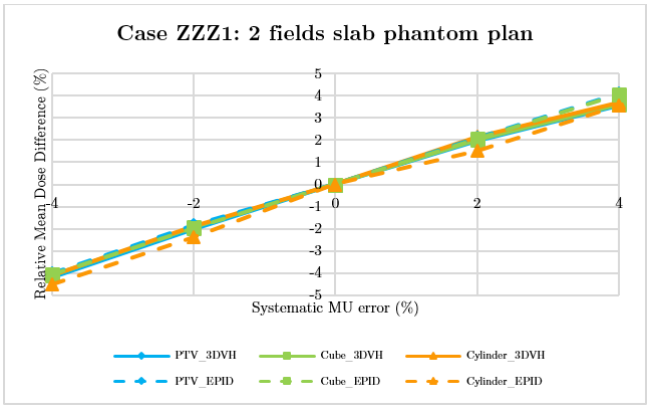

Figure 4.16: Relative Mean Dose Difference of PTV, Cube and Cylinder of the case ZZZ1, 2 fields slab phantom plan. The data obtained by 3DVH is compared with the data from EPID obtained by pdDVH for the Systematic MU Errors.

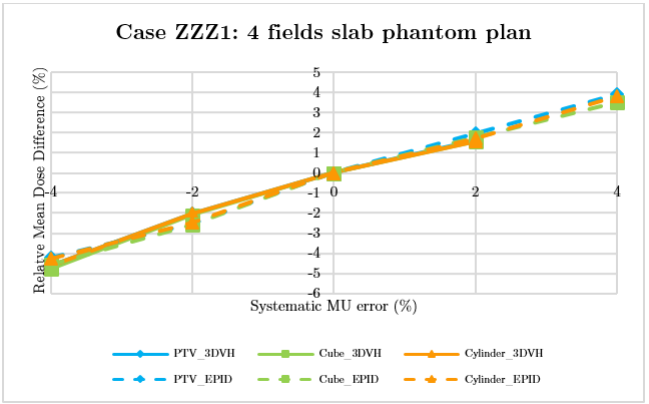

Figure 4.17: Relative Mean Dose Difference of PTV, Cube and Cylinder of the case ZZZ1, 4 fields slab phantom plan. The data obtained by 3DVH is compared with the data from EPID obtained by pdDVH for the Systematic MU Errors.

Figures 4.15, 4.16 and 4.17, show that the systems detect accurately the errors, because the relative mean dose obtained for all cases are approximately equal to the error introduction, that is, the deviations measured were the same as predicted. Thus, the dose value measured is approximately equal to the dose value predicted.

MU results are better than results of MLC errors. In all plans, linear straights are observed

for all structures, indicating a proportional relation between the error and the relative mean dose difference.

For all the plans, both systems demonstrate capabilities in the detection of the errors and show results very equals: the relative dose mean presents approximately the same value of the errors introduced; and the straight obtained are very linear, indicating the proportionality between the errors and the mean dose differences. A symmetry is also seen, which means, the negative errors cause the same effects that the positive errors. However, in the last plan, the negative errors cause approximately 1% more effects than the positive errors. Probably because the LINAC may deliver less dose and the high errors compensate this less. Despite some low deviations, the errors cause the same effects in the three structures for all cases, as expected. In 3DVH analysis, there is no value for the MU error of 4%, because the software did not perform this calculation.

It is also seen that the negative errors cause underdose, because the relative mean dose difference results indicate a reduction of 2 and 4%, as expected; and the positive errors cause overdose, that is, increase the dose delivery, because the relative mean dose difference results show that the dose increase 2 and 4%.

Comparing with gamma analysis, a lack of correlation is observed. This analysis shows that the negative and positive errors cause approximately the same effects in the plans that the positive errors and the gamma analysis presents that the positive errors cause more effects.

4.2 Patients Test

The second section describes the results relative to the patient tests. After the systems and software had been tested using the square fields tests and its predictions, in this section, they will be evaluated using the patient plans analysis.

In this case, it was not possible to predict quantitatively the results of MLC errors, just theoretically, because these cases are IMRT cases. However, for MU errors the predictions were possible. Once again, the data, with MLC and MU errors, and without errors were previously acquired by ArcCHECK and EPID and analysed with their respective software, SNC and Predose, and with 3DVH as well.

Gamma analysis and DVH analysis were used for dose distribution evaluation. In this case, DVH analysis were carried out only with 3DVH. The pdapp just can be used with data of measurements with patient and phantom, as described in the last chapter. For square fields test, it was possible to perform phantom measurements with errors, because a slab phantom was used. However, in the case of patients, *in vivo* measurements with errors were of course not possible. Thus, the pdDVH did not have the necessary data to create the respective DVHs.

As many data were acquired and it is impossible to show all of them, only one IMRT breast case and one VMAT prostate case will be analysed in detail in this section.

4.2.1 Comparison of Gamma Criterion

Gamma passing rate, for patient plans, was calculated using PreDose, SNC and 3DVH, the specific software to analyse the data from EPID and ArcCHECK measurements, respectively in order to

compare the performance of these software to obtain %GP. The gamma analysis was performed for both MLC and MU errors tests with the 3%/3mm criteria, 10% of dose threshold for 2D gamma analysis using PreDose and SNC (referred as ArcCHECK in the tables and graphs), and with the 3%/3mm criteria, 50% of dose threshold for 3D gamma analysis using 3DVH, and with 90% of acceptance threshold, which is clinically used.

MLC Errors

The MLC errors, which means, errors in the leaf position, affect the dose delivered to the patient. They increase or decrease the volume affected by the field and also its delivered dose quantity.

In the case of IMRT and VMAT treatments, the MLC moves while the dose is delivered. This allows to irradiate only the PTV with high dose, trying to spare as much as possible the surrounding organs. The planning is also done to avoid damages in these organs. When the MLC errors are introduced, the leaves open and close, depending on the error. Contrary to what occurs in square fields tests, dose inside the PTV is affected and it is expected that it is more affected than the organs at risk. It is also expected that the dose value decreases or increases with the volumes change, contrary to the square fields, where few changes in the dose delivered where seen. Once again, the larger (±3, ±2 mm) errors cause more effects than the smaller (±1, ±0.5 mm); and the negatives errors cause underdose, whereas the positive errors cause overdose.

Table 4.5 shows the effects of the MLC errors (systematic of ±3, ±2, ±1, ±0.5 mm and random of 1, 2, 3, 4 and 5 mm) in the %GP calculated by 3DVH, ArcCHECK and Predose. These data are the %GP mean, and respectively standard deviation, of the six patient that were tested.

Table 4.5: Mean and standard deviation of the Gamma Passing Rate (%γ<1) for the six patient cases tested for both systematic (sys) and random (ran) MLC errors.

%γ<1	3DVH	ArcCHECK	PreDose
Errors (%)	**Mean ± SD**	**Mean ± SD**	**Mean ± SD**
sys -3	46.1 ± 5.2	61.7 ± 9.4	28.6 ± 6.4
sys -2	64.4 ± 8.7	77.3 ± 9.9	58.0 ± 11.2
sys -1	94.7 ± 1.0	92.5 ± 4.7	85.4 ± 12.7
sys -0.5	99.1 ± 0.4	96.4 ± 1.3	93.1 ± 8.0
0	99.7 ± 0.1	97.2 ± 1.4	98.1 ± 2.7
sys 0.5	98.5 ± 0.2	93.4 ± 3.9	98.5 ± 1.0
sys 1	94.6 ± 2.5	83.6 ± 11.4	93.2 ± 4.7
sys 2	53.5 ± 9.8	54.0 ± 24.4	68.8 ± 10.6
sys 3	NA	35.1 ± 15.9	44.1 ± 8.9
ran 1	97.5 ± 3.1	96.3 ± 2.1	97.6 ± 2.9
ran 2	96.4 ± 4.8	95.5 ± 3.0	96.5 ± 3.1
ran 3	96.9 ± 3.9	93.2 ± 4.1	94.8 ± 5.4
ran 4	97.1 ± 3.6	91.7 ± 4.3	92.5 ± 6.8
ran5	92.8 ± 12.5	87.6 ± 4.8	92.0 ± 3.5

Looking at Table 4.5 it is possible to observe the effects of the errors in the %GP calculated by all the systems, which means, they detect the presence of the both MLC errors. Larger errors cause more effects than the smaller and the %GP without errors is quite good. In random

errors, their effects are also observed and they increase with the large error as well, but in small intensity than seen in systematic errors. Their results are above the acceptance threshold, unless for random error of 5 mm of ArcCHECK measurements (87.6 ± 4.8%), which means, these errors are less relevant for the treatment. It is not possible to understand if the errors cause underdose or overdose, just looking at the %GP value. It is necessary to look at the dose maps of the field provided by the software used.

Comparing the results obtained by the three systems, it is possible to observe some differences between 3DVH and ArcCHECK. It can be justified by the explanations referred to in the Square Fields Test Section (subsubsection 4.1.1), such as for the 3DVH analysis, a dose threshold different from the one used with ArcCHECK analysis was adopted, because 3DVH provides a 3D gamma analysis and ArcCHECK provides a 2D gamma analysis. The PreDose, in systematic errors, shows more sensibility in negative errors than in positive errors, resulting in an asymmetry, as seen in square fields errors. Again, it can be related with the threshold chosen and with the different systems used, that can react in a different way. Even without errors, PreDose detects less dose than is planned and it also takes into account the output variations of the LINAC, unlike ArcCHECK. Therefore, the positive errors may correct the dose delivery system and present better %GP than negative errors and even the reference situation.

For the systematic error of 3 mm there are no results, because 3DVH did not work for all the patient plans with large deviations. It did not work for other points in VMAT patient plans, such as systematic errors of -3, 2, and 3 mm. The 3DVH detects many deviations in VMAT plans, being more difficult than for the system to calculate VMAT plans than IMRT plans, because the VMAT is a treatment with more parameters (for instance related with gantry rotation) than IMRT.

Once again, Figures 4.18 and 4.19 are an illustrative example , that is, they show the %GP obtained with 3DVH, SNC and PreDose just for two patient cases, one IMRT breast patient and one VMAT prostate patient. Figures 4.18 (a) and 4.19 (a) show the %GP of systematic errors and Figures 4.18 (b) and 4.19 (b) show the %GP of random errors.

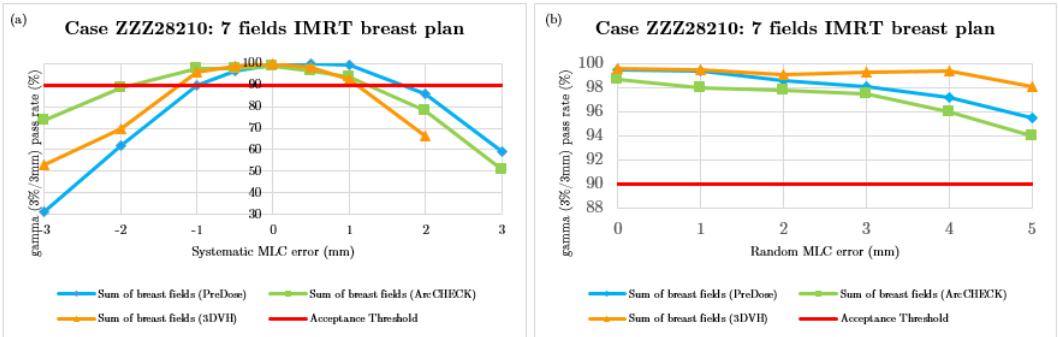

Figure 4.18: Gamma Passing Rates as function of MLC errors for the case of the patient ZZZ28210, 7 fields IMRT breast plan. The analysis was done for 3%/3mm criteria and 10% of dose threshold for PreDose and ArcCHECK; and for 3%/3mm criteria and 50% of dose threshold for 3DVH, with 90% as acceptance threshold.

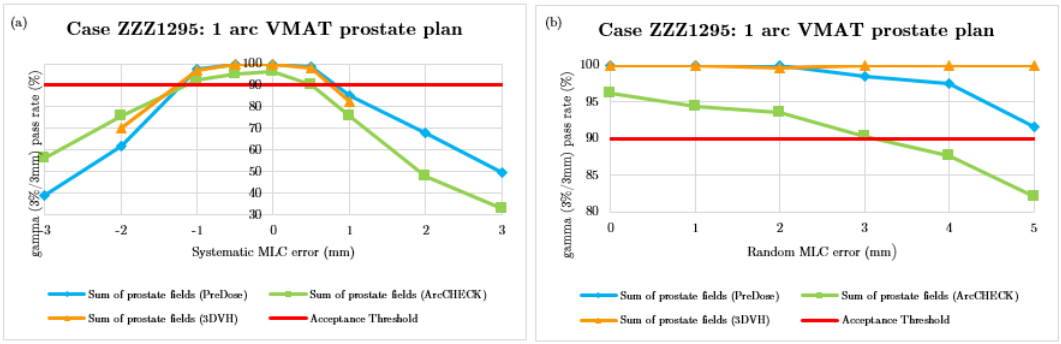

Figure 4.19: Gamma Passing Rates as function of MLC errors for the case of patient ZZZ1295, 1 arc VMAT prostate plan. The analysis was done for 3%/3mm criteria and 10% of dose threshold for PreDose and ArcCHECK; and for 3%/3mm criteria and 50% of dose threshold for 3DVH, with 90% as acceptance threshold.

Looking at Figures 4.18 and 4.19, it is possible to see the effect of all MLC errors in the patient plans through the %GP, as seen in Table 4.5; and again, the consequences of them are seen more clearly for the larger errors than for the smaller, in both patient plans.

For systematic errors, the ArcCHECK and 3DVH present many similarities in the first plan (Figure 4.18 (a)). The PreDose shows once again, more sensibility for the negative errors in both plans. On the other hand, the ArcCHEK and 3DVH show more sensibility for the positive errors, which means, the systems show different asymmetries. In the second plan (Figure 4.19 (a)), 3DVH could not calculate three plans of the ZZZ1295 patient case, correspondents to the systematic errors of -3, 2 and 3 mm.

For random errors, the ArcCHECK and PreDose show some similarities for the first patient plan (Figure 4.18 (b)). Few significant effects of the random errors are observed in the first plan. Unlike in the last one, in the second plan (Figure 4.19 (b)), more consequences are detected, mainly with the ArcCHECK. 3DVH does not detect any effects in the second plan, being constant. Probably, this is due to the fact that for IMRT and VMAT there are so many segments that the effect of random leaf errors will generally cancel out.

MU Errors

The MU errors cause changes in the patient plans, as well. Modifying the MU value, the dose delivered to the patient increases or decreases, depending on the error magnitude, which means, the dose is directly affected. As the MUs are directly related with the dose, all the dose of the field is affected, as in the square fields tests.

Table 4.6 shows the effects of the MU errors in six patient fields. It is possible to observe the mean %GP, and its respective standard deviation, calculated by 3DVH and SNC, using ArcCHECK measurements and PreDose, using EPID measurements, for each MU error (±4 and ±2%).

Table 4.6: Mean and standard deviation of the Gamma Passing Rate (%γ<1) for the six patient cases tested for MU errors.

%γ<1	3DVH	ArcCHECK	PreDose
Errors (%)	Mean ± SD	Mean ± SD	Mean ± SD
-4	79.6 ± 6.6	93.7 ± 1.5	71.3 ± 7.2
-2	96.1 ± 2.4	97.2 ± 1.4	89.0 ± 7.6
0	98.2 ± 2.2	97.4 ± 1.9	96.7 ± 4.4
2	92.4 ± 6.6	94.8 ± 3.2	97.4 ± 2.8
4	70.5 ± 9.0	87.3 ± 6.8	92.7 ± 8.2

Looking at Table 4.6 and comparing the systems, the positive errors affect more than the negative errors in 3DVH and ArcCHECK. PreDose keeps to be sensitive to negative errors. Once again, this is caused by underdose already present in the plan without errors, possibly caused by the outputs variations of the LINAC and that is taken into account by the PreDose.

Figures 4.20 and 4.21 show the relation between the MU errors and the %GP only for two examples of the six treatment plans measured previously analysed for MLC errors as well.

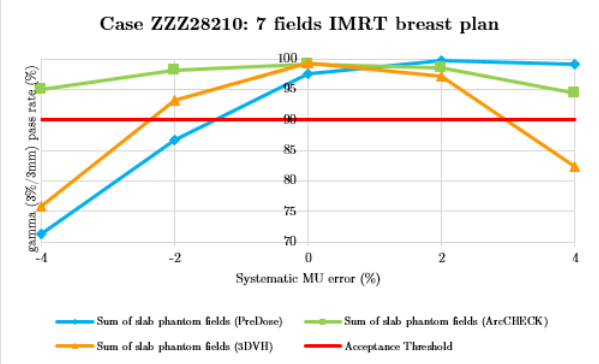

Figure 4.20: Gamma Passing Rates as function of Mu errors for the case of the patient ZZZ28210, 7 fields IMRT breast plan. The analysis was done for 3%/3mm criteria and 10% of dose threshold for PreDose and ArcCHECK; and for 3%/3mm criteria and 50% of dose threshold for 3DVH, with 90% as acceptance threshold.

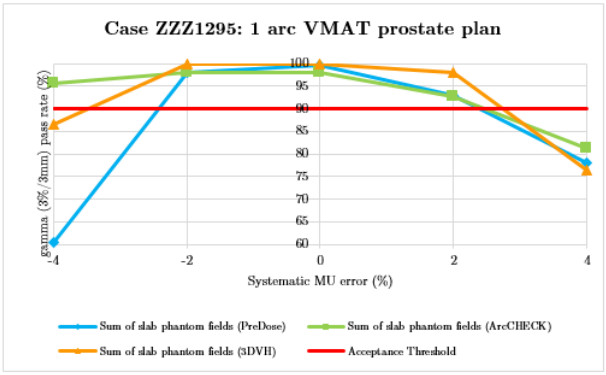

Figure 4.21: Gamma Passing Rates as function of MU errors for the case of patient ZZZ1295, 1 arc VMAT prostate plan. The analysis was done for 3%/3mm criteria and 10% of dose threshold for PreDose and ArcCHECK; and for 3%/3mm criteria and 50% of dose threshold for 3DVH, with 90% as acceptance threshold.

Figures 4.20 and 4.21 show the same effects of the MU errors in the patient plans seen in the Table 4.6. For both patient plans the errors are detected. Larger errors (±4%) cause more relevant

effects in the plans. On the other hand, the smaller errors (±2%) do not cause significant effects, its %GP are above the acceptance criteria.

In the first plan, a symmetry is approximately observed for ArcCHECK. 3DVH and the PreDose show an asymmetry with more deviations detected in negative errors. For the second plan, ArcCHECK and 3DVH detect more deviations for the positive errors comparatively to the negative ones and the PreDose detects the opposite.

4.2.2 Analysis of DVHs

DVHs showed to be an accurate and powerful tool for dose evaluation in the square fields test. In this subsection, its performance in detecting MLC and MU errors will be tested for patient plans.

As described previously, this analysis will be done just using data from 3DVH for two patient plans, one IMRT breast plan and one VMAT prostate plan, also used in the gamma analysis. For the first case, DVHs for PTV and the most important organs at risk, heart and lung (in this case the left lung, because it is a treatment of a breast left cancer) were obtained. For the second case, DVHs for PTV, bladder and rectum were also obtained.

MLC Errors

The MLC errors were also detected in the DVH analysis. In Figure 4.22, the comparison between the planned data, from Monaco and the measured data from ArcCHECK and calculated with 3DVH is observed.

Figures 4.23, 4.24, 4.25 and 4.26 present the DVH for each structure of the plans with errors. The first two figures correspond to the IMRT breast plan; and the last two figures correspond to the VMAT prostate plan.

DVHs of the structures affected by the systematic errors of ± 2 mm for the first patient plan, the DVHs of the ones affected by the systematic errors of ± 1 mm for the second patient plan, and the DVHs of the structures affected by the random errors of 1 and 5 m for both plans will be presented. The 3DHV did not calculate the DVHs of systematic errors of ± 3 mm for the IMRT plan and the DVHs of systematic errors ±3 and ± 2 mm for the VMAT plan.

The comparison is done between the reference, which is the error-free data, and the measured, which is the error data measured with ArcCHECK. It allows to compare the data without errors with the data with errors and see the deviation between them and what occurs when a MLC error is introduced. All the data was analysed by the 3DVH.

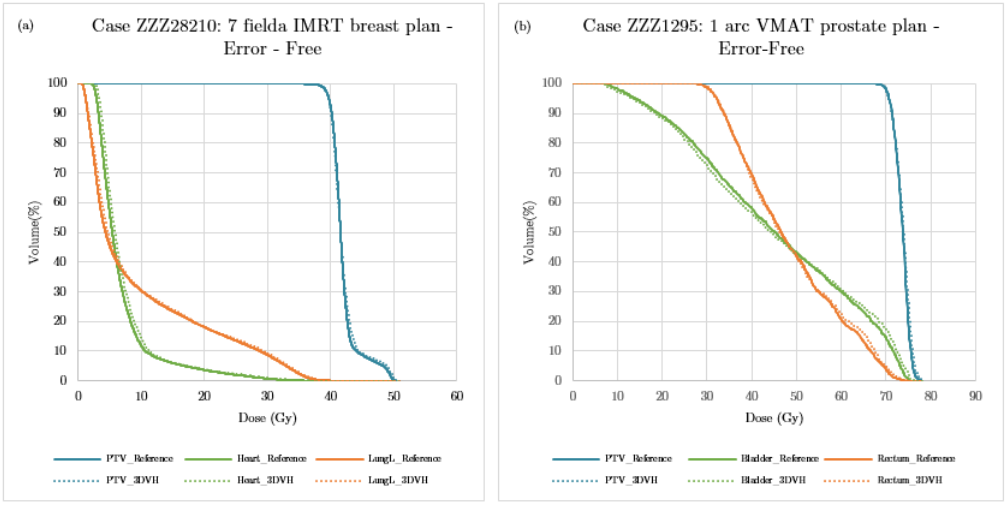

Figure 4.22: DVHs of the structures, PTV and organs at risk, of the two patient cases, ZZZ28210 and ZZZ1295, Error-Free. (a) corresponds to the ZZZ28210, 7 fields IMRT breast plan and (b) corresponds to ZZZ1295, 1 arc VMAT prostate plan. The reference data, obtained by Monaco, is compared with the measured data without errors acquired by the ArcCHECK and analysed with 3DVH.

Looking at Figure 4.22, some differences between the Monaco reference and the measured are observed. Just small deviations are seen, meanly in the organs art risk. However, they are not very relevant, which means that the treatment is able to be performed.

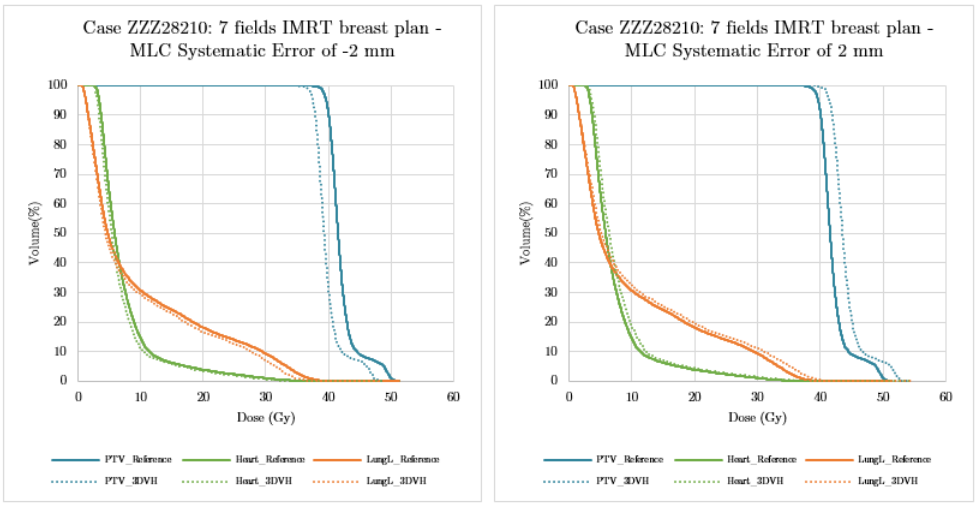

Figure 4.23: DVHs of the structures, PTV, Heart and Left Lung, of the patient case ZZZ28210, 7 fields IMRT breast plan, MLC Systematic Errors. (a) corresponds to systematic errors of -2 mm, and (b) corresponds to systematic errors of 2 mm. The reference data, i.e. the error-free data, is compared with the measured data with errors acquired by the ArcCHECK and analysed with 3DVH.

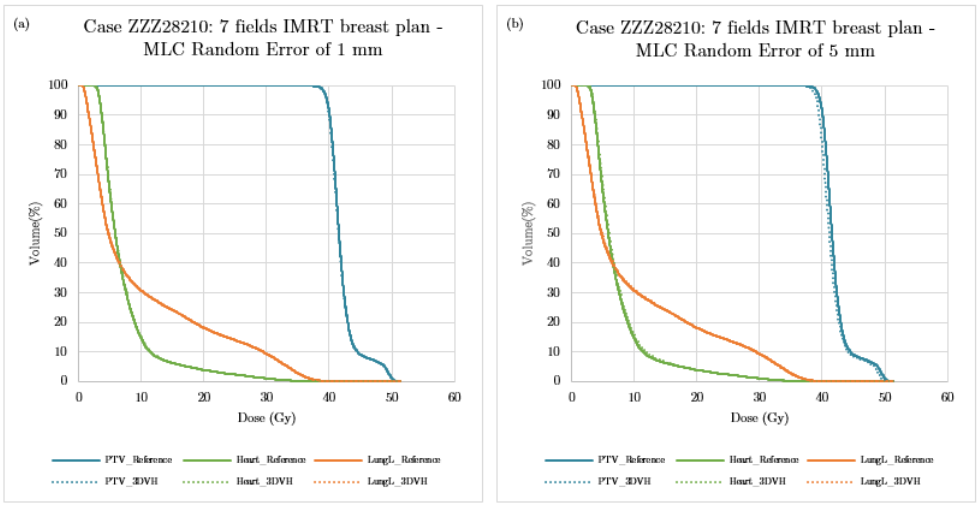

Figure 4.24: DVHs of the structures, PTV, Heart and Left Lung, of the patient case ZZZ28210, 7 fields IMRT breast plan, MLC Random Errors. (a) corresponds to random errors of 1 mm, and (b) corresponds to random errors of 5 mm. The reference data, i.e. the error-free data, is compared with the measured data with errors acquired by the ArcCHECK and analysed with 3DVH.

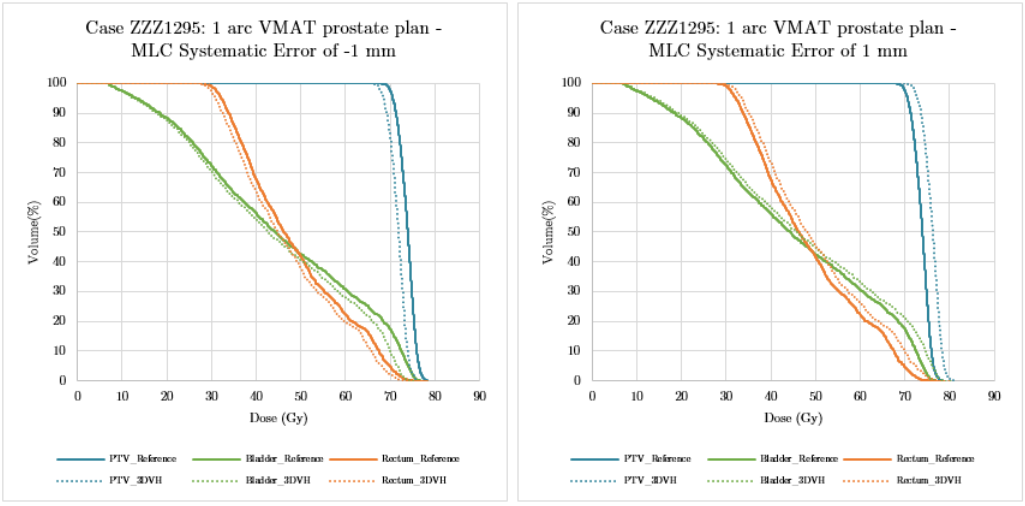

Figure 4.25: DVHs of the structures, PTV, bladder and rectum, of the patient case ZZZ1295, 1 arc VMAT prostate plan, MLC Systematic Errors. (a) corresponds to systematic errors of -1 mm, and (b) corresponds to systematic errors of 1 mm. The reference data, i.e. the error-free data, is compared with the measured data with errors acquired by the ArcCHECK and analysed with 3DVH.

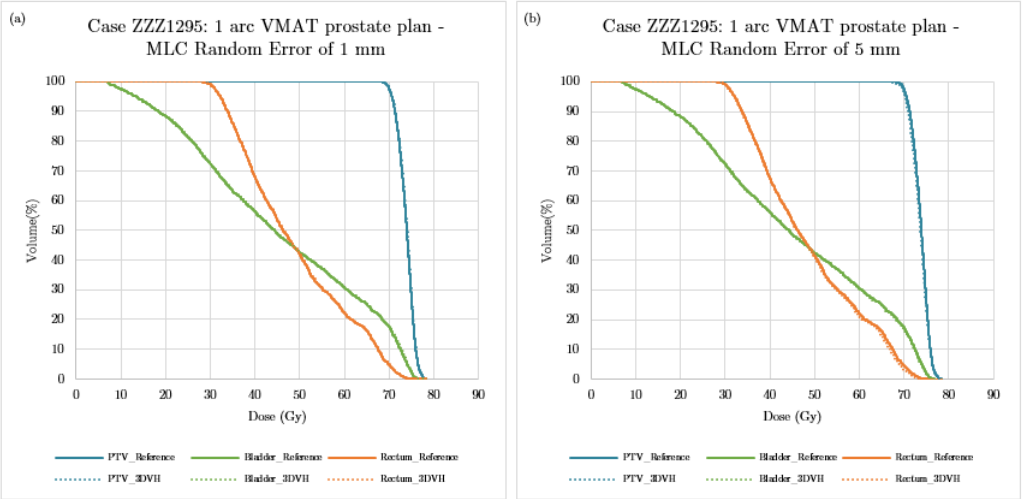

Figure 4.26: DVHs of the structures, PTV, Bladder and Rectum, of the patient case ZZZ1295, 1 arc VMAT prostate plan, MLC Random Errors. (a) corresponds to random errors of 1 mm, and (b) corresponds to random errors of 5 mm. The reference data, i.e. the error-free data, is compared with the measured data with errors acquired by the ArcCHECK and analysed with 3DVH.

The previous figures (Figures 4.23, 4.24, 4.25 and 4.26) show the expected effects caused by the introduction of the MLC errors in the patient plans.

In theory, the negative systematic errors cause underdose in the patient, which means, reduces the dose delivered. It is reflected by the movement of the DVH to the left, comparing with the reference. On the other hand, the positive systematic errors cause overdose, which means, increase the dose delivered. This effect is seen by the movement of the DVH to the right, comparing with the reference.

Both negative and positive systematic errors cause deviations between the reference and measured data, and are approximately the same. These deviations are more clear in PTV than in organs at risk, mainly for the IMRT patient. The deviations caused by the negative errors are detected, because the maximum dose decreases, so the DVH moves to the left. The effects of the positive errors increase the dose and the DVH moves to the right, as expected. Unlike gamma analysis, relevant difference between the negative and the positive errors is not observed, they cause approximately the same effect in the plans.

In the case of random errors, any relevant effects are not observed, in both plans. There are some differences between the plan with systematic errors of 5 mm and with systematic errors of 1 mm, but very smooth. Unlike this, the gamma analysis shows some differences, mainly the data from SNC. As described in square fields, the random errors do not affect the treatment plans, because the leaves move in a randomly way and this movement can cancel itself, not affecting too much the dose in the different volumes.

Thus, this analysis allows to understand if the plan is appropriate for the treatment, but also informs how the errors affect the structures and which ones are affected. DVH gives more clinically relevant information than gamma analysis. However, this analysis was obtained with 3DVH, which was not effective in detecting the MLC errors in square fields plans, presenting less accurate results. However, since there is no an alternative measurement or predictions yet, these results may not be very reliable.

MU Errors

The perturbations of the MU errors can also be detected by the DVH. Following figures (Figures 4.27, 4.28 and 4.29) show the respective DVH of each structure. The first two are of breast plan and the last two are of prostate plan. For both plans, the DVHs of MU errors of ±4 and ±2% will be analysed.

Figure 4.27 presents the deviations between the reference, data from Monaco, and the measured, which is the measurements data from the two patient plans without errors. As in the square fields tests, the reference case was repeated for MU errors, because these measurements were performed several months later.

Figures 4.28 and 4.29 present the DVH of each structure for the two patient cases in analysis, allowing the comparison between the reference and the measured. The reference data is the error-free data and the measured data is the data with the errors measured by the ArcCHECK. All the data was analysed by the 3DVH.

The first comparison allows to observe the usual errors of the dose delivery system and the second comparison allows to take into account only the effect of the errors.

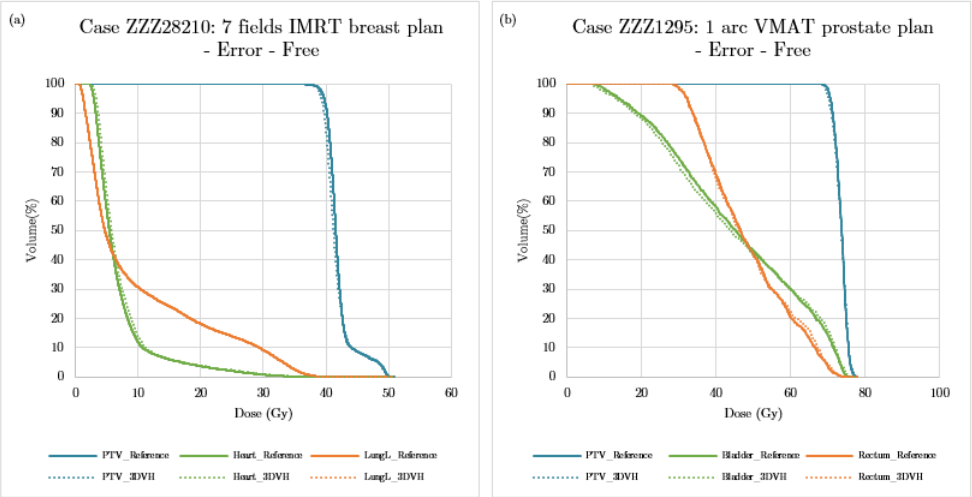

Figure 4.27: DVHs of the structures, PTV and organs at risk, of the two patient cases, ZZZ28210 and ZZZ1295, Error-Free. (a) corresponds to the ZZZ28210, 7 fields IMRT breast plan and (b) corresponds to ZZZ1295, 1 arc VMAT prostate plan. The reference data, obtained by Monaco, is compared with the measured data without errors acquired by the ArcCHECK and analysed with 3DVH.

Looking at Figure 4.27, it is possible to observe some differences between the reference and the measured. Small deviations are observed, indicating an underdose, mainly in PTV for the first plan and the organs at risk for the VMAT plan. However, they are not very relevant, which means that the treatment is able to be performed.

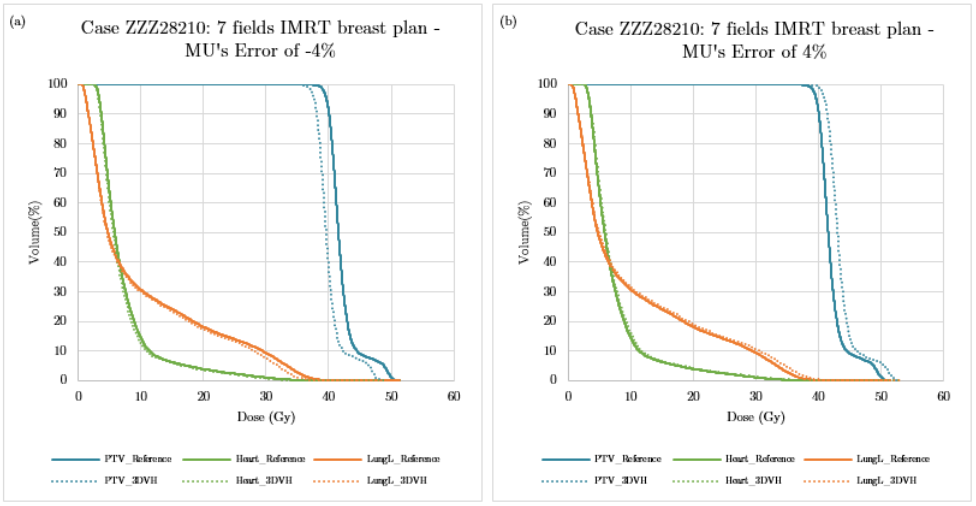

Figure 4.28: DVH of the structures, PTV, Heart and Left Lung, of the patient case ZZZ28210, 7 fields IMRT breast plan, MU errors. (a) corresponds to MU errors of -4%, and (b) corresponds to MU errors of 4%. The reference data, i.e. the error-free data, is compared with the measured data with errors acquired by the ArcCHECK and analysed with 3DVH.

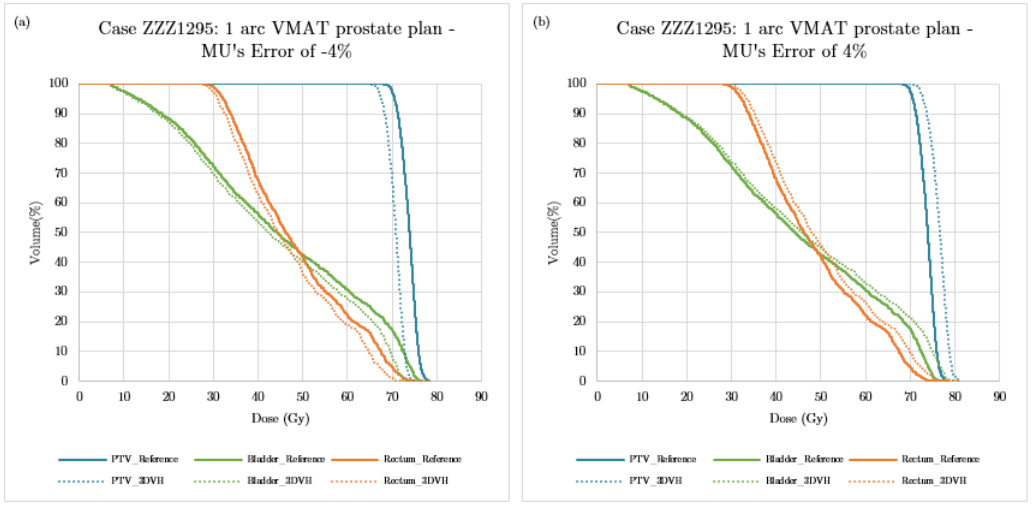

Figure 4.29: DVH of the structures, PTV, Bladder and Rectum, of the patient case ZZZ1295, 1 arc VMAT prostate plan, MU errors. (a) corresponds to MU errors of -4%, and (b) corresponds to MU errors of 4%. The reference data, the error-free data, is compared with the measured data with errors acquired by the ArcCHECK and analysed with 3DVH.

Unlike the analysis obtained for MLC errors, it is expected that the MU errors results are more reliable than the MLC errors results, because the square fields tests indicated better results for the MU errors analysis. It is also expected that the errors affect all the structures in the same way, because these errors interfere in the dose delivered to the field, which contains the PTV and also the organs at risk.

For both plans (Figures 4.28 and 4.29) more deviations between the reference and the measured in negative errors than in positive errors are observed. However, in the VMAT plan, the deviations between the reference and measured are more smooth. Figure 4.27 presents an underdose, which means the LINAC delivers less dose than it was planned, because the leaves might be more closed. Therefore, the positive errors can cause less effects that the negative errors.

The PTV DVH shows more deviations between the reference and the measured than the other structures, mainly for the first plan, which was not the expected. The negatives errors affect the maximum dose detected, which means, it decreases, and the DVH move to the left. Contrary, the positive errors increase the dose delivered to the patient. Thus, the maximum dose seen in the DVH will also increase, which means, the DVH moves to the right.

4.2.3 Comparison of Relative Mean Dose Difference

Analysing the mean dose of the structures is also an important evaluation of the effect of the errors. It is a helpful analysis obtained from DVH analysis. This consists in analysing the difference between the measured data (data with errors) and the reference data (error-free data). This difference is presented in this subsection as the relative mean dose difference.

This analysis was performed for the six patient plans, using the 3DVH, for the MLC errors and MU errors, and, in this subsection, all the results are presented.

MLC Errors

The MLC errors are also detected by analysing the mean dose difference, because, in the case of IMRT and VMAT patient plans, the MLC errors affect more the delivered dose to the patient than in the case of square fields tests.

Figures 4.30 to 4.35 show these effects in PTV and in organs at risk of the six patients analysed.

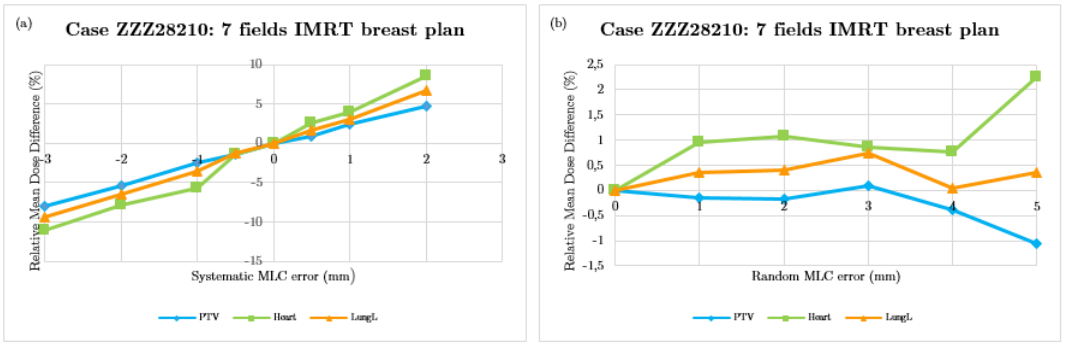

Figure 4.30: Relative Mean Dose Difference of PTV, Heart and Left Lung of the case ZZZ28210, 7 fields IMRT breast plan, MLC Errors, obtained by 3DVH. (a) corresponds to Systematic Errors and (b) corresponds to Random Errors. The scale of both graphs is different.

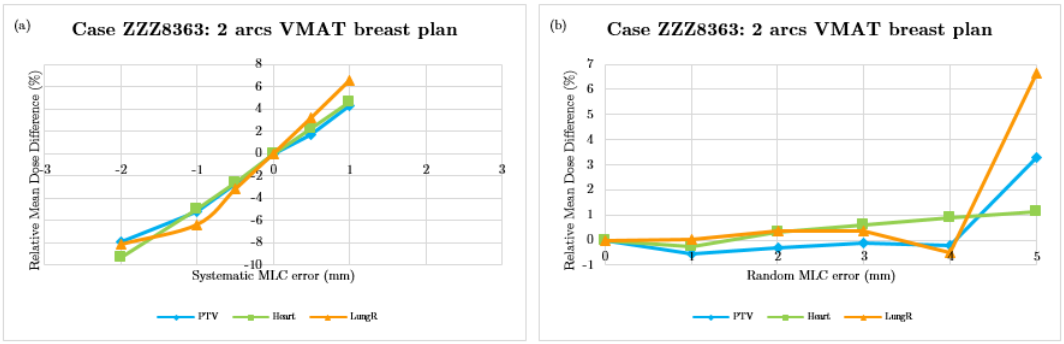

Figure 4.31: Relative Mean Dose Difference of PTV, Heart and Right Lung of the case ZZZ8363, 2 arcs VMAT breast plan, MLC Errors, obtained by 3DVH. (a) corresponds to Systematic Errors and (b) corresponds to Random Errors. The scale of both graphs is different.

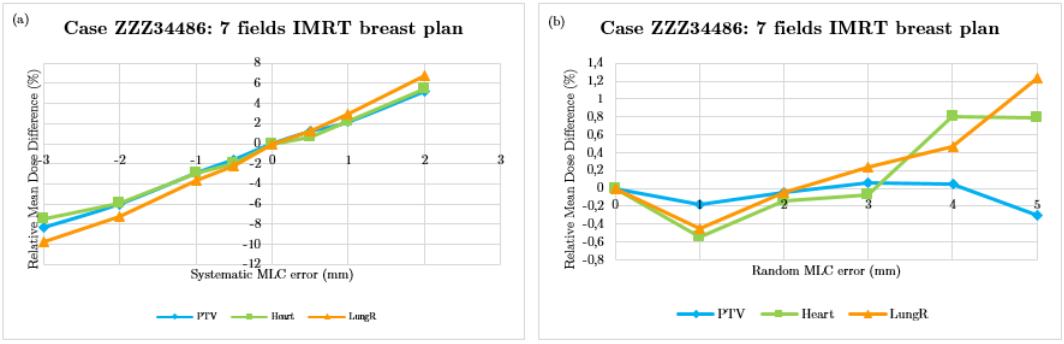

Figure 4.32: Relative Mean Dose Difference of PTV, Heart and Right Lung of the case ZZZ34486, 7 fields IMRT breast plan, MLC Errors, obtained by 3DVH. (a) corresponds to Systematic Errors and (b) corresponds to Random Errors. The scale of both graphs is different.

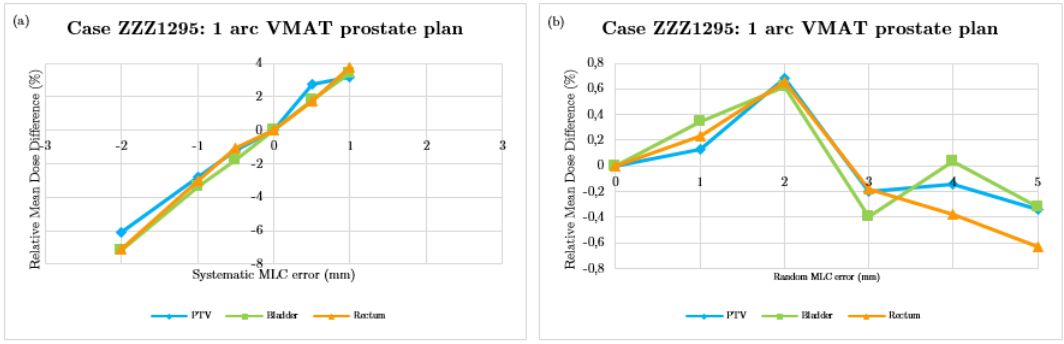

Figure 4.33: Relative Mean Dose Difference of PTV, Bladder and Rectum of the case ZZZ1295, 1 arc VMAT prostate plan, MLC Errors, obtained by 3DVH. (a) corresponds to Systematic Errors and (b) corresponds to Random Errors. The scale of both graphs is different.

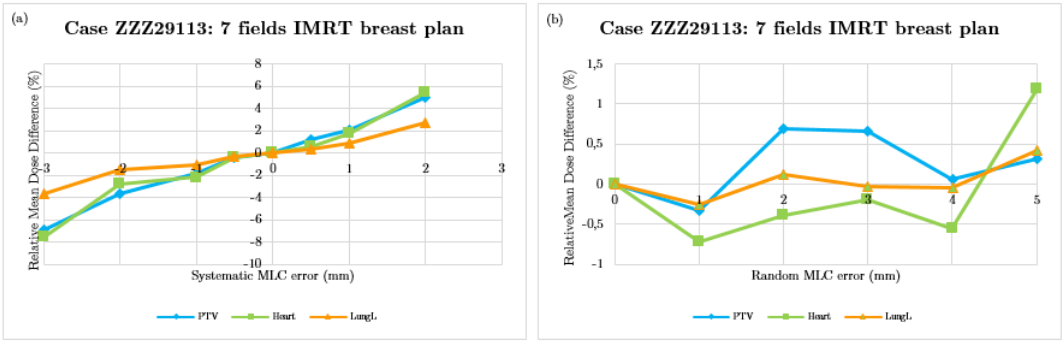

Figure 4.34: Relative Mean Dose Difference of PTV, Heart and Left Lung of the case ZZZ29113, 7 fields IMRT breast plan, MLC Errors, obtained by 3DVH. (a) corresponds to Systematic Errors and (b) corresponds to Random Errors. The scale of both graphs is different.

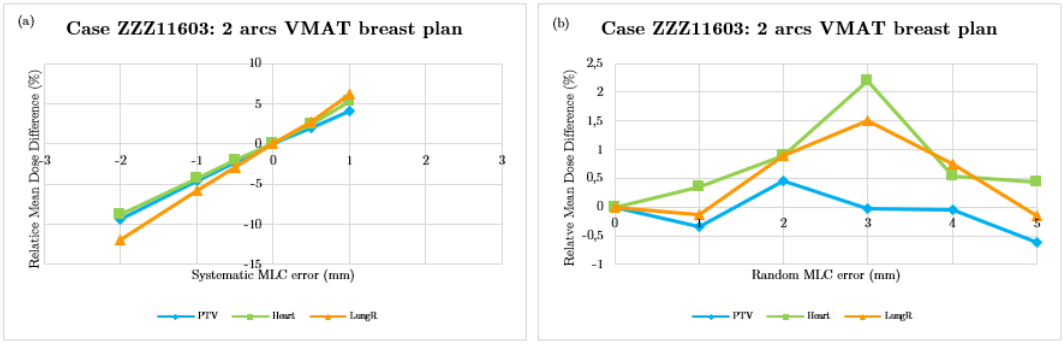

Figure 4.35: Relative Mean Dose Difference of PTV, Heart and Right Lung of the case ZZZ11603, 2 arcs VMAT breast plan, MLC Errors, obtained by 3DVH. (a) corresponds to Systematic Errors and (b) corresponds to Random Errors. The scale of both graphs is different.

In the systematic errors (Figures 4.30 (a) to 4.35 (a)), for all plans few deviations between PTV and the other structures are observed. It was expected that the PTV would be most affected by the errors, but this is not the case.

In all plans, a symmetry is observed, which means, the positive errors cause approximately the same effects that the negative errors, being the relative mean dose differences of the structures approximately the same, in module, for all situations. It is also noticed that different plans can be more or less sensitive to the same systematic leaf error: for ZZZ34486 a 2 mm errors causes a 5-6% mean dose difference, whereas for ZZZ11603 this would be about 10%. This might be due to a different number of segments (i.e. control points) used in the treatment plans, that is, the more segments, the larger the dose deviation. 3DVH did not calculate DVH and mean doses for the systematic errors of 3 mm of IMRT plans and for systematic errors of -3, 2 and 3 mm of VMAT plans, which is a disadvantage.

Looking at the random error results (Figures 4.30 (b) to 4.35 (b)), there is no relation between errors and dose for all plans, that is, larger errors do not cause more perturbation than smaller. Once more, it is proven that these errors do not cause many relevant effects in the treatment plans. There is also no seen any correlation between the gamma analysis and DVH analysis. In the gamma analysis, the random errors, mainly the larger, cause the higher perturbations and a relation between the error and the %GP is seen.

MU Errors

The MU errors also interfere with the dose delivered to the patient. As carried out in square fields tests, this analysis allows to predict if the system is efficient in detecting the errors. It is expected that the all mean PTV doses increase or decrease with 2 and 4%, i.e. once again a linear relation between the MU error and dose. Therefore, the relative dose difference obtained for the plans with errors should be the same that the error introduced.

Figures 4.36 to 4.41 show the effects of these errors in the PTV and in the organs at risk of all patient cases.

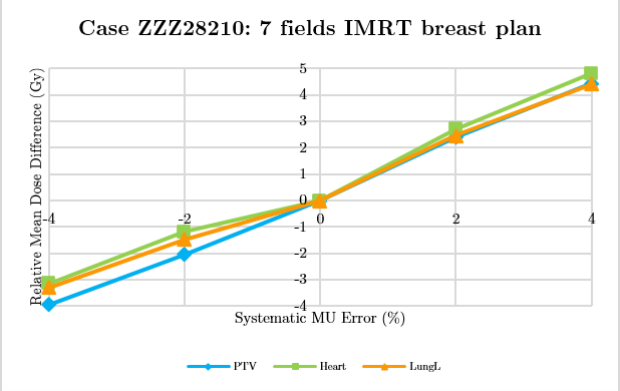

Figure 4.36: Relative Mean Dose Difference of PTV, Heart and Left Lung of the case ZZZ28210, 7 fields IMRT breast plan, MU Errors, obtained by 3DVH.

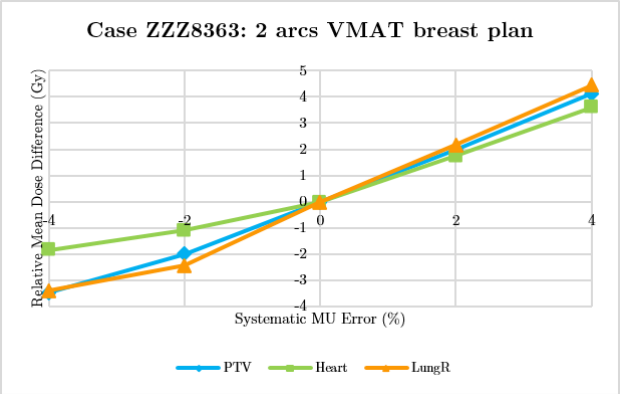

Figure 4.37: Relative Mean Dose Difference of PTV, Heart and Right Lung of the case ZZZ8363, 2 arcs VMAT breast plan, MU Errors, obtained by 3DVH.

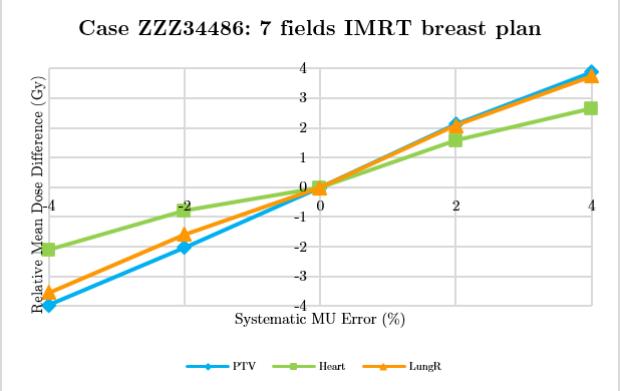

Figure 4.38: Relative Mean Dose Difference of PTV, Heart and Right Lung of the case ZZZ34486, 7 fields IMRT breast plan, MU Errors, obtained by 3DVH.

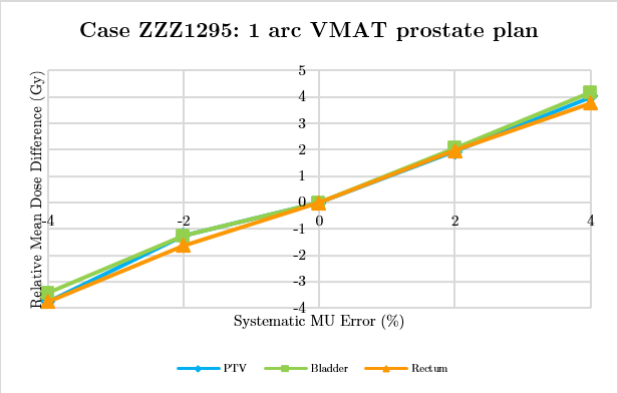

Figure 4.39: Absolute Mean Dose Difference of PTV, Bladder and Rectum of the case ZZZ1295, 1 arc VMAT prostate plan, MU errors, obtained by 3DVH.

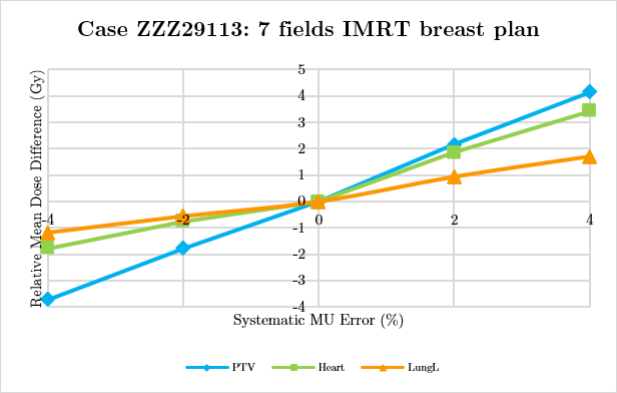

Figure 4.40: Relative Mean Dose Difference of PTV, Heart and Left Lung of the case ZZZ29113, 7 fields IMRT breast plan, MU Errors, obtained by 3DVH.

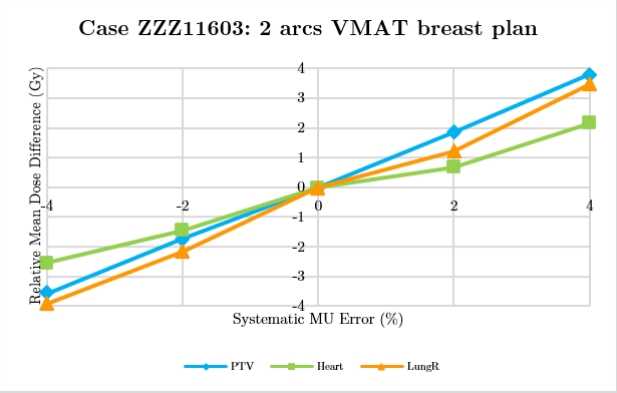

Figure 4.41: Relative Mean Dose Difference of PTV, Heart and Right Lung of the case ZZZ11603, 2 arcs VMAT breast plan, MU Errors, obtained by 3DVH.

Looking at Figure 4.39, it is possible to see that the ZZZ1295 patient plan obtained relative mean dose difference many close to the MU errors, that is, for this plan the system was effective in detecting the errors. For this plan is also observed that the structures are affected in the same way and there is a proportionality between the errors and the relative mean dose difference, obtaining more values for the large errors. A symmetry between the negative and positive errors is also seen, that is both negative and positive errors cause approximately the same perturbations, as

seen in the DVH. These results do not correlate with the ones obtained in gamma analysis with PreDose and ArcCHECK, which show an asymmetry between the negative and positive errors.

The other patient plans (Figures 4.36,4.37, 4.38 and 4.41) also present straight lines, that is the larger the error, the worse the perturbation caused by the errors in the plan. ZZZ28210, ZZZ8363, ZZZ34486 and ZZZ11693 patient cases show mainly differences between the structures in negative errors and also in positive errors, where in the heart, the predictions are not observed, unlike in the other two structures, where the relative mean differences are approximately equal to errors value.

In ZZZ29113 results (Figure 4.40), the predictions are equal to the errors introduced just for the PTV and heart in the negative errors. The LungL does not suffer relevant perturbations. The fact that the OARs show less steep relation between the error and mean dose probably has to do with the fact that, in contrast to the PTV, these organs are partly outside the treatment beams: increasing the MU will therefore not increase the dose in these parts and mean dose increase will be less than the MU increase.

4.3 Errors

In general, there are some factors that may have affected the results. Beside normal differences between the systems that will interfere with the results, there are some external factors that can also perturb the data such as:

- Interlocks: During the measurements, the LINAC system has many moments that it stops to deliver dose. This should not affect the treatment, because, after restarting, it delivers all the dose. However, when it occurs many times during one measurement, it may interfere in the way how the system acquired the dose.
- Couch interferences: When the dose is delivered between 90° and 270°, the couch is between the dose source and the dose acquiring system, absorbing some dose.
- Discretization errors: For square fields, in the DVHs, some fluctuations are seen, which can be related with the existence of points that do not calculate dose.

CHAPTER 5

Conclusion

As mentioned at the beginning of this study, in the last years, a great growth and development in the radiotherapy treatment was observed, due to the rapid advance of new, accurate and improved technology. This changed completely the way radiotherapy is planned and performed. Subsequently, a new way to perform the QA of the treatment had to be conceived, that responded accurately to all these new enhancements, in order to provide the patient with the best treatment possible.

The patient-specific QA is an important step during the treatment preparation. It assures the quality of the treatment, allowing to understand whether or not that treatment is the correct one to be administered to the patient. It consists of a measurement, which simulates the treatment, and of a comparison between the plan, performed by the TPS, and the measurement data, in order to see if there are differences and errors to overcome.

The dose evaluation in the QA has been performed by the gamma analysis for many years. This metric uses both dose and spatial criteria to analyse the dose differences. However, many recent studies have shown incoherencies, poor accuracy, sensitivity, and specificity of this method. This study, in its turn, also showed this lack of accuracy and relevant information. In effect, the main goal of this study was to test a new way to perform dose distribution evaluation, DVH, which might replace the gamma analysis in the QA process.

Our study was carried out at the Champalimaud Foundation, where the QA is performed using ArcCHECK, as the phantom/dosimeter to acquire dose, and using its specific software, which applies the gamma analysis to make the dose distribution evaluation. We wanted to implement a new way to perform dose evaluations using the DVH, a graph that illustrates the dose distribution in a structure per volume, using the 3DVH, a software compatible with ArcCHECK. The capacity of EPID dosimetry to calculate DVHs was tested too. To test this, MLC errors and MU errors were introduced in open square fields plans and in patient plans to compare both methods and both systems.

By comparing the gamma method with the DVH analysis, this study proved that the gamma analysis is not the best dose evaluation method to use in QA, being limitative and incoherent. It analyses point to point dose difference and distance and considers any point, taking into account the criteria used; and if there are a lot of points in accordance with the gamma criteria chosen in irrelevant structures, they will affect the evaluation and hide significant errors in regions

clinically important or showing errors where they do not really exist. These effects were seen in the square field tests and in the patient tests. In the cases where the gamma analysis did not show errors, when they effectively existed, it was possible to see, by looking at the DVH, deviations between the reference and the measured data, that is, a lack of correlation between gamma analysis and DVH analysis was observed. The other problem is related with the small amount of information provided by this method. It merely gives a value that either accepts or rejects the treatment, and the software also shows dose profiles and a dose map of the field with the fail and pass points. However, these points are not placed in and related with the patient CT, which means, it does not provide information about which regions are affected and it does not provide information directly related with the dose delivered as well. It is also very complicated to decide which criteria should be chosen. As mentioned in the Chapter 2 (subsubsection 2.3.2), 3%/3mm criteria and 10% as dose threshold criterion are the most clinically used. However, it depends on what type of evaluation is required. The dose threshold is related with the maximum planned dose, instead of the measured dose, because the measured dose has many oscillations. However, relevant points can be out of the area analysed and are not taken into account, because only the points that pass the threshold are analysed in the measured plan.

DVH analysis comes as an answer to overcome these disadvantages and limitations. It provides information about the dose distribution in a structure per volume, i.e. the dose evaluation is individual and specific to each organ. Both square field tests and patient tests showed good results in the DVH analysis. Two correlations were observed: one between the errors and the expected DVH and the other one between the errors and the dose mean differences. Thus, it gives more clinically relevant information to decide whether to accept or reject the plan and the dose evaluation is significantly more complete. However, there are some doubts about which dose constraints should be analysed. There are specific dose constraints for each structure used in the planning, that can be an option. However, there are external factors, such as the output variations of the LINAC, that have to be taken into account in the dose constraints, because the output variations of the LINAC automatically interfere in the treatment.

3DVH was the software tested. It provides both 3D gamma analysis and DVH analysis. 3DVH uses the ArcCHECK measurements, just like its specific software, SNC, which provides 2D gamma analysis. However, 3DVH considers for the analysis more points than the SNC, which only considers the number of the ArcCHECK diodes. This accounts for some of the differences between the 3DVH and the SNC data. 3DVH software is more complete, which means, it provides many types and options of analysis, such as the dose map of gamma analysis in the CT of the patient, the individual analysis gamma, the DVHs of each structure and specific statistics. These analyses are very important to see which area is affected by the error. However, it has some disadvantages, such as, it does not calculate measured plans with many deviations relatively to the reference. Its analysis is also time-consuming, because it goes beyond a simple calculation of a number, as done in gamma analysis. In case of square fields, this study showed smaller sensibility in MLC errors detection, comparing with the EPID, for the square fields test, i.e. it is questionable if 3DVH can detect all errors. However, its results for MU errors detections are very good and similar to the EPID results, proving that it can detect these errors. In case of patients, it shows better results for MLC errors than in case of square fields. However, as some

lesser results were observed in square fields, the ones obtained for the patients may be not very reliable. For the MU errors results, in most the plans, it detects the presence of them, i.e. the results were approximately equal to the predictions, as in square field tests. For now, 3DVH is the best solution, because it provides DVH analysis that is better than gamma analysis and it is a compatible software with ArcCHECK.

Another system was tested in this study, EPID, which has been demonstrating accurate and sensitive capabilities in dosimetry. In Champalimaud Foundation, its capabilities have been investigated, in order to be integrated in the QA process. So, EPID measurements and its respective software were also tested for gamma analysis and for DVHs analysis performance. In both analyses, it showed more sensibility in the detection of the errors. In the case of the square fields for DVH analysis, it obtained approximately the same results as previously calculated and predicted, that is, it shows capabilities to measure DVHs. In terms of measurements, EPID has more resolution than the ArcCHECK and is linked to the gantry, perpendicularly positioned relatively of the dose source, which means that it follows the dose source during all the measurement, acquiring dose in all angles and its set-up is not time-consuming. ArcCHECK presents as well a great geometry for accurately acquiring dose in all angles. However, there are diodes overlapping and gaps between the diodes where dose is not measured. This affects the MLC errors detection, because the gaps size (1 cm) is larger than the introduced errors, this being the main cause of some lesser results of 3DVH. ArcCHECK is a good option to perform the QA, but EPID proved to be better.

For now, it is necessary to find the dose constraints for the DVHs analysis, understand how to perform this analysis and how the QA routine will be done with this new tool. It is also important to trust this the new software, 3DVH, which shows many advantages in the dose distribution evaluation, in order to try to implement it clinically. To this end, another test could be performed: creating patient plans in the slab phantom to compare the DVH analysis of 3DVH with the one of EPID. It allows to understand if the deviations detected by the 3DVH in the patient plans are relevant and real, comparing with the EPID that has shown better results, mainly in MLC errors. The comparison between the DVH analysis of patient plans from EPID with the one from 3DVH was not performed in this study, and it would be interesting to see if EPID works accurately in analysing these plans as well.

In sum, the DVH analysis proved to be an important and accurate analysis for the dose evaluation during the specific-patient QA. It was seen that 3DVH has the capabilities to execute this analysis. In addition to this, it was proven that EPID dosimetry is also a good, if not a better, option to be implemented, due to its precise capabilities to perform DVHs analysis, requiring simply improvement of the analysis systems, because many of them are research software.

Bibliography

[1] Global Burden of Disease Cancer Collaboration, "The Global Burden of Cancer 2013." *JAMA oncology*, vol. 1, no. 4, pp. 505–527, 2015.

[2] R. Baskar, K. A. Lee, R. Yeo, and K.-w. Yeoh, "Cancer and Radiation Therapy : Current Advances and Future Directions." *International Journal of Medical Sciences*, vol. 9, no. 3, pp. 193–199, 2012.

[3] J. Ferlay, E. Steliarova-Foucher, J. Lortet-Tieulent, S. Rosso, J. Coebergh, H. Comber, D. Forman, and F. Bray, "Cancer incidence and mortality patterns in Europe: Estimates for 40 countries in 2012," *European Journal of Cancer*, vol. 49, no. 6, pp. 1374–1403, 2013.

[4] L. N. Mcdermott, "On radiotherapy dose verification with a flat-panel imager." Ph.D. dissertation, 2007.

[5] M. Wendling, R. J. W. Louwe, L. N. Mcdermott, J.-j. Sonke, M. V. Herk, and B. J. Mijnheer, "Accurate two-dimensional IMRT verification using a back-projection EPID dosimetry method." *Medical Physics*, vol. 33, no. 2, pp. 259–273, 2006.

[6] S. M. J. J. G. Nijsten, "Portal Dosimetry in Radiotherapy." Ph.D. dissertation, 2009.

[7] P. Arthur Boyer, P. Peter Biggs, D. James Galvin, M. Eric Klein, P. Thomas LoSasso, P. Daniel Low, M. Katherine Mah, and D. Cedric Yu, "Basic Applications of Multileaf Collimators." *AAPM Report No. 72 , Report of Task Group No. 50, Radiation Therapy Committee*, p. 56, 2001.

[8] A. Ismail, G. N. Lu, R. Sihanath, P. Pittet, J. M. Galvan, and J. Balosso, "Radiotherapy quality insurance by individualized in vivo dosimetry : State of the art." *Cancer/Radiothérapie*, vol. 13, no. 3, pp. 182–189, 2009.

[9] M. Lopes, "Um século de terapia com radiação," *Gazeta de Física*, vol. 30, no. 14, pp. 14–29, 2005.

[10] J. Stroom, "Safety margins for geometrical uncertainties in radiotherapy." Ph.D. dissertation, 2000.

[11] W. Owadally and J. Staffurth, "Principles of cancer treatment by radiotherapy." *Surgery (Oxford)*, vol. 33, no. 3, pp. 127–130, 2015.

[12] I. Rosenberg, *Radiation Oncology Physics: A Handbook for Teachers and Students.* Nature Publishing Group, 2008.

[13] C. M. Washington and D. T. Leaver, *Principles and Practice of Radiation Therapy*. Elsevier Health Sciences, 2015.

[14] P. M. McCowan, D. W. Rickey, P. Rowshanfarzad, P. B. Greer, W. Ansbacher, and B. M. McCurdy, "An investigation of gantry angle data accuracy for cine-mode EPID images acquired during arc IMRT," *Journal of Applied Clinical Medical Physics*, vol. 15, no. 1, pp. 187–201, 2014.

[15] M. Dalaryd, "Dosimetric effects of removing the flattening filter in radiotherapy treatment units," Ph.D. dissertation, 2015.

[16] D. Georg, T. Knöös, and B. McClean, "Current status and future perspective of flattening filter free photon beams." *Medical Physics*, vol. 38, no. 3, pp. 1280–1293, 2011.

[17] M. Dalaryd, G. Kragl, C. Ceberg, D. Georg, B. McClean, S. af Wetterstedt, E. Wieslander, and T. Knöös, "A Monte Carlo study of a flattening filter-free linear accelerator verified with measurements." *Physics in Medicine and Biology*, vol. 55, no. 23, pp. 7333–7344, 2010.

[18] S. Ashokkumar, N. A. Nambi Raj, S. N. Sinha, G. Yadav, R. Thiyagarajan, K. Raman, and M. B. Mishra, "Comparison of Head Scatter Factor for 6MV and 10MV flattened (FB) and Unflattened (FFF) Photon Beam using indigenously Designed Columnar Mini Phantom." *Journal of Medical Physics / Association of Medical Physicists of India*, vol. 39, no. 3, pp. 184–191, 2014.

[19] M. Goitein, *Radiation Oncology: A Physicist's-Eye View*. Springer, 2008.

[20] A. Kacprowska and J. Jassem, "Hypofractionated radiotherapy for early breast cancer: Review of phase III studies." *Reports of Practical Oncology & Radiotherapy*, vol. 17, no. 2, pp. 66–70, 2012.

[21] S. T. Lutz, E. L. Chow, W. F. Hartsell, and A. A. Konski, "A review of hypofractionated palliative radiotherapy." *Cancer*, vol. 109, no. 8, pp. 1462–1470, 2007.

[22] A. Taylor, "Intensity-modulated radiotherapy - what is it?." *Cancer Imaging*, vol. 4, no. 2, pp. 68–73, 2004.

[23] Y. Nishimura and R. Komaki, *Intensity-Modulated Radiation Therapy: Clinical Evidence and Techniques*. Springer, 2015.

[24] S. Webb, "The physical basis of IMRT and inverse planning." *The British Journal of Radiology*, vol. 76, no. 910, pp. 678–689, 2003.

[25] A. Brahme, J. E. Roos, and I. Lax, "Solution of an integral equation encountered in rotation therapy." *Physics in Medicine and Biology*, vol. 27, no. 10, pp. 1221–1229, 1982.

[26] A. Brahme, "Optimization of stationary and moving beam radiation therapy techniques." *Radiotherapy and Oncology : Journal of the European Society for Therapeutic Radiology and Oncology*, vol. 12, no. 2, pp. 129–140, 1988.

[27] V. Feygelman, "Dose Verification in IMRT and VMAT." *Concepts and Trends in Medical Radiation Dosimetry: Proceedings of SSD Summer School.*, vol. 1345, no. 1, pp. 145–164, 2011.

[28] H. Zhen, "Improving Patient-Specific Pre-Treatment Quality Assurance." Ph.D. dissertation, 2012.

[29] G. M. Mancuso, "Evaluation of Volumetric Modulated Arc Therapy (VMAT) Patient Specific Quality Assurance." Ph.D. dissertation, 2011.

[30] C. X. Yu, "Intensity-modulated arc therapy with dynamic multileaf collimation: an alternative to tomotherapy." *Physics in Medicine and Biology*, vol. 40, no. 9, pp. 1435–1449, 1995.

[31] A. Sdrolia, K. Brownsword, J. Marsden, K. Alty, C. Moore, and A. Beavis, "Retrospective review of locally set tolerances for VMAT prostate patient specific QA using the COMPASS® system." *Physica Medica*, vol. 31, no. 7, pp. 792–797, 2015.

[32] "Patient Specific Quality Assurance for IMRT and VMAT based on Radiochromic Film Dssimetry with EBT2/EBT3 Film." [Online]. Available: http://slidegur.com/doc/1136257/patient-specific-quality-assurance-for-imrt-and-vmat

[33] International Commission on Radiation Units and Measurements (ICRU) Ed., "Prescribing, Recording, and Reporting Photon Beam Therapy (Report 50)." 1993.

[34] International Commission on Radiation Units and Measurements (ICRU), "Prescribing, Recording, and Reporting Photon Beam Therapy (Report 62) (Supplement to ICRU Report 50)," 1999.

[35] Animesh, "Advantages of multiple algorithm support in treatment planning system for external beam dose calculations," *Journal of Cancer Research and Therapeutics*, vol. 1, no. 1, pp. 12–20, 2005.

[36] C. Nieder, J. Langendijk, and M. Baumann, *Re-irradiation: New Frontiers Fractionation Concepts*. Springer, 2011.

[37] T. J. FitzGerald, M. Urie, K. Ulin, F. Laurie, J. Yorty, R. Hanusik, S. Kessel, M. B. Jodoin, G. Osagie, M. G. Cicchetti, R. Pieters, K. McCarten, and N. Rosen, "Processes for quality improvements in radiation oncology clinical trials." *International Journal of Radiation Oncology, Biology, Physics*, vol. 71, no. 1, pp. 76–79, 2008.

[38] Intensity Modulated Radiation Therapy Collaborative Working Group, "Intensity-modulated radiotherapy: current status and issues of interest." *International Journal of Radiation Oncology, Biology, Physics*, vol. 51, no. 4, pp. 880–914, 2001.

[39] G. A. Ezzell, J. M. Galvin, D. Low, J. R. Palta, I. Rosen, M. B. Sharpe, P. Xia, Y. Xiao, L. Xing, and C. X. Yu, "Guidance document on delivery, treatment planning, and clinical implementation of IMRT: Report of the IMRT subcommittee of the AAPM radiation therapy committee." *American Association of Physicists in Medicine*, vol. 30, no. 8, pp. 2089–2115, 2003.

[40] B. Mijnheer and D. George, "Guidelines for the verification of IMRT." in *Physics for Clinical Radiotherapy - ESTRO Booklet no 9*, 2008.

[41] A. Fredh, J. B. Scherman, L. S. Fog, and P. Munck af Rosenschöld, "Patient QA systems for rotational radiation therapy: a comparative experimental study with intentional errors." *Medical Physics*, vol. 40, no. 3, p. 1716, 2013.

[42] M. F. Chan, "Patient Clinically Relevant Dose QA for Head and Neck IMRT," 2011.

[43] B. E. Nelms and J. a. Simon, "A survey on planar IMRT QA analysis." *Journal of Applied Clinical Medical Physics / American College of Medical Physics*, vol. 8, no. 3, p. 2448, 2007.

[44] B. Fraass, K. Doppke, M. Hunt, G. Kutcher, G. Starkschall, R. Stern, and J. Van Dyke, "American Association of Physicists in Medicine Radiation Therapy Committee Task Group 53: quality assurance for clinical radiotherapy treatment planning." *American Association of Physicists in Medicine*, vol. 25, no. 10, pp. 1773–1829, 1998.

[45] D. A. Low, "Quality Assurance of Intensity-Modulated Radiotherapy." *Seminars in Radiation Oncology*, vol. 12, no. 3, pp. 219–228, 2002.

[46] J. M. Galvin, G. Ezzell, A. Eisbrauch, C. Yu, B. Butler, Y. Xiao, I. Rosen, J. Rosenman, M. Sharpe, L. Xing, P. Xia, T. Lomax, D. A. Low, and J. Palta, "Implementing IMRT in clinical practice: a joint document of the American Society for Therapeutic Radiology and Oncology and the American Association of Physicists in Medicine." *International Journal of Radiation Oncology, Biology, Physics*, vol. 58, no. 5, pp. 1616–1634, 2004.

[47] D. A. Low, J. M. Moran, J. F. Dempsey, L. Dong, and M. Oldham, "Dosimetry tools and techniques for IMRT." *American Association of Physicists in Medicine*, vol. 38, no. 3, pp. 1313–1338, 2011.

[48] S. Amerio, A. Boriano, F. Bourhaleb, R. Cirio, M. Donetti, A. Fidanzio, E. Garelli, S. Giordanengo, E. Madon, F. Marchetto, U. Nastasi, C. Peroni, A. Piermattei, C. J. Sanz Freire, A. Sardo, and E. Trevisiol, "Dosimetric characterization of a large area pixel-segmented ionization chamber." *Medical Physics*, vol. 31, no. 2, pp. 414–420, 2004.

[49] M. Stasi, S. Giordanengo, R. Cirio, A. Boriano, F. Bourhaleb, I. Cornelius, M. Donetti, E. Garelli, I. Gomola, F. Marchetto, M. Porzio, C. J. Sanz Freire, A. Sardo, and C. Peroni, "D-IMRT verification with a 2D pixel ionization chamber: dosimetric and clinical results in head and neck cancer." *Physics in Medicine and Biology*, vol. 50, no. 19, pp. 4681–4694, 2005.

[50] J. Herzen, M. Todorovic, F. Cremers, V. Platz, D. Albers, A. Bartels, and R. Schmidt, "Dosimetric evaluation of a 2D pixel ionization chamber for implementation in clinical routine." *Physics in Medicine and Biology*, vol. 52, no. 4, pp. 1197–1208, 2007.

[51] B. Poppe, A. Blechschmidt, A. Djouguela, R. Kollhoff, A. Rubach, K. C. Willborn, and D. Harder, "Two-dimensional ionization chamber arrays for IMRT plan verification." *Medical Physics*, vol. 33, no. 4, pp. 1005–1015, 2006.

[52] J. G. Li, G. Yan, and C. Liu, "Comparison of two commercial detector arrays for IMRT quality assurance." *Journal of Applied Clinical Medical Physics*, vol. 10, no. 2, p. 2942, 2009.

[53] E. Spezi, a. L. Angelini, F. Romani, and A. Ferri, "Characterization of a 2D ion chamber array for the verification of radiotherapy treatments." *Physics in Medicine and Biology*, vol. 50, no. 14, pp. 3361–3373, 2005.

[54] R. Sadagopan, J. a. Bencomo, R. L. Martin, G. Nilsson, T. Matzen, and P. a. Balter, "Characterization and clinical evaluation of a novel IMRT quality assurance system." *Journal of Applied Clinical Medical Physics*, vol. 10, no. 2, p. 2928, 2009.

[55] S. Both, I. M. Alecu, A. R. Stan, M. Alecu, A. Ciura, J. M. Hansen, and R. Alecu, "A study to establish reasonable action limits for patient-specific quality assurance in intensity-modulated radiation therapy." *Journal of Applied Clinical Medical Physics*, vol. 8, no. 2, pp. 1–8, 2007.

[56] P. A. Jursinic and B. E. Nelms, "A 2-D diode array and analysis software for verification of intensity modulated radiation therapy delivery." *Medical Physics*, vol. 30, no. 5, pp. 870–879, 2003.

[57] D. Létourneau, M. Gulam, D. Yan, M. Oldham, and J. W. Wong, "Evaluation of a 2D diode array for IMRT quality assurance." *Radiotherapy and Oncology*, vol. 70, no. 2, pp. 199–206, 2004.

[58] M. Bucciolini, F. B. Buonamici, and M. Casati, "Verification of IMRT fields by film dosimetry." *Medical Physics*, vol. 31, no. 1, pp. 161–168, 2004.

[59] S. G. Ju, Y. C. Ahn, S. J. Huh, and I. J. Yeo, "Film dosimetry for intensity modulated radiation therapy: dosimetric evaluation." *Medical Physics*, vol. 29, no. 3, pp. 351–355, 2002.

[60] B. E. Nelms, K. H. Rasmussen, and W. A. Tomé, "Evaluation of a fast method of EPID-based dosimetry for intensity modulated radiation therapy." *Journal of Applied Clinical Medical Physics*, vol. 11, no. 2, pp. 1–28, 2010.

[61] J. L. Bedford, Y. K. Lee, P. Wai, C. P. South, and A. P. Warrington, "Evaluation of the Delta 4 phantom for IMRT and VMAT verification." *Physics in Medicine and Biology*, vol. 54, no. 9, pp. 167–176, 2009.

[62] S. Korreman, J. Medin, and F. Kjær-Kristoffersen, "Dosimetric verification of RapidArc treatment delivery." *Acta Oncologica*, vol. 48, no. 2, pp. 185–191, 2009.

[63] V. Feygelman, G. Zhang, C. Stevens, and B. E. Nelms, "Evaluation of a new VMAT QA device, or the "X" and "O" array geometries." *Journal of Applied Clinical Medical Physics*, vol. 12, no. 2, p. 3346, 2011.

[64] D. L. Defoor, L. A. Vazquez-quino, P. Mavroidis, N. Papanikolaou, and S. Stathakis, "Anatomy-based , patient-specific VMAT QA using EPID or MLC log files." *Journal of Applied Clinical Medical Physics*, vol. 16, no. 3, pp. 206–215, 2015.

[65] D. Letourneau, J. Publicover, J. Kozelka, D. J. Moseley, and D. A. Jaffray, "Novel dosimetric phantom for quality assurance of volumetric modulated arc therapy." *Medical Physics*, vol. 36, no. 5, pp. 1813–1821, 2009.

[66] G. Yan, B. Lu, J. Kozelka, C. Liu, and J. G. Li, "Calibration of a novel four-dimensional diode array." *Medical Physics*, vol. 37, no. 1, pp. 108–115, 2010.

[67] G. Li, Y. Zhang, X. Jiang, and S. Bai, "Evaluation of the ArcCHECK QA system for IMRT and VMAT verification." *Physica Medica*, vol. 29, no. 3, pp. 295–303, 2013.

[68] A. L. Petoukhova, "The ArcCHECK diode array for dosimetric verification of HybridArc." *Physics in Medicine and Biology*, vol. 56, no. 16, p. 5411, 2011.

[69] E. M. Mckenzie, "An Evaluation of the Consistency of IMRT Patient-Specific QA Techniques." Ph.D. dissertation, 2013.

[70] A. Van Esch, C. Clermont, M. Devillers, M. Iori, and D. P. Huyskens, "On-line quality assurance of rotational radiotherapy treatment delivery by means of a 2D ion chamber array and the Octavius phantom." *Medical Physics*, vol. 34, no. 10, pp. 3825–3837, 2007.

[71] W. V. Elmpt, L. Mcdermott, S. Nijsten, M. Wendling, P. Lambin, and B. Mijnheer, "A literature review of electronic portal imaging for radiotherapy dosimetry." *Radiotherapy and Oncology*, vol. 88, no. 3, pp. 289–309, 2008.

[72] H. Meertens, M. van Herk, and J. Weeda, "A liquid ionisation detector for digital radiography of therapeutic megavoltage photon beams." *Physics in Medicine and Biology*, vol. 30, no. 4, pp. 313–321, 1985.

[73] M. van Herk and H. Meertens, "A matrix ionisation chamber imaging device for on-line patient setup verification during radiotherapy." *Radiotherapy and Oncology : Journal of the European Society for Therapeutic Radiology and Oncology*, vol. 11, no. 4, pp. 369–378, 1988.

[74] H. Meertens, M. van Herk, J. Bijhold, and H. Bartelink, "First clinical experience with a newly developed electronic portal imaging device." *International Journal of Radiation Oncology, Biology, Physics*, vol. 18, no. 5, pp. 1173–1181, 1990.

[75] M. van Herk, "Physical aspects of a liquid-filled ionization chamber with pulsed polarizing voltage." *Medical Physics*, vol. 18, no. 4, pp. 692–702, 1991.

[76] E. J. Morton, W. Swindell, D. G. Lewis, and P. M. Evans, "A linear array, scintillation crystal-photodiode detector for megavoltage imaging." *Medical Physics*, vol. 18, no. 4, pp. 681–691, 1991.

[77] L. E. Antonuk, Y. El-Mohri, W. Huang, K. W. Jee, J. H. Siewerdsen, M. Maolinbay, V. E. Scarpine, H. Sandler, and J. Yorkston, "Initial performance evaluation of an indirect-detection, active matrix flat-panel imager (AMFPI) prototype for megavoltage imaging." *International Journal of Radiation Oncology, Biology, Physics*, vol. 42, no. 2, pp. 437–454, 1998.

[78] L. E. Antonuk, J. Yorkston, W. Huang, J. H. Siewerdsen, J. M. Boudry, Y. El-Mohri, and M. V. Marx, "A real-time, flat-panel, amorphous silicon, digital x-ray imager." *Radiographics*, vol. 15, no. 4, pp. 993–1000, 1995.

[79] J. C. Gore, Y. S. Kang, and R. J. Schulz, "Measurement of radiation dose distributions by nuclear magnetic resonance (NMR) imaging." *Physics in Medicine and Biology*, vol. 29, no. 10, pp. 1189–1197, 1984.

[80] V. Chandraraj, S. Stathakis, R. Manickam, C. Esquivel, S. S. Supe, and N. Papanikolaou, "Comparison of four commercial devices for RapidArc and sliding window IMRT QA." *Journal of Applied Clinical Medical Physics / American College of Medical Physics*, vol. 12, no. 2, pp. 338–349, 2011.

[81] M. Hussein, P. Rowshanfarzad, M. A. Ebert, A. Nisbet, and C. H. Clark, "A comparison of the gamma index analysis in various commercial IMRT/VMAT QA systems." *Radiotherapy and Oncology*, vol. 109, no. 3, pp. 370–376, 2013.

[82] S. B. Jiang, G. C. Sharp, T. Neicu, R. I. Berbeco, S. Flampouri, and T. Bortfeld, "On dose distribution comparison." *Physics in Medicine and Biology*, vol. 51, no. 4, pp. 759–776, 2006.

[83] J. Van Dyk, R. B. Barnett, J. E. Cygler, and P. C. Shragge, "Commissioning and quality assurance of treatment planning computers." *International Journal of Radiation Oncology, Biology, Physics*, vol. 26, no. 2, pp. 261–273, 1993.

[84] W. B. Harms, D. A. Low, J. W. Wong, and J. A. Purdy, "A software tool for the quantitative evaluation of 3D dose calculation algorithms." *Medical Physics*, vol. 25, no. 10, pp. 1830–1836, 1998.

[85] D. A. Low, "Gamma Dose Distribution Evaluation Tool." *Journal of Physics: Conference Series*, vol. 250, no. 1, p. 2071, 2010.

[86] M. Dinesh Kumar, N. Thirumavalavan, D. Venugopal Krishna, and M. Babaiah, "QA of intensity-modulated beams using dynamic MLC log files." *Journal of Medical Physics / Association of Medical Physicists of India*, vol. 31, no. 1, pp. 36–41, 2006.

[87] D. A. Low, W. B. Harms, S. Mutic, and J. A. Purdy, "A technique for the quantitative evaluation of dose distributions." *Medical Physics*, vol. 25, no. 5, pp. 656–661, 1998.

[88] D. A. Low and J. F. Dempsey, "Evaluation of the gamma dose distribution comparison method." *Medical Physics*, vol. 30, no. 9, pp. 2455–2464, 2003.

[89] B. E. Nelms, H. Zhen, and W. A. Tome, "Per-beam, planar IMRT QA passing rates do not predict clinically relevant patient dose errors." *Medical Physics*, vol. 38, no. 2, pp. 1037–1044, 2011.

[90] H. Zhen, B. E. Nelms, and W. A. Tome, "Moving from gamma passing rates to patient DVH-based QA metrics in pretreatment dose QA." *Medical Physics*, vol. 38, no. 10, pp. 5477–5489, 2011.

[91] M. Stasi, S. Bresciani, A. Miranti, A. Maggio, V. Sapino, and P. Gabriele, "Pretreatment patient-specific IMRT quality assurance: a correlation study between gamma index and patient clinical dose volume histogram." *Medical Physics*, vol. 39, no. 12, pp. 7626–7634, 2012.

[92] L. Coleman and C. Skourou, "Sensitivity of volumetric modulated arc therapy patient specific QA results to multileaf collimator errors and correlation to dose volume histogram based metrics." *Medical Physics*, vol. 40, no. 11, p. 1715, 2013.

[93] G. Heilemann, B. Poppe, and W. Laub, "On the sensitivity of common gamma-index evaluation methods to MLC misalignments in Rapidarc quality assurance." *Medical Physics*, vol. 40, no. 3, p. 1702, 2013.

[94] B. E. Nelms, M. F. Chan, G. Jarry, M. Lemire, J. Lowden, C. Hampton, and V. Feygelman, "Evaluating IMRT and VMAT dose accuracy: Practical examples of failure to detect systematic errors when applying a commonly used metric and action levels." *Medical Physics*, vol. 40, no. 11, p. 1722, 2013.

[95] P. Carrasco, N. Jornet, A. Latorre, T. Eudaldo, A. Ruiz, and M. Ribas, "3D DVH-based metric analysis versus per-beam planar analysis in IMRT pretreatment verification," *Medical Physics*, vol. 39, no. 8, pp. 5040–5049, 2012.

[96] J. Gordon and J. Siebers, "Addressing a gap in current IMRT quality assurance." *International Journal of Radiation Oncology, Biology, Physics*, vol. 87, no. 1, pp. 20–21, 2013.

[97] S. Stojadinovic, L. Ouyang, X. Gu, A. Pompoš, Q. Bao, and T. D. Solberg, "Breaking bad IMRT QA practice." *Journal of Applied Clinical Medical Physics*, vol. 16, no. 3, pp. 154–165, 2015.

[98] R. Drzymala, R. Mohan, L. Brewster, J. Chu, M. Goitein, W. Harms, and M. Urie, "Dose-volume histograms." *International Journal of Radiation Oncology, Biology, Physics*, vol. 21, no. 1, pp. 71–78, 1991.

[99] M. J. Dance, "A comparative Analysis for Verification of IMRT and VMAT Treatment Plans using a 2D and 3D Diode Array," Ph.D. dissertation, 2014.

[100] C. Mai, "Technology Development in QA and Dosimetry." [Online]. Available: http://www.tmps.or.th/12AOCMP/presentation/Therapy{_}room/11122012/11122012{_}0930{_}MaxTang.pdf

[101] F. M. G. de Moura, "Amorphous silicon detector panel damage: correlating physical parameters to clinical usability," Ph.D. dissertation, 2008.

[102] M. G. Herman, J. M. Balter, D. A. Jaffray, K. P. Mcgee, P. Munro, S. Shalev, M. V. Herk, and J. W. Wong, "Clinical Use of Electronic Portal Imaging : Report of AAPM Radiation Therapy Committee Task Group 58 AAPM Refresher Course – Salt Lake City July 2001," *Medical Physics*, vol. 28, no. 5, pp. 712–737, 2001.

[103] W. V. Elmpt, "3D dose verification for advanced radiotherapy," Ph.D. dissertation, 2008.

[104] J. B. Scherman, "Development and evaluation of methods for comparison of dose distributions in radiotherapy using calculated, synthetic and simulated measured dose distributions." Ph.D. dissertation, 2009.

[105] T. Depuydt, A. Van Esch, and D. P. Huyskens, "A quantitative evaluation of IMRT dose distributions: Refinement and clinical assessment of the gamma evaluation." *Radiotherapy and Oncology*, vol. 62, no. 3, pp. 309–319, 2002.

[106] É. Y. Watanabe, "Avaliação do dispositivo eletrônico de imagem portal "portal dosimetry" no controle de qualidade de radioterapia de intensidade modulada," Ph.D. dissertation, 2010.

[107] G. A. Ezzell, J. W. Burmeister, N. Dogan, T. J. LoSasso, J. G. Mechalakos, D. Mihailidis, A. Molineu, J. R. Palta, C. R. Ramsey, B. J. Salter, J. Shi, P. Xia, N. J. Yue, and Y. Xiao, "IMRT commissioning: Multiple institution planning and dosimetry comparisons, a report from AAPM Task Group 119." *Medical Physics*, vol. 36, no. 11, pp. 5359–5373, 2009.

[108] P. S. Basran and M. K. Woo, "An analysis of tolerance levels in IMRT quality assurance procedures." *Medical Physics*, vol. 35, no. 6, pp. 2300–2307, 2008.

[109] M. Yoon, "A new homogeneity index based on the statistical analysis of dose volume histogram," *Journal of Applied Clinical Medical Physics*, vol. 8, no. 2, pp. 9–17, 2007.

[110] International Commission on Radiation Units and Measurements (ICRU) Ed., "Prescribing, Recording, and Reporting Intensity-Modulated Photon-Beam Therapy (IMRT)(ICRU Report 83)," 2010.

[111] S. Dieterich, E. Ford, D. Pavord, and J. Zeng, *Practical Radiation Oncology Physics*. Elsevier, 2016.

[112] M. Oliver, K. Bush, S. Zavgorodni, W. Ansbacher, and W. A. Beckham, "Understanding the impact of RapidArc therapy delivery errors for prostate cancer." *Journal of Applied Clinical Medical Physics / American College of Medical Physics*, vol. 12, no. 3, p. 3409, 2011.

[113] L. W. Brady and T. E. Yaeger, Eds., *Encyclopedia of Radiation Oncology*. Springer Berlin Heidelberg, 2013.

[114] R. Thiyagarajan, A. Nambiraj, S. N. Sinha, G. Yadav, A. Kumar, V. Subramani, and Kothandaraman, "Analyzing the performance of ArcCHECK diode array detector for VMAT plan," *Reports of Practical Oncology & Radiotherapy*, vol. 21, no. 1, pp. 50–56, 2016.

[115] Sun Nuclear Corporation, "ArcCHECK ® Reference Guide The Ultimate 4D QA Solution."

[116] "Your Most Valuable QA and Dosimetry Tools." [Online]. Available: http://www.sunnuclear.com/documents/datasheets/arccheck3dvh.pdf

[117] S. Deshpande, A. Xing, L. Holloway, P. Metcalfe, and P. Vial, "Dose calibration of EPIDs for segmented IMRT dosimetry," *Journal of Applied Clinical Medical Physics*, vol. 15, no. 6, p. 4895, 2014.

[118] W. D. Renner, K. Norton, and T. Holmes, "A method for deconvolution of integrated electronic portal images to obtain incident fluence for dose reconstruction," *Journal of Applied Clinical Medical Physics*, vol. 6, no. 4, pp. 22–39, 2004.